



Calhoun: The NPS Institutional Archive

Theses and Dissertations

Thesis Collection

1987

The fractal dimension as a petrophysical parameter.

Cowan, Kenneth Lee.

<http://hdl.handle.net/10945/22815>



Calhoun is a project of the Dudley Knox Library at NPS, furthering the precepts and goals of open government and government transparency. All information contained herein has been approved for release by the NPS Public Affairs Officer.

Dudley Knox Library / Naval Postgraduate School
411 Dyer Road / 1 University Circle
Monterey, California USA 93943

<http://www.nps.edu/library>



WILLIAM KNOX LIBRARY
607 1/2 - 10TH AVENUE - 1ST FLOOR
ANN ARBOR, MICHIGAN 48106-1000

THE FRACTAL DIMENSION AS A
PETROPHYSICAL PARAMETER

THE FRACTAL DIMENSION AS A
PETROPHYSICAL PARAMETER

by

KENNETH LEE COWAN, B.S.

THESIS

Presented to the Faculty of the Graduate School of
The University of Texas at Austin
In Partial Fulfillment
of the Requirements
for the Degree of

MASTER OF SCIENCE IN ENGINEERING

THE UNIVERSITY OF TEXAS AT AUSTIN

AUGUST, 1987

ACKNOWLEDGMENTS

I would like to thank the many people who assisted me in this project. Dr. Mukul M. Sharma, my supervising professor, for his guidance and direction throughout the course of this project and for working within the very tight schedule that was maintained. Dr. Mark A. Miller for his time spent reading and commenting on this paper. The United States Navy for providing me with the time and the financial support to accomplish this task. Larry Mack for teaching me how to use the Scanning Electron Microscope. All of my friends who encouraged me and provided support for me throughout this project. Finally, my wife, Julie, who always provided a positive attitude and much needed moral support throughout the duration of this project-- I could not have accomplished this project without her constant support.

Kenneth Lee Cowan

The University of Texas at Austin

July, 1987

ABSTRACT

The secondary electron emission from a Scanning Electron Microscope (SEM) was used to determine that the pore spaces of seven sandstones and four dolomites exhibited fractal behavior over certain length scales. Data from the SEM measurements produced log-log plots that not only verified the fractal nature of the rocks, but also allowed for the determination of their fractal dimensions.

To model the transport properties of fractal lattices, a two dimensional model known as the Sierpinski Carpet was used as a starting point. Results developed by Sharma and Gupta (1987) for the petrophysical properties of such fractal lattices, such as porosity, permeability, capillary pressure, etc. are presented here. Although the results cannot be directly compared with experiments, they demonstrate a methodology that can be applied to three dimensional lattices as well.

A variation of a three dimensional fractal structure known as the Menger Sponge was used to model the pore spaces in rocks in an attempt to determine transport properties of rocks from fractal data. The fractal data on the rock samples obtained from the SEM

was combined with corresponding core analysis data to test the model. It was determined that the simple Menger Sponge was an inadequate model for fractal pore space within rocks as it estimated porosity values much higher than those commonly encountered in rock samples. However, a modified version of this model showed potential for accurately representing the pore space of rocks as it produced porosity values that were in the same range as those of the rock samples.

TABLE OF CONTENTS

Acknowledgments	iv
Abstract	v
Table of Contents	vii
Chapter 1: Introduction	1
Chapter 2: Definition of Fractal	5
Chapter 3: Measurement of Fractal Dimension	25
3.1: Manual Methods of Measurement	25
3.2: Automated Methods of Measurement	29
3.3: X-ray Scattering	34
3.4: Adsorption of Molecules	36
3.5: Scanning Electron Microscope	41
Chapter 4: Experimental Procedure and Results	45
4.1: Summary.....	45
4.2: Preparation of Rock Samples.....	45
4.3: Intensity Measurements.....	48
4.4: Results... ..	49
4.5: Discussion.....	52
Chapter 5: Fractals and Transport Properties of Rocks	69
5.1: Summary.....	69
5.2: Two Dimensional Model: The Sierpinski Carpet.....	70
5.2.1: Porosity.....	75
5.2.2: Specific Surface Area.....	77
5.2.3: Pore Size Distribution.....	77
5.2.4: Permeability.....	79
5.2.5: Capillary Pressure Curves.....	82
5.2.6: Relative Permeability Curves.....	84
5.2.7: Discussion	86

5.3: Three Dimensional Model: The Menger Sponge.....	86
5.3.1: Porosity.....	95
5.3.2: Results.....	97
5.4: Modified Menger Sponge.....	98
5.5: Future Work.....	99
Chapter 6: Conclusion	103
Appendix A: Photographs	105
Appendix B: Menger Sponge Graphs.....	134

LIST OF FIGURES

Figure 2-1: Examples of Euclidean geometrical figures.	6
Figure 2-2: Example of a fractal line.	10
Figure 2-3: Log-log plot of $L(r)$ vs r .	12
Figure 2-4: Triadic Koch Island.	15
Figure 2-5: Cantor Set with fractal dimension < 1 .	18
Figure 2-6: Sierpinski Carpet with $b=8$, $c=4$, and $D=1.8617$.	19
Figure 2-7: Menger Sponge.	21
Figure 3-1: Example of Flook's method.	30
Figure 3-2: Computer's technique for selecting coordinates.	33
Figure 3-3: Molecules of different sizes.	38
Figure 3-4: Typical secondary electron intensity display from an SEM.	42
Figure 4-1: Rock sample mounted to an aluminum cylinder.	47
Figure 4-2: Log-log plot for Berea sandstone.	56
Figure 4-3: Log-log plot for uncompacted Frio sandstone, 9178.3 ft.	57
Figure 4-4: Log-log plot for compacted Frio sandstone, 9177.5 ft.	58

Figure 4-5: Log-log plot for uncompacted Frio sandstone, 9189.5 ft.	59
Figure 4-6: Log-log plot for compacted Frio sandstone, 9189.5 ft	60
Figure 4-7: Log-log plot for Travis Peak sandstone, 7449.4 ft.	61
Figure 4-8: Log-log plot for Travis Peak sandstone, 7456.3 ft.	62
Figure 4-9: Log-log plot for San Andres dolomite, 3350 ft.	63
Figure 4-10: Log-log plot for San Andres dolomite, 3414 ft.	64
Figure 4-11: Log-log plot for San Andres dolomite, 3464 ft.	65
Figure 4-12: Log-log plot for San Andres dolomite, 3492 ft.	66
Figure 4-13: Porosity vs fractal dimension.	67
Figure 4-14: Permeability vs fractal dimension.	68
Figure 5-1: Sierpinski Carpet with high lacunarity.	72
Figure 5-2: Sierpinski Carpet with low lacunarity.	73
Figure 5-3: Porosity vs D for varying lacunarity.	76
Figure 5-4: Pore size distribution for varying lacunarity.	80
Figure 5-5: Permeability vs D for varying lacunarity.	81
Figure 5-6: Capillary pressure curves for varying lacunarity.	83
Figure 5-7: Relative permeability curves for varying D.	85

Figure 5-8: Original cube divided into b^3 smaller cubes.	88
Figure 5-9: Effects of changing the value of b .	90
Figure 5-10: When $b=6$ and $c=2$, the total cubes removed from each face is c^2 or 4.	91
Figure 5-11: Removal of cubes creates passageway through large cube.	93
Figure 5-12: porosity vs D for $b=100$ and $L_2/L_1=1000$.	100
Figure 5-13: porosity vs D for $b=100$ and $L_2/L_1=35000$.	101
Figure A-1: Frio Sandstone, 9178.3 ft, x31, x53.	106
Figure A-2: Frio Sandstone, 9178.3 ft, x103, x260.	107
Figure A-3: Frio Sandstone, 9178.3 ft, x550, x1030.	108
Figure A-4: Frio Sandstone, 9178.3 ft, x2600, x4800.	109
Figure A-5: Frio Sandstone, 9178.3 ft, x9300, x18500.	110
Figure A-6: Travis Peak Sandstone, 7456.3 ft, x34, x55.	111
Figure A-7: Travis Peak Sandstone, 7456.3 ft, x130, x220.	112
Figure A-8: Travis Peak Sandstone, 7456.3 ft, x260, x520.	113
Figure A-9: Travis Peak Sandstone, 7456.3 ft, x1100, x2900.	114
Figure A-10: Travis Peak Sandstone, 7456.3 ft, x5400, x9500.	115

Figure A-11: Frio Sandstone, 9189.5 ft, x29, x58.	116
Figure A-12: Frio Sandstone, 9189.5 ft, x100, x250.	117
Figure A-13: Frio Sandstone, 9189.5 ft, x510, x750.	118
Figure A-14: Frio Sandstone, 9189.5 ft, x1000, x2700.	119
Figure A-15: Frio Sandstone, 9189.5 ft, x5100, x10000.	120
Figure A-16: Frio Sandstone, 9189.5 ft, x18000.	121
Figure A-17: San Andres dolomite, 3350 ft, x31, x54.	122
Figure A-18: San Andres dolomite, 3350 ft, x102, x240.	123
Figure A-19: San Andres dolomite, 3350 ft, x510, x760.	124
Figure A-20: San Andres dolomite, 3350 ft, x990, x2500.	125
Figure A-21: San Andres dolomite, 3350 ft, x5200, x10000.	126
Figure A-22: San Andres dolomite, 3350 ft, x17000.	127
Figure A-23: San Andres dolomite, 3464 ft, x27, x54.	128
Figure A-24: San Andres dolomite, 3464 ft, x102, x230.	129
Figure A-25: San Andres dolomite, 3464 ft, x510, x730.	130
Figure A-26: San Andres dolomite, 3464 ft, x1030, x2400.	131
Figure A-27: San Andres dolomite, 3464 ft, x5100, x10300.	132
Figure A-28: San Andres dolomite, 3464 ft, x18300.	133

Figure B-1: Porosity vs D for $b=10$ and $L2/L1=1000$.	135
Figure B-2: Porosity vs D for $b=100$ and $L2/L1=1000$.	136
Figure B-3: Porosity vs D for $b=200$ and $L2/L1=1000$.	137
Figure B-4: Porosity vs D for $b=10$ and $L2/L1=10000$.	138
Figure B-5: Porosity vs D for $b=100$ and $L2/L1=10000$.	139
Figure B-6: Porosity vs D for $b=200$ and $L2/L1=10000$.	140
Figure B-7: Porosity vs D for $b=10$ and $L2/L1=35000$.	141
Figure B-8: Porosity vs D for $b=100$ and $L2/L1=35000$.	142
Figure B-9: Porosity vs D for $b=200$ and $L2/L1=35000$.	143

Chapter 1

Introduction

The conceptual ideas behind fractal geometry have been known for quite some time. As early as the 1920's, mathematicians such as Cantor, Peano and many others developed some of the mathematical concepts that set the foundation for fractal theory (Mandelbrot 1983). Many of these concepts were merely expanded versions of old ideas; however, much of the thought was completely revolutionary. It was not until 1975 that Mandelbrot brought forth his idea of a fractal dimension. Since that time, the popularity of fractals has increased significantly. The available literature on the subject has grown exponentially through published books, journals and other professional papers. It seems as if we are just beginning to understand the concepts behind fractals and their importance in almost every aspect of science and nature. In fact, it is now apparent that fractal forms are much more common and more useful than anyone had first anticipated.

Studies have recently shown that fractal forms occur quite often in many engineering practices, and that they can be modeled and utilized to help explain many natural phenomena. For example, Winslow (1985) conducted experiments with cement pastes and discovered that the surfaces of these pastes are fractals.

Furthermore, this fractal nature of cement paste explained many of the anomalies observed in previous vapor sorption experiments. This fractal property of cement may also have future implications in the construction industry where it is often used in the construction of buildings, walls, walkways, etc. There could possibly be a relationship between the fractal dimension of the cement surface and the strength and adhesive properties of the cement.

Van Damme, Obrecht, Levitz, Gatineau and Laroche (1986) conducted experiments with clay slurries and discovered that the interface between injected water and clay slurries formed a fractal boundary. This fractal interface may have some far reaching implications in the Petroleum industry. Nearly all drilling fluids used in drilling operations contain a mixture of clay and water. The fractal boundary between these two substances may prove to be significant in drilling operations. In addition, the filtrate from the drilling mud usually invades the adjacent formation during drilling operations causing a change in the formation petrophysical properties near the wellbore. In formations containing high percentages of clays, the filtrate from the drilling mud will most likely come into contact with these clays. Since the water/clay boundary has been shown to be a fractal, there may be a connection

between the fractal nature of this boundary and the petrophysical properties of the invaded zone.

Many others have also investigated the properties of fractals, and the results are very interesting. Jacquin and Adler (1985) discovered that the interface between the gas phase and the liquid phase in a displacement process is of a fractal nature. This fact could prove to be very significant in many of the enhanced oil recovery processes that involve the displacement of oil and water by a gas (i.e. steamfloods, carbon dioxide floods, etc.). Pentland (1983) used the concepts fractals combined with computer graphic techniques to create three dimensional models of structures containing fractal surfaces.

These are only a few examples of the significance of fractal figures in the areas of science and engineering. A more complete discussion of applications of fractals is deferred to a later chapter.

This thesis will investigate the application of fractal concepts to reservoir rocks. The first goal is to determine whether or not some well known reservoir rocks exhibit fractal behavior. This will be determined through appropriate measurements made on a Scanning Electron Microscope (SEM). The second goal of this thesis is to be able to accurately measure the fractal dimension of these rocks (if they indeed are fractals) using the SEM measurements. The final goal is to use this fractal property of

rocks to obtain a better description of the rock in terms of its petrophysical properties. The fractal models used here are the Sierpinski Carpet (in two dimensions) and the Menger Sponge (in three dimensions).

Chapter 2

Definition of Fractal

The term "fractal" was coined by Benoit Mandelbrot in the 1970's to represent dimensions that are non-integers. Mandelbrot (1983) defined a fractal as "a set for which the Hausdorff Besicovitch dimension strictly exceeds the topological dimension". Although this definition may be correct, it is not the easiest way to understand the concept of fractals. There are many ways to define the "fractal dimension". The purely geometric interpretation of fractals provides perhaps the best illustration. One method of explaining fractal surfaces is to compare them with Euclidean surfaces.

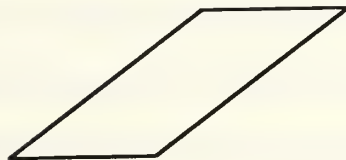
In conventional Euclidean geometry, forms can be grouped into points, lines, surfaces and volumes, and each form has a characteristic number of dimensions to describe it. For example, a point has no dimensions, a line has one dimension, a plane has two, and a volume has three (see Figure 2-1). These forms are also considered to be smooth (everywhere differentiable) and of finite length, area, etc. However, in reality, forms are not so simple. Nearly all forms have some surface roughness, and when viewed at



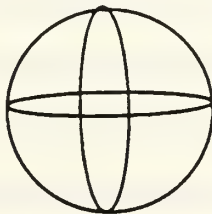
A point: zero dimensions



A line: one dimension



A plane: two dimensions



A sphere: three dimensions

Figure 2-1: Examples of Euclidean geometrical shapes.

higher and higher magnifications, these surfaces may appear as a series of "peaks and valleys".

Examine a piece of sanded wood for instance. Initially, it may appear that the wood is smooth, but examination at a higher magnification will reveal a very rough surface filled with these so called peaks and valleys. If the magnification were continually increased, it may be discovered that these peaks may themselves be composed of even smaller peaks. If this process were to continue at all levels of magnification, the surface would be discontinuous everywhere and have infinite area!

In order to be classified as a self-similar fractal, the structure and general appearance of these smaller peaks and valleys must remain the same as the larger ones. Thus, a form must appear the same or similar at high magnifications as it does at low magnifications. For instance, a desert scene in the middle of Death Valley, California may possess this characteristic. The basic texture of the desert floor appears approximately the same from 30,000 feet in the air as it does from the ground. From the air, the many dried up creekbeds and lakebeds appear very similar to the smaller mudcracks observed by someone standing near the desert floor. In addition, the desert floor most likely appears similar when observed at even higher magnifications due to the properties of the soil present. Thus, the desert landscape could possibly be a

fractal due to its repetitive nature at many different levels of magnification. However, it would most likely be considered only approximately self-similar, since the desert does not appear exactly the same at all levels of magnification.

Not all irregular shapes possess this self-similar characteristic. Some shapes may only exhibit this behavior over a specific range of magnifications, and can therefore be considered self-similar fractals for that range. For magnifications above or below that range of magnifications, the shape can be considered Euclidean in nature.

It is possible that a shape may be considered a fractal, but still not possess the self-similarity previously described. Such shapes are called random fractals. Random fractals are shapes that still possess the fractal nature, but they do not have the self-similarity trait that was just discussed. When these types of shapes are observed at different magnifications, they appear generally the same, except the peaks and valleys do not look exactly the same at all magnifications. It may be possible that the characteristic shapes observed at one magnification were formed in a probabilistic manner. Hence, the minor difference in appearance. These types of fractal surfaces are not as well studied as self-similar fractals.

Obviously, forms with fractal characteristics cannot be adequately described by the concepts of Euclidean geometry alone.

The concepts of fractal geometry allow for a quantitative description of irregular forms that do not have smooth edges and surfaces. The concepts of points, lines, surfaces and volumes in one, two or three dimensions are still valid in fractal geometry; however, they are allowed to have non-integer dimensions, and the amount by which a fractal form's dimension exceeds its Euclidean counterpart is a measure of its irregularity. For instance, a line with a fractal dimension of 1.7 is more irregular than a line with a fractal dimension of 1.3, and both are more irregular than the Euclidean line of dimension 1.

A simple example in one dimension may help to clarify these concepts. Consider the line in Figure 2-2(a). Clearly this line has a dimension of one, if it assumed that it is perfectly straight between the endpoints. In Figure 2-2(b) the line is made more irregular by dividing it up into eight line segments, each of which is $1/4$ the original length of the line. Although the distance between the endpoints has not changed, the total length of the line has increased from a length of one to a length of $8 \times (1/4) = 2$. If the eight line segments are again divided up in the exact same way, the individual line segments get smaller, and the total length increases again (see Figure 2-2(c)). If this process were continued indefinitely, the length of the line segments would approach zero, and the total length of the curve would approach infinity! A curve of this nature

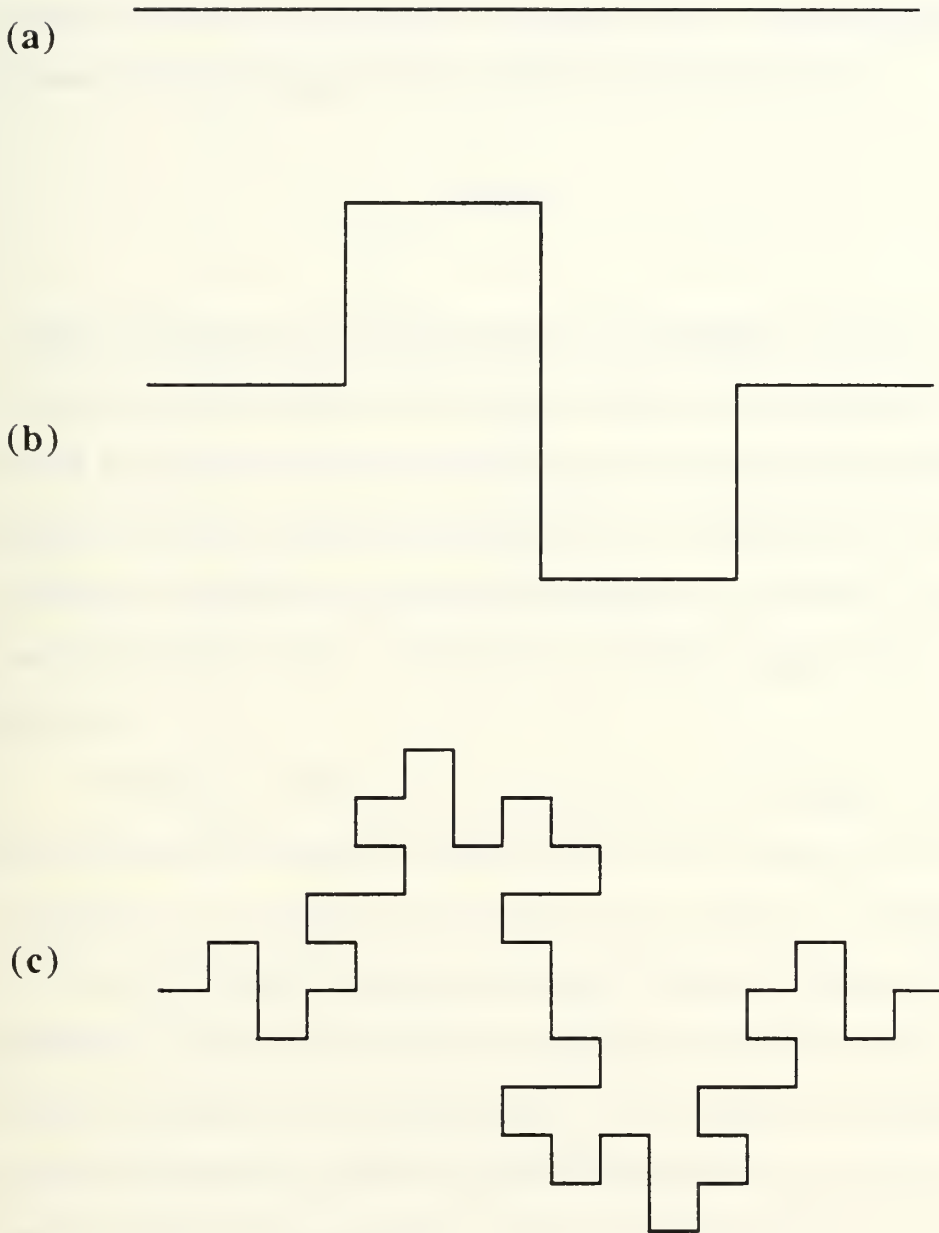


Figure 2-2: Example of a fractal line.

would be considered a self-similar fractal, because its wiggles repeat themselves at all levels of magnification. The relationship between the total length, $L(r)$, and the fractal dimension is

$$r = r^{-(D-1)} \quad (2.1)$$

where D is the fractal dimension and r is the length of the line segments used to measure the length of the curve. In Figure 2-2(b), $r=1/4$, because the line was divided up into line segments that are equal to $1/4$ the length of the original line. A log-log plot of $L(r)$ vs r results in a straight line with slope equal to $1-D$. Figure 2-3 is an example of such a plot. For the curve shown in Figure (2-2), $D=1.5$.

Numerous fractal curves, such as the curve in Figure 1, can be constructed manually through the use of an "initiator" and a "generator". An initiator may be any curve, surface, or volume that is used to establish the general shape of the fractal form. The generator, on the other hand, is the fractal portion of the curve which is repeated at all magnifications. The initiator is combined with the generator by replacing specific portions of the initiator with the shape of the generator. For the fractal in Figure 1, the straight line in Figure 2-2(a) is the initiator, because it is the shape used to start, or initiate the curve. The shape in Figure 2-2(b) is the

Log (L) vs Log (r)

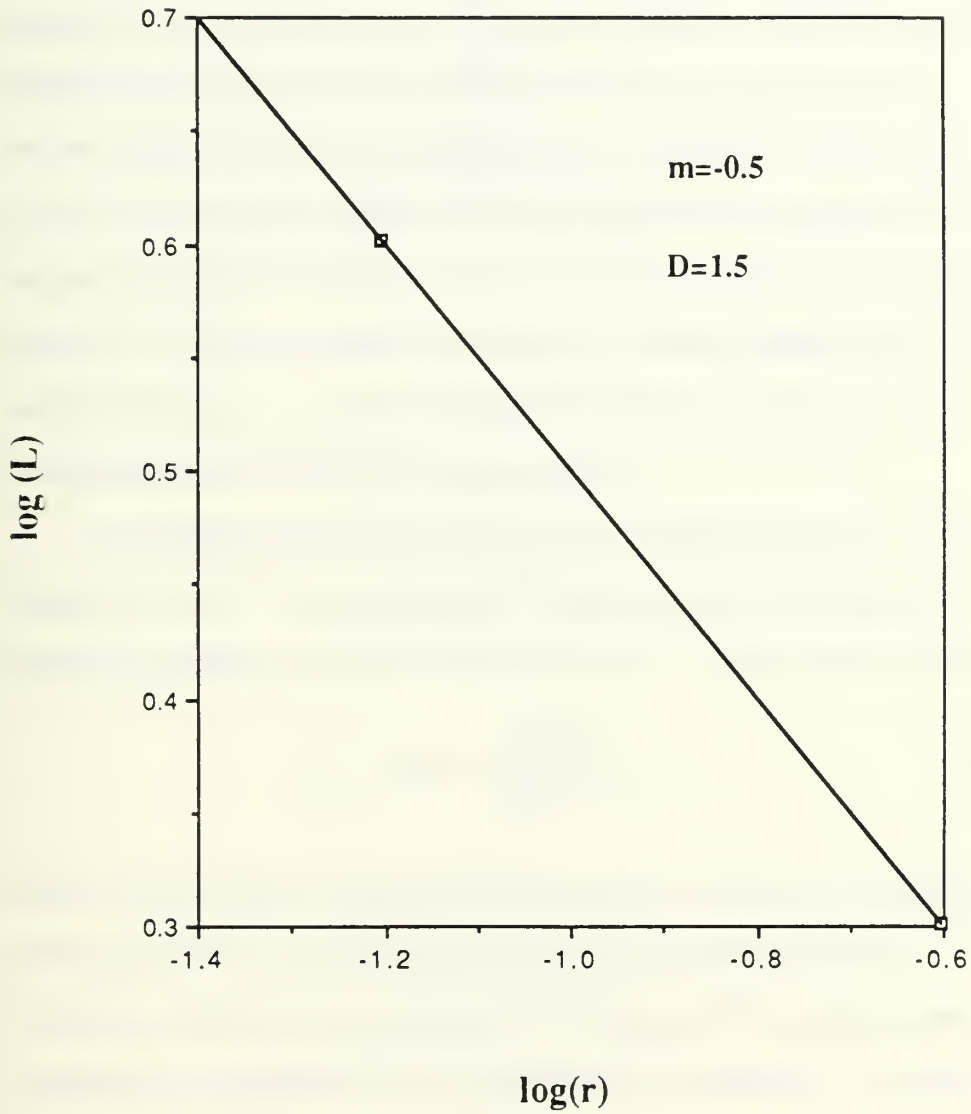


Figure 2-3: Log-log plot of $L(r)$ vs r . Note that the slope of the line is equal to $1-D$.

generator, because it is used to modify the initiator to form the fractal curve. Figure 2-2(b) is an example of the line after the generator is inserted in place of the original line. As this process is repeated, each line segment of the curve must be replaced (in proper proportion) with the shape of the generator. Thus, the curve very quickly becomes a series of smaller and smaller line segments combined to form a unique pattern. Figure 2-2(c) is an example of the curve after this process has been repeated twice. As stated earlier, the curve becomes a fractal as the process is continuously repeated to all length scales.

The fractal dimension of a manually generated fractal is a function of only N and r , where N is the number of segments of length r replacing the original line segment. The actual formula is

$$D = \frac{\log N}{\log 1/r} \quad (2.2)$$

which is equivalent to the previous equation relating total length, fractal dimension, and segment length at any magnification.

However, with this formula, only the shapes of the initiator and generator are required to obtain the fractal dimension. The total length and individual segment lengths do not need to be known at every magnification, but they can be easily calculated if desired.

The fractal curves and surfaces that can be formed in this

manner are practically limitless. They can take many different forms in one, two, or three dimensions. Mandelbrot gives many examples of such curves in his book *The Fractal Geometry of Nature* (1983).

Figure 2-4 is another example of a generated fractal surface in which the initiator is an equilateral triangle of side length b (see Figure 2-4(a)), and the generator is made up of four line segments, each of length b/r as shown in Figure 2-4(b). Each side of the triangle is replaced with the generator, and the resulting form is shown in Figure 2-4(c). As before, the process is continued indefinitely so that the curve becomes self-similar at all magnifications. Using the formula from above, the fractal dimension of this curve is

$$D = \frac{\log N}{\log 1/r} = \frac{\log 4}{\log 3} = 1.2618 \quad (2.3)$$

Note that $N = 4$ and $r = 1/3$ since each side of the triangle is replaced with four line segments of length $1/3$ (of original line segment). This curve was originally constructed by Helge Von Koch, and it is called a triadic Koch Island.

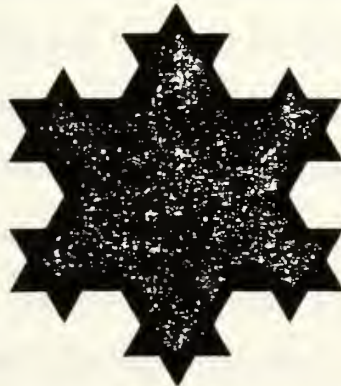
The line in Figure 2-1 and the Koch Island in Figure 2-4 are both examples of irregular forms that can be characterized as fractals. Both curves have fractal dimensions greater than one and



Initial Triangle



After first generation



After second generation

Figure 2-4: Triadic Koch Island

less than two. This range of fractal dimensions implies that the curves are more irregular than a Euclidean line of dimension one, and that the curves fill less area than a Euclidean planar surface of dimension two. As stated earlier, fractals represent distributions containing fractional dimensions somewhere between the dimensions of conventional Euclidean geometry.

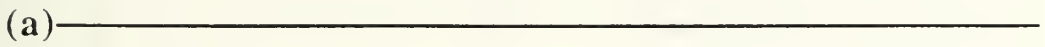
Thus far, only linear type fractals have been considered; however, fractal distributions can pertain to an area or volume as well as a length. In fact, the more irregular a line, the higher the fractal dimension, and the closer D becomes to two. In other words, highly irregular lines become space filling and approach planar figures rather than linear curves. It may be easier to model highly irregular curves as Euclidean planes with some area removed, rather than a line with a high degree of irregularity.

A similar analogy can be made for surfaces with fractal dimensions between two and three. These types of surfaces can be modeled as either conventional planar surfaces with a degree of irregularity, or they can be modeled as Euclidean volumes with some specific volume removed. Examine a piece of paper for instance. At first glance, the paper may seem to be a very good approximation of a planar surface of dimension two. It has length and width, but relatively little depth. However, further examination of the paper surface under high magnifications will

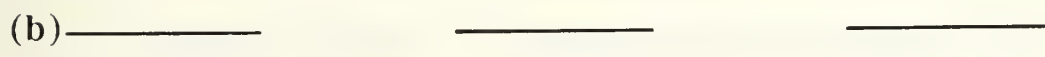
reveal the strands of wood fiber used to construct the paper. At these magnifications, the fibrous material will not appear planar at all; rather, it will appear three dimensional with peaks and valleys between the individual strands. Thus, a simple piece of paper could possibly be a fractal surface for some range of magnifications. Fractal or not, the paper will most definitely appear highly irregular and not planar. Obviously, the surface would have a characteristic dimension somewhere between two and three.

Thus, another way to think of fractals is that they can be modeled as lines, surfaces and volumes that do not entirely fill space. In Euclidean geometry, a line fills all the space between the two endpoints and has a dimension of one. However, a fractal line can be created that has a fractal dimension less than one by removing regular intervals of the line as shown in Figure 2-5. This type of line is a special type of fractal, because it has a fractal dimension less than one, and it is called a Cantor set. (Mandelbrot 1983). Similarly, a Euclidean plane is a surface with only length and width, and it has all of the area filled in between the boundaries. On the other hand, some fractal surfaces can be modeled as planar surfaces with some interval of area removed. These fractal surfaces have fractal dimensions between one and two.

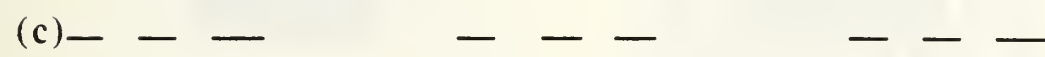
The Sierpinski Carpet in Figure 2-6 is an example of such a surface. It is formed by dividing a square into b^2 smaller squares



Original line

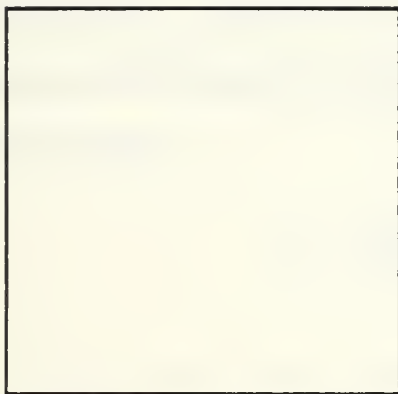


After one generation

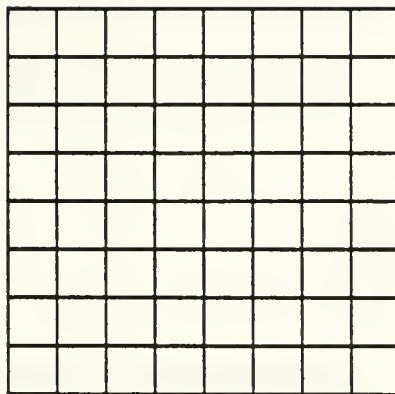


After two generations

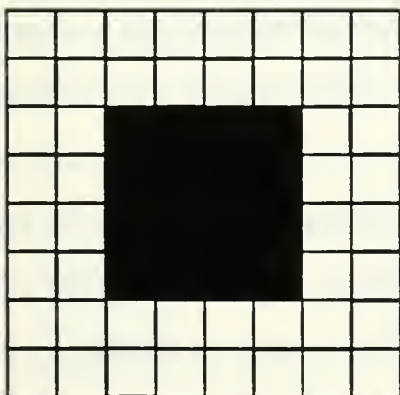
Figure 2-5: Cantor Set with fractal dimension < 1 .



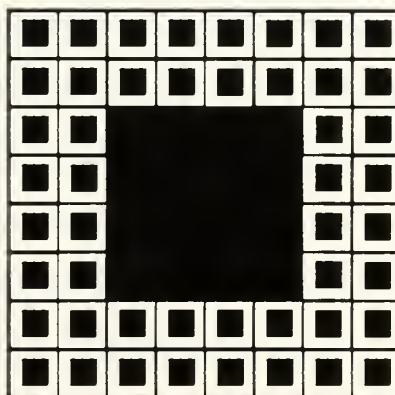
Original square



Divided into 64 smaller squares



16 squares removed from center



process repeated

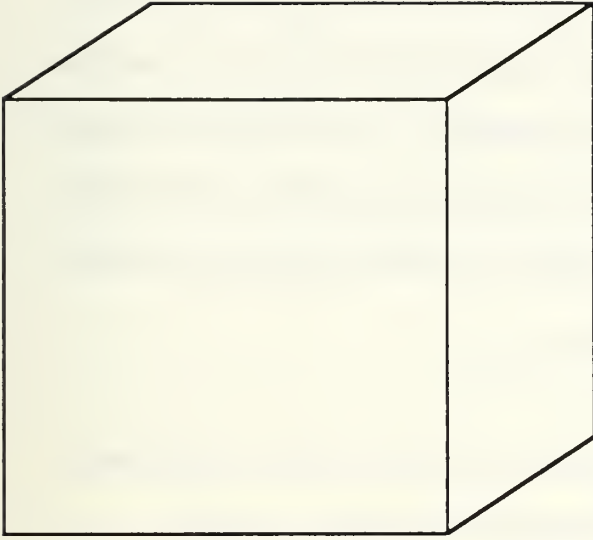
Figure 2-6: Sierpinski Carpet with $b=8$, $c=4$, and $D=1.8617$.

as shown. Then, by removing c^2 of these squares, a surface is formed that has some finite amount of area removed. This process is continuously repeated so that the resulting surface is a fractal with dimension

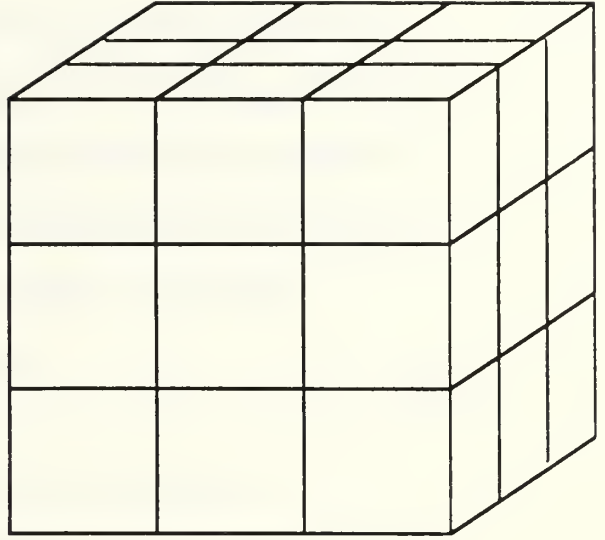
$$D = \frac{\log (b^2 - c^2)}{\log b} \quad (2.4)$$

In the same manner, some fractal volumes can be modeled as Euclidean volumes with some finite amount of space removed. These volumes will have fractal dimensions between two and three compared to Euclidean volumes of dimension three. One such example is the Menger Sponge shown in Figure 2-7. It is formed in a manner very similar to the Sierpinski carpet, except that it is three dimensional rather than two dimensional. A cube is divided into a series of smaller cubes each of side $1/b$ and volume $1/b^3$. Then, as in the Sierpinski carpet, some of the cubes are removed in some regular pattern to form a void space within the structure. This process is repeated indefinitely so that the volume becomes a fractal lattice.

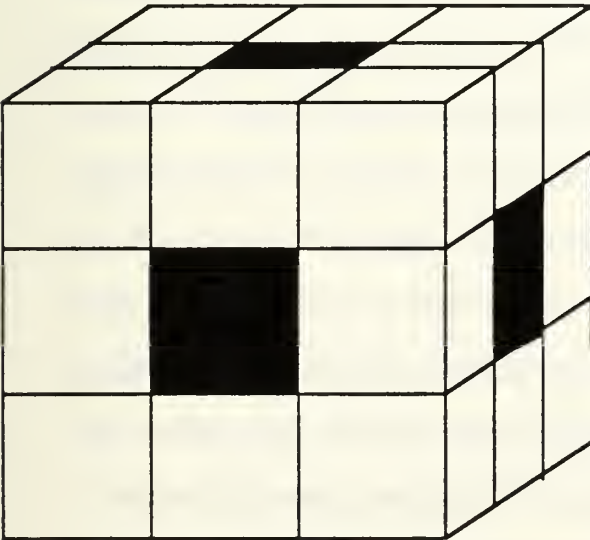
Although only squares and lines were used to create these fractal forms, it is evident that any regular shape (triangles, rectangles, circles, etc.) can be used. As stated earlier, fractals can be thought of as either Euclidean figures (lines, planes, or



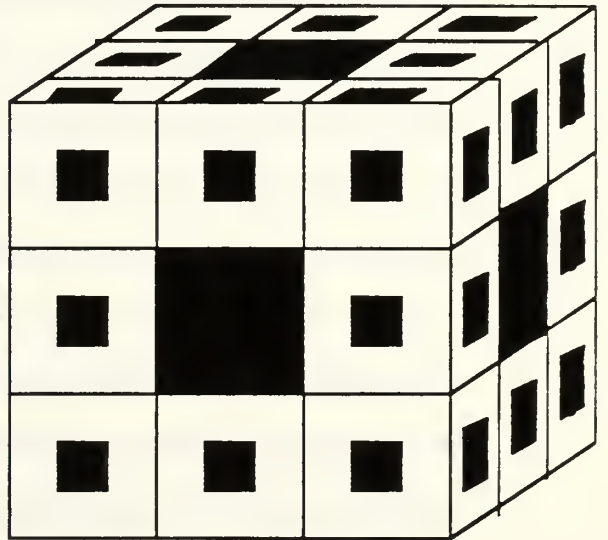
Initial cube



Divided into 27 smaller cubes



Center cube on each face removed



Process repeated for smaller cubes

Figure 2-7: Menger Sponge.

volumes) that become more irregular as the fractal dimension increases, or they can be thought of as Euclidean figures that do not completely fill space. Whichever model is used, the concepts of fractals still remain the same and are characterized by a relation between a number density, N , and a scale, r , in the form

$$N = r^{f(D)} \quad (2.5)$$

where $f(D)$ is some function of the fractal dimension.

Thus far, only man-made fractal forms have been discussed. The irregular line, the Koch Island, the Sierpinski carpet and the Menger sponge are all exact fractal forms generated through the principles of fractal geometry. However, fractal forms abound in nature. Mountains, for example, are not cones formed in perfect regular patterns. They are rugged, irregular surfaces that can vary greatly in size and shape. These same mountains may also exhibit a high degree of self-similarity when examined at different length scales. In fact, most mountains are self-similar over some range. The surfaces of rocks tend to look the same when viewed from afar or viewed closeup, and they will usually appear the same even when observed at length scales over several orders of magnitude. It is this characteristic of rocks that give mountains their fractal properties.

On a similar note, clouds are not perfect spheres, lightning

does not form regular patterns and coastlines are not straight lines. Just a casual glance towards the sky will reveal the highly irregular nature of clouds. The general shape of a cloud is usually not circular, and the edges are usually very irregular. This fact implies that a cloud is definitely not a regular form and may indeed be a fractal for some range of length scale. Lightning and coastlines are both similar to clouds in that they are irregular forms that may very well exhibit fractal behavior. These are only a few of the natural forms that exhibit fractal behavior, but there are undoubtedly many more. In fact, most of the forms in nature are not regular and probably exhibit fractal behavior over some length scale.

Although these surfaces do have characteristic fractal dimensions to describe the degree of irregularity, these fractal dimensions may be very difficult to measure. These figures have no characteristic initiators and generators that can be used to determine the fractal dimensions through mathematical formulas. The only way to determine the fractal dimension of such figures is to establish relationships between the lengths, areas or volumes over various ranges and obtain a log-log plot of density vs scale. The slope of this graph will be related to the fractal dimension in some way depending on the type of fractal form and the type measurements made. In the line of Figure 2-1, the slope of $\log L$ vs

$\log r$ is equal to $-(D-1)$ where D is the fractal dimension. The relationship may be slightly different when measuring surface areas or volumes. Thus, the fractal dimensions of manually generated fractals can be determined through mathematical formulas before the surface is generated, whereas the fractal dimensions of naturally occurring fractals must be determined through some type of density measurements made over a variety of scale ranges.

Chapter 3

Measurement of Fractal Dimension

3.1 Manual Methods of Measurement

Since fractal shapes can take many forms (i.e. lines, surfaces, volumes etc.), there are many different ways to measure their fractal dimensions. As stated earlier, fractal dimensions are related to some type of density measurements made over a range of length scales. Hence, methods must be developed for observing fractal forms at these different scales and for making the proper density measurements. These methods can be quite different depending on the type of fractal form involved. For example, the measurement for a fractal line requires that the length of the line be measured using different length scales, while the measurement for a fractal surface requires that the surface area be measured. In order to observe these lengths and areas over more than one order of magnitude, the figures must be observed at several magnifications. So far many different methods have been developed for making the required measurements.

One method of measuring fractal dimensions involves the use of mathematical formulas based on the initiator/ generator model.

This type of fractal figure has already been discussed in the previous section. These formulas apply only to the fractals that are generated through the use of an initiator and generator. The exact shape of these types of figures is known at all levels of magnifications, and the shape remains consistent over these ranges as well. Hence, the formulas developed for these figures apply over the entire range of self-similarity. For a line, the formula

$$L(r) = r^{-(1-D)} \quad (3.1)$$

relates the fractal dimension to the selected values of L and r , which were defined in Chapter 2. Since these values of L and r are pre-selected before generating the fractal line, the fractal dimension is actually predetermined for any particular figure and can be easily changed by changing the values of L and r .

In the above method, there were no experimental measurements required to determine the fractal dimension of these manually generated fractals. However, natural fractal forms require some kind of experimental measurements, because the parameters L and r are not known. In addition, they may not be exactly self-similar nor possess fractal properties over all length scales. There are several kinds of measurements used to determine L and r and the length scale over which the sample is a fractal.

The method of measuring the perimeter using line segments

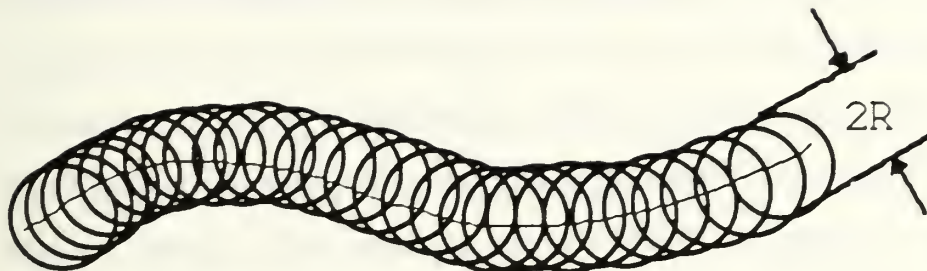
of varying length scale can be applied to natural fractals. As an example, it is desired to determine whether or not the coastline of an island is a fractal. One could conceivably measure the length of the coastline using different length scales. Start by using one mile as the length scale and measure the length of the coastline in one mile increments. Obviously this length will not include the numerous small features and irregularities that are smaller than one mile. However, as the length scale is decreased to one half-mile, one yard, one foot, one inch, etc., the resulting lengths of the coastline will consistently increase as the smaller and smaller irregularities (inlets, bays, estuaries, etc.) are included in the measurements. A log-log plot of the total length vs the length scale will result in a straight line if the coastline is a fractal. The slope of this line will be related to the fractal dimension in a manner very similar to the formula discussed previously. Theoretically, the total length of the coastline would approach infinity as the length scale used to measure it approached zero, provided the coastline was a fractal over all length scales. In practice, there are definite limitations on the length scales that can be used for making these measurements (Mandelbrot 1983).

This same method can be applied to innumerable shapes and figures that behave as fractals, provided that there is a means of changing the length scale and making the necessary measurements.

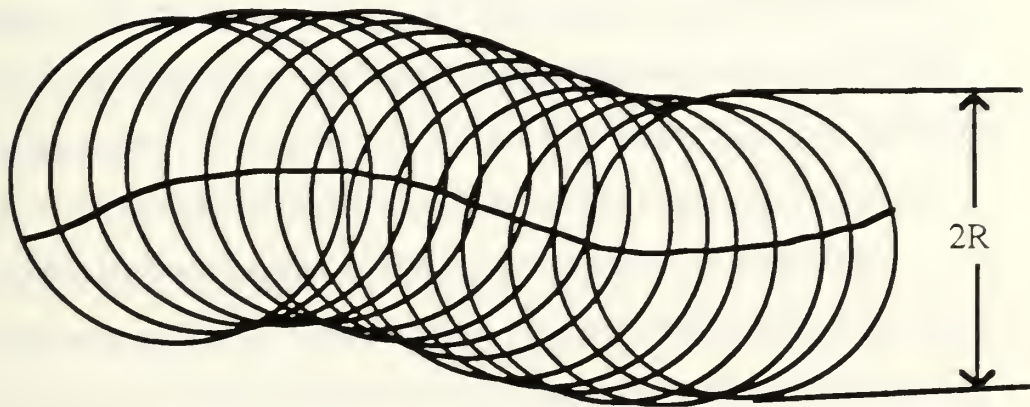
Anything that has a fractal silhouette in two dimensional space can be analyzed in this manner. For instance the pore space in a reservoir rock appears to be a fractal when viewed in a thin section Krohn (1987). The silhouette of a mountain or of a cloud also appears to have this property Mandelbrot (1983). As long as the magnification and the length scale can be changed, then the fractal dimension of these figures can be determined. Obviously the thin section of a rock can be viewed at various magnifications. The circumference of a pore space boundary can be measured at each magnification by using some value of length to make the measurements. As the magnification is continuously increased, irregularities will appear that were not visible at lower magnifications. Hence, the length of the pore space/ rock boundary will increase with magnification due to the inclusion of these irregularities. As before, a log-log plot of total length vs length scale may result in a straight line from which the fractal dimension can be determined. The technology currently exists to make these types of measurements on very small outlines and boundaries as well as on large ones. Thus, the fractal dimension of pore spaces and mountains can be measured using basically the same method.

3.2 Automated Methods of Measurement

Although it is possible to make all the necessary measurements to determine the fractal dimension, it can be a very cumbersome and tedious task to obtain the data manually. However, computerized techniques have been developed to automate the above procedure, thereby making the measurements much easier to obtain. Many schemes have been developed to computerize the process of counting lengths at various scales. Kaye (1978) developed several computer-compatible strategies based on image analysis software, and Flook (1978) developed another such algorithm based on the use of a Quantimet 720 fitted with a 2D Amender module. Kaye's methods were based on the process of determining total length by counting the number of lengths r required to complete the curve in question. However, Flook's method was based on a slightly different approach in which r was calculated by a method used by Cantor to "tame" non-differentiable curves. In this method, the curve is considered a series of closely spaced points. A series of overlapping circles of radius R is drawn with their centers on each of the points of the curve as shown in Figure 3-1. This series of circles describes a path of width $2R$ around the length of the curve. The area of this curve divided by



Overlapping circles with centers
located on the curve



Increased radius R . Note the loss of detail resulting
from the increase

Figure 3-1: Example of Flook's Method.

it's width gives an estimate of the total length of the curve. As R is increased, the circles have a greater degree of overlap and obscure more and more of the fine details of the curve so that the length estimate of the curve will decrease. This process is very similar to decreasing magnification so that the finer details of an object become obscured, and only the larger details are observed. As with the first method, a log-log plot of length vs R will result in a straight line whose slope is related to the fractal dimension. This entire process was computerized by Flook (1978) utilizing the 2D Amender module to perform the dilation process that was just described. The detector threshold was set for full detection of the particle and the contiguity output from the detector was used as input to the amender. The use of contiguity ensures that only the common boundary points between detected and undetected video are measured. The area of this dilated boundary was then measured for increasing steps of dilation. Each dilated boundary area was divided by the diameter of the dilation element to obtain the perimeter estimate. The resulting values of the perimeter are used to calculate the fractal dimension of the curve. Flook verified this method by using it to determine the fractal dimension of some known figures. First he used it to determine that the fractal dimension of a Euclidean circle (which is everywhere differentiable) is indeed unity. He also verified the fractal

dimension of the Triadic Koch Island and the Quadratic Koch Island which are fractal curves of known fractal dimensions (Mandelbrot 1983).

Schwarz and Exner (1980) also developed a computerized technique to measure fractal dimensions. This technique is based on the use of a semi-automatic image analyzer combined with digitizing tablets. It works by tracing the profile of the image under investigation with a cursor, and then transferring the coordinates of the profile points into a microprocessor. From these coordinates, conventional software is used to transform these points into characteristic parameters of the curve such as area, perimeter, shape factor, etc. In addition, the computer can determine the fractal dimension of this curve in a manner similar to that already discussed. It automatically calculates the length of the curve for any given value of length scale. Initially, a starting point is chosen somewhere on the curve. The computer then determines the coordinates of the point which is a distance equal to the length scale from the starting point (see Figure 3-2). The next point is found in a similar manner, and the process is continued until the starting point is reached again. The total length of the curve is then calculated by multiplying the number of points times the length scale. As before, the length of the curve increases as the length scale decreases, because the small irregularities begin to show up,

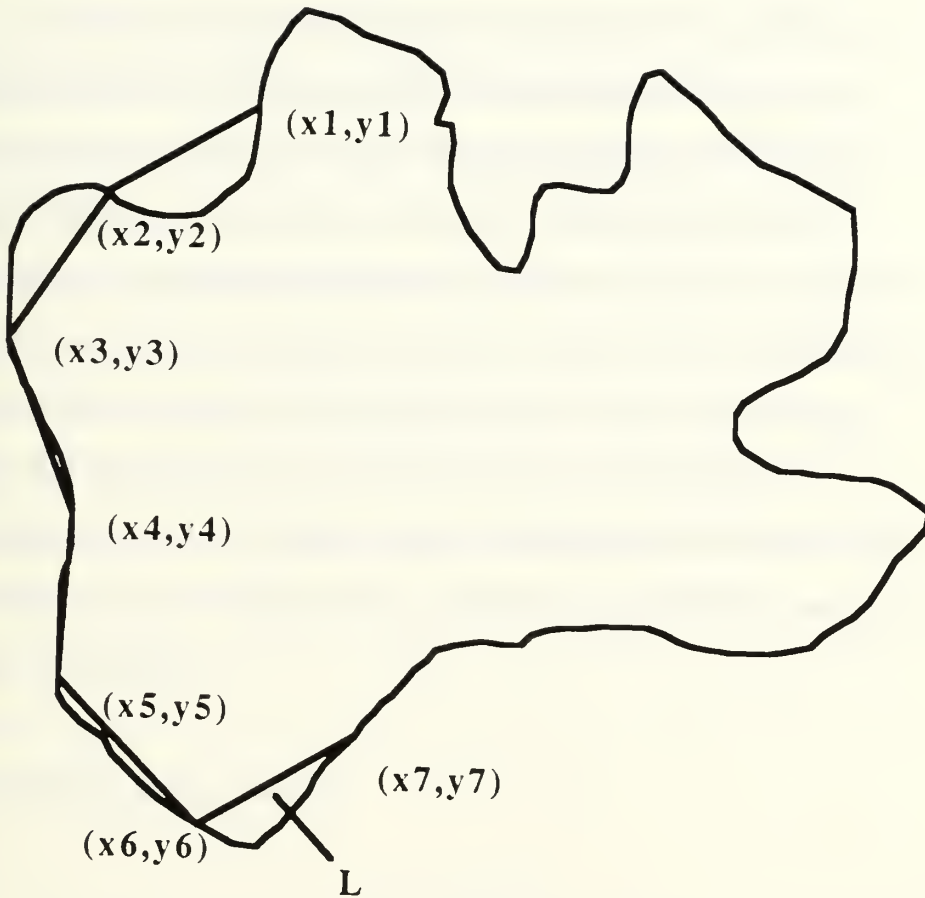


Figure 3-2: Example of computerized technique. Computer selects each point by locating the coordinates of the point which is a distance L from the previous point.

and a log-log plot of curve length vs length scale results in straight line with the slope related to the fractal dimension.

Schwarz and Exner (1980) also verified this method by measuring the fractal dimensions of some known curves and comparing the results to results obtained by Flook (1978) and Koch. This comparison showed that this automated method accurately measures the fractal dimension of curves. It must be pointed out that this method can only be used on curves that can be traced by the computer and digitized into a set of coordinates. Thus, the difficult part of this method may be finding a way to digitize the curve. In addition, this method is only accurate for a particular range of length scales, which is limited by the resolution of the equipment.

3.3 X-Ray Scattering

It has also been found that small angle X-ray scattering can be used to measure the fractal dimension of porous materials. Winslow (1985) demonstrated the use of this method by measuring the fractal dimension of cement pastes. When X-rays are passed through porous materials, they are scattered at small angles that are related to the intensity of the scattered radiation. Porod (1951) demonstrated that intensity decreases with the negative third power

of the scattering angle (for a slit-collimated X-ray beam). It is assumed that the material consists of two distinct phases, the solid phase and the pore space. These two phases are assumed to be of uniform electron density with sharp, abrupt interfaces.

However, it has been discovered that for some interfaces, the intensity decreases at some power other than negative three. Before the concept of fractals was introduced, it was thought that these deviations from Porod's law were due to electron density fluctuations and to the absence of a distinct interface. Since that time, it has been shown that this deviation is expected if the interface is a fractal. Furthermore, the amount of deviation can be used to estimate the fractal dimension of the interface.

For small angle scattering, a transformed version of the scattering angle is often used to describe the degree of scattering. The transformed parameter, h , is defined as

$$h = \frac{4\pi \sin\theta}{\lambda} \quad (3.2)$$

where λ is the X-ray wavelength. Porod's law suggests that the intensity, I , should be proportional to h to the negative third power. However, recent analysis of scattering from fractal surfaces shows that the intensity is proportional to $-(5-D)$, where D is the fractal dimension of the surface. Thus, Porod's law is

actually a simplified version of scattering where the surface is a smooth Euclidean plane of dimension two. Therefore, this method is used to measure the fractal dimension of surfaces with dimensions between two and three. The other methods discussed previously were only valid for curves with dimensions between one and two.

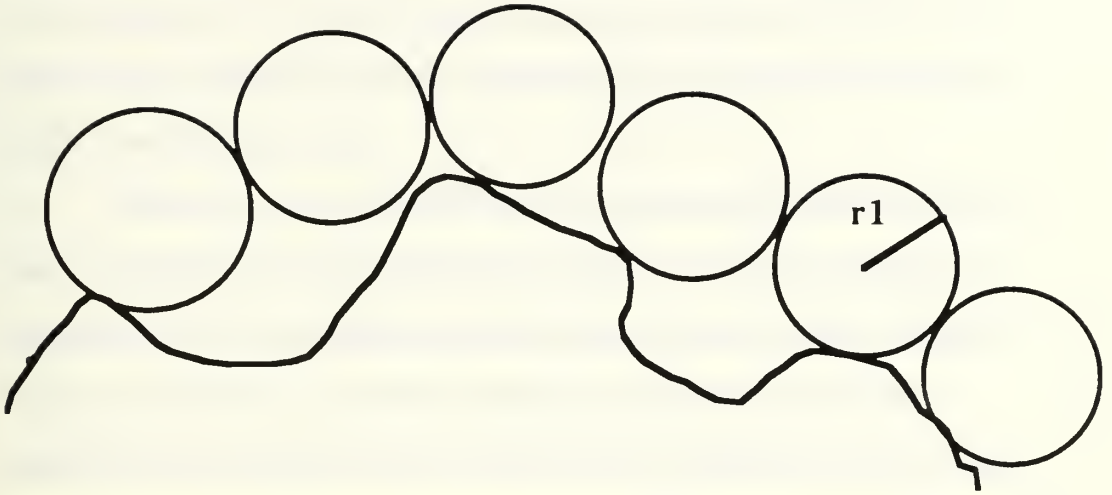
3.4 Adsorption of Molecules

Another method that has been developed for the measurement of fractal dimensions is the adsorption of molecules. This method involves the adsorption of adsorbate molecules on the surface of an adsorbent, thereby estimating the number of moles required to form a monolayer around the adsorbent. The surface area of the adsorbent can be determined from this process, if the molecular radius of the adsorbate molecules is known. Consider a three dimensional surface with a surface area equal to A . Next, consider a series of molecules of radius r packed tightly around this surface, forming a monolayer. It has been shown by Pfeifer and Avnir (1983) that the specific surface area (A) of the adsorbent is given by

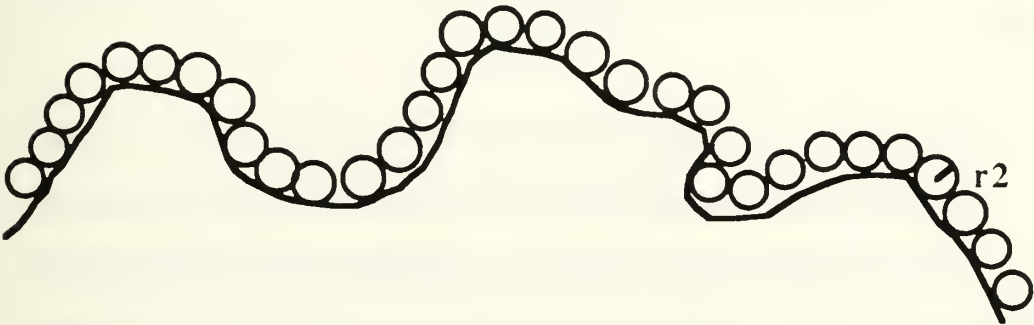
$$A \propto \sigma^{(2-D/2)} \quad (3.3)$$

where σ is effective cross-sectional area of the adsorbate and D is the fractal dimension. In order to experimentally obtain the fractal dimension from this information, one must use a variety of adsorbates (having different effective molecular cross-sectional areas) to obtain a series of corresponding surface areas. This process is equivalent to changing the length scale in the previous methods, because each different adsorbate molecule will investigate the surface with a different length scale. In the previous methods, different total length values were obtained by altering the length scale used to make the measurements. In this case, it is the effective cross-sectional areas that are changed to obtain different total surface areas. Figure 3-3 shows why the larger adsorbate molecules result in a smaller surface area. Note how the larger molecules skip over the small irregularities in the curve, while the smaller molecules include these irregularities in the surface area measurement. One important fact to note about this process is that each of the different adsorbate molecules used must be the same shape. These molecules do not have to be exactly spherical, but must be geometrically and chemically similar.

In a manner similar to the other methods, the fractal dimension is obtained using a log-log plot of surface area, A , vs effective cross-sectional area, σ . This plot results in a straight line



Large adsorbate molecules of radius r_1



Smaller adsorbate molecules of radius r_2

Figure 3-3: Molecules of different sizes. Note how the large molecules skip over the irregularities.

relationship in which the slope of the line is equal to $(2-D)/2$. So just as before, the slope of the characteristic log-log plot is related to the fractal dimension.

Pfeifer and Avnir (1983) also showed that this process can be used to determine the fractal dimension of a surface by changing the grain size of the adsorbent and keeping the size of the adsorbate molecules constant. Instead of probing a single surface with yardsticks of varying size, he used a fixed yardstick to probe larger and larger specimens of the same substrate. The theory is much the same as that for varying the size of the adsorbate molecules. If the substance in question is considered to be a spheroid of radius R , then it has been shown that

$$A \propto R^{D-3} \quad (3.4)$$

where A is the total surface area corresponding to a spheroid of radius R . By increasing the size of the spheroid (and therefore increasing R), one will obtain varying values of surface area.

Again, a log-log plot of surface area vs radius results in a straight line whose slope is equal to $D-3$. As before, it is required that all of the surfaces have essentially the same shape in order for the above relationship to hold true (i.e. all adsorbent particles must be geometrically similar).

Avnir, Farin and Pfeifer (1983) used the above method of molecule adsorption to measure the fractal dimension of many common substances such as carbon black, graphite, and crushed glass. They found that this method seemed to be an accurate way to measure the fractal dimension of such substances utilizing both the concepts of varying adsorbate size and varying adsorbent size. It is important to note that all of the tested materials had characteristic surface areas that were large compared to the average reservoir rock. Subsequent work by Gupta (1987) has shown that this method is not very practical for the measurement of fractal dimensions in common sandstones and carbonates, because the surface areas of these rocks are not large enough show a clear distinction between the areas obtained using different adsorbates.

3.5 Scanning Electron Microscope

Katz and Thompson (1985) developed a method for measuring fractal dimensions which appears to be accurate for measurements with reservoir rocks. They used the secondary electron emission from a scanning electron microscope (SEM) to identify surface features along a linear trace on the rock. They found that there is a one-to-one correspondence between the secondary electron intensity extrema and the edges of the surface features that intersect the SEM trace. Thus, the number of surface features is obtained by counting the number of peaks on the secondary electron intensity output. Figure 3-4 is a sample of a secondary electron intensity trace. Each of the jagged peaks represents a surface feature on the rock surface

The fractal dimension is obtained by counting the number of features at different magnifications and constructing a log-log plot of the number of surface features vs the length scale. The length scale is obtained by dividing the width of the SEM screen by the magnification. The resulting number is the actual length of portion of the rock currently visible on the SEM screen. Thus, the length scale is different for each magnification. The log-log plot results in

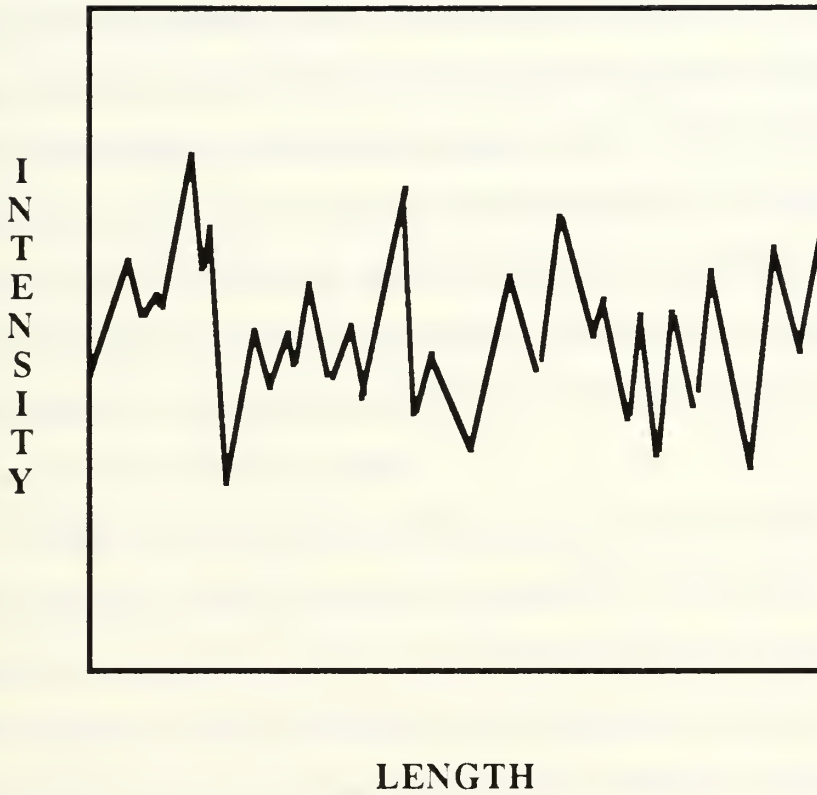


Figure 3-4: Typical secondary electron intensity display from an SEM. Each peak represents a surface feature.

a straight line (if the rock is a fractal) for which the slope is equal to $2-D$.

The important part of this procedure is obtaining a correct count of the surface features at each magnification. This task can be accomplished manually, but it requires good judgement to identify which of the intensity peaks are caused by the presence of surface features and which are caused by random noise. Some criteria must be established in order to make this determination. To some extent, this procedure is subjective, and the results may vary depending on the individual making the measurements. However, as long as the measurements are made consistently, the results are adequate to determine the fractal dimension.

Krohn and Thompson (1986) automated this counting process utilizing a digitizer and a low pass filter. The basic procedure was the same with a couple of exceptions. First, the SEM images for 18 to 20 different magnifications were digitized using a digitizing system based on the Hewlett-Packard 9836C computer. A digital low pass filter was then convolved with the data in order to establish uniform resolution at all magnifications. The number of features was automatically calculated, and a feature histogram was created for each magnification. These histograms were placed on log-log plots with the number of features plotted against feature size. Just as in the manual method, the slope of the

resulting straight line was related to the fractal dimension. One important fact about the automatic counting process was that the computer distinguished between surface features and random noise through the use of an amplitude threshold. This value was programmed into the computer, so that the computer only selected intensity values that exceeded this threshold value. This automated technique allows for a much faster analysis of the SEM data. In the experience of (1987), the automated technique does not provide a significant advantage in terms of the measurement accuracy.

Chapter 4

Experimental Procedure and Results

4.1 Summary

The Scanning Electron Microscope was used in this project to make measurements on various reservoir rocks. Due to the lack of necessary equipment for automated measurements, the manual method previously described was used to make measurements on eleven different rocks. Measurements were made on seven sandstone rocks, of which four were from the Frio formation in Louisiana, two were tight gas sandstones from the Travis Peak formation in Texas, and one was a Berea sandstone from Ohio. The other four samples were all dolomites from the San Andres formation in West Texas. All but one of these samples was obtained from the core repository at Balcones Research Center in Austin, Texas.

4.2 Preparation of Rock Samples

Before any measurements were made on the SEM, the samples had to be properly prepared. Only a very small piece of each sample (approximately 1 cubic cm) was required for the

measurements. Samples larger than this cannot be viewed on the SEM. The samples were partially cut with a special saw and then broken so that at least one of the faces of the rock was a fractured surface. It was important that the measurements were made on the fractured surface and not the cut surface, because the results of any measurements made on the cut surface would not be representative of the rock; rather, these results would identify properties of the smooth and crushed grains. Once these samples were cut and broken to the proper size, they were mounted to small aluminum cylinders as shown in Figure 4-1. The samples were mounted with a clear glue, similar to model glue.

In order for the samples to be observed in the SEM, the surfaces of these samples had to be conductive. These samples were made conductive by coating them with a thin layer of gold. This layer of gold was deposited on the surface of the rock samples through the ionization of gold particles inside a vacuum chamber. This gold layer was thin enough (only a few angstroms) so that it did not alter the surface features of the rock samples. Finally, several stripes were painted down the side of each rock, from the top surface to the point where the rock was connected to the cylinder. A highly conductive, carbon based paint was used to paint these stripes, and the purpose of the stripes was to insure good electrical contact between the rock and the cylinder.

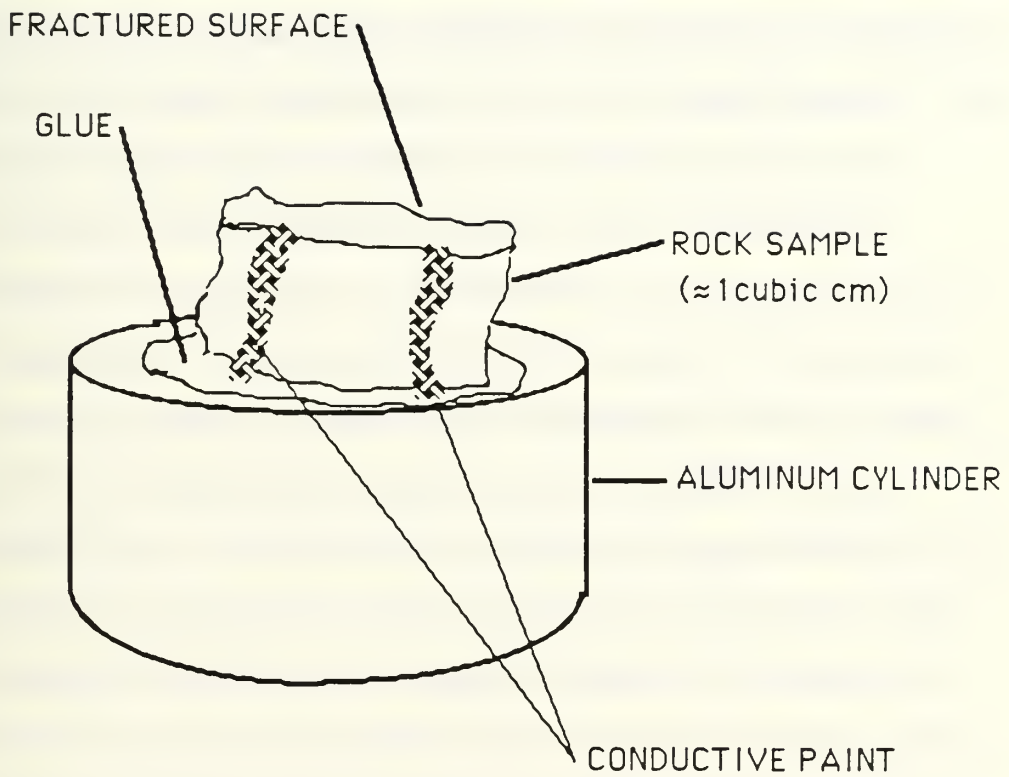


Figure 4-1: Rock sample mounted to aluminum cylinder.
Note that the sample is \approx 1cc and is not to scale.

4.3 Intensity Measurements

After the samples had been prepared, as described above, they were ready for observation in the SEM. Each sample was placed in the SEM chamber and observed at a series of magnifications. The actual visual image of the sample was observed as well as the secondary electron emission intensity trace. As described in Chapter 3, the number of surface features was determined at each magnification by counting the number of peaks on the secondary electron intensity emission trace. The number of surface features and the corresponding length scales were recorded for each magnification. Each sample was observed at approximately eleven different magnifications ranging from approximately 25 - 30X to as high as 21,000X, and the appropriate data was recorded each time. This process was repeated at five different locations on each sample to ensure that the "average" rock values were obtained. Care was always taken to ensure that the measured locations on the surface of the samples were free of any large voids or irregularities that could significantly alter the number of surface features on the rock. In some cases, a set of photographs was taken of the visual image of the rock overlain by the secondary electron emission intensity trace (see photographs in Appendix A). A set of

photographs consisted of a group of pictures taken at various magnifications for one specific location on the sample.

Once the data was obtained, a log-log plot of the number of features per centimeter vs. the length scale was plotted for each rock using the combined data from all five locations. The best-fit line was plotted through these points, and the fractal dimension of each sample was determined from the slopes of these lines.

4.4 Results

Figures 4-2 through 4-12 at the end of this chapter are log-log plots of surface features per centimeter vs length scale for the eleven rock samples observed in the SEM. As seen from these graphs, each set of data appears to have a straight line relationship over the length scales observed. As discussed in Chapter 3, the straight line relationship indicates fractal behavior over the length scale in question. Furthermore, the fractal dimension is related to the slope of the line through the formula

$$m = 2-D \quad (4.1)$$

where m is the slope of the line and D is the fractal dimension.

The least squares method of linear regression was used to plot the best-fit straight line through the data points on the log-log

scale. In all samples, the regression was a good fit, indicating that the data points do have a linear relationship when observed on a log-log scale. Table 4-1 is a compilation of the results of the SEM measurements along with the results of previous core analysis obtained from Balcones Research Center in Austin, Texas. Table 1 shows that the fractal dimension, D , varied from 2.58 to 2.75, while the porosity and permeability of the samples varied from 6.8% to 28.5% and from .06 md to 2266 md respectively.

Two other plots, D vs porosity and D vs permeability, were constructed in an attempt to find a simple correlation between the fractal dimension and these two parameters. The results are shown in Figures 4-13 and 4-14. These plots reveal the fact that there is no simple relationship between the fractal dimension and the other parameters. The data points are highly scattered and there is no pattern evident. This suggests that the relationship between the fractal dimension and other petrophysical properties involves additional parameters. The next chapter discusses what these parameters might be.

Table 4-1: Core Analysis Data

Sample	D	Error	Porosity (%)	Permeability (md)
Berea SS	2.75	0.11	21	300
Travis Peak SS (7449.4 ft)	2.615	0.12	17.3	129
Travis Peak SS (7456.3 ft)	2.58	0.13	6.9	0.06
Frio SS (9177.5 ft) uncompacted	2.72	0.107	28.5 16.5	2266
Frio SS (9177.5 ft) compacted	2.74	0.195	8.5 11.2	----
Frio SS (9189.5 ft) uncompacted	2.70	0.089	21.7 17.8	1382
Frio SS (9189.5 ft) compacted	2.74	0.092	6.8 8.5	----
San Andres dol. (3350 ft)	2.61	0.092	17.6	302 (max)
San Andres dol. (3414 ft)	2.64	0.089	12.3	0.09 (max)
San Andres dol. (3464 ft)	2.66	0.121	14.9	56 (max)
San Andres dol. (3492)	2.64	0.114	15.6	3.0 (max)

4.5 Discussion

The results of the SEM measurements indicated that the rock samples are fractals and that the range of fractal dimensions varied between 2.58 and 2.75; however, these measurements did not identify the upper and lower length scales, L1 and L2, nor did they indicate the percentage of fractal porosity in the pore space. In addition, the measurement did not give any indication of the cause of the fractal behavior exhibited by the rock samples. As previously stated, the measurements made on the SEM could only be used to verify the presence of fractal geometry and to quantitatively measure the fractal dimension.

Additional work by others (Krohn and Thompson, 1986) has shown that more data in addition to the SEM data is required to obtain the upper and lower length scale limits of fractal geometry. Katz and Thompson (1985) used optical correlation data along with SEM data to estimate the value of L2 for various sedimentary rocks. This method seemed to provide a fairly accurate value of L2 as it produced results consistent with known properties of the rocks. They assumed a value of L1 to be approximately 20 angstroms, which is the minimum size of a crystal nucleus in a pore

space. Knowing the values of L_2 and L_1 , they calculated the "fractal" porosity of the fractal pore space using the formula

$$\phi = A(L_1/L_2)^{3-D} \quad (4.2)$$

where ϕ is the fractal porosity, $A=1$, and D is the fractal dimension. The fractal porosity includes the contribution to the pore volume from features with length scales between L_1 and L_2 . Note that this fractal porosity may be different than the absolute porosity of the rock, because most rocks are only fractals over a limited length scale.

Krohn (1987a) verified that sedimentary rocks such as sandstones contain two separate types of porosities, fractal porosity and Euclidean porosity. She used both SEM data and thin section data to verify that sandstones contained a pore volume distribution with a short-length fractal regime and a long-length Euclidean regime. The fractal pores were identified by a power-law relationship in both types of measurements, while the Euclidean pores demonstrated a lack of power-law behavior. Results showed that two of the four rock samples were dominated by fractal porosity and the other two were dominated by Euclidean porosity. She concluded that diagenesis was at least partially responsible for the fractal geometry in the rocks, because the rocks that were

predominantly fractals contained many authigenic minerals and pore filling clays.

Krohn (1987b) conducted further experiments on sedimentary rocks and concluded that diagenesis was indeed a major contributor to the presence of the fractal pore space. She conducted the tests on a variety of rocks, including various sandstones, cherts, carbonates and shales. In most cases, the samples that contained mainly fractal pore space had also undergone a significant amount of diagenesis, while those samples that were mainly Euclidean in nature were relatively free of any diagenetic material. Structures such as euhedral quartz overgrowths, druse quartz, calcite, dolomite and clays dominated the pore space of the fractal rocks. Although there may have been traces of these structures in the Euclidean rocks, the amount was relatively insignificant in comparison. She concluded that understanding the distribution of fractal and Euclidean pores within the samples may be important in determining their transport properties.

Krohn's conclusions seem consistent with the results of this project. First, all rock samples seem to contain fractal pore space as verified by the SEM measurements; however, the extent of the fractal pore space could not be determined from the SEM data alone. Also, there appears to be no direct relationship between the

fractal dimension of the samples and their corresponding values of porosity and permeability. Finally, almost all samples showed evidence of diagenesis. The photographs in Appendix A show a variety of authigenic material within the pore space of the samples. The photographs of the Frio sandstone show a great deal of material in and around the pore spaces of the rock. There appears to be large amounts of crystal growth as well as clay particles interspersed within the matrix of the sand grains. Only one of the photographs in the Travis Peak series shows the visual image of the rock. The others show only the secondary electron emission trace. In spite of this fact, the one photograph of the Travis Peak sandstone shows that there was also a great deal of diagenetic material in this formation. Although there are no photographs for higher magnifications, observation of these samples in the SEM showed that the amount of diagenesis in this formation was significant. There appears to be a large quantity of clay particles and some crystal growth within the pore spaces of the rock sample. In addition, observation of the San Andres dolomite photographs shows the significant amount of dolomite crystal growth within and around the pore spaces of the rock samples. The presence of diagenetic materials in these samples and the verification of fractal pore spaces is consistent with Krohn's theory.

Berea Sandstone

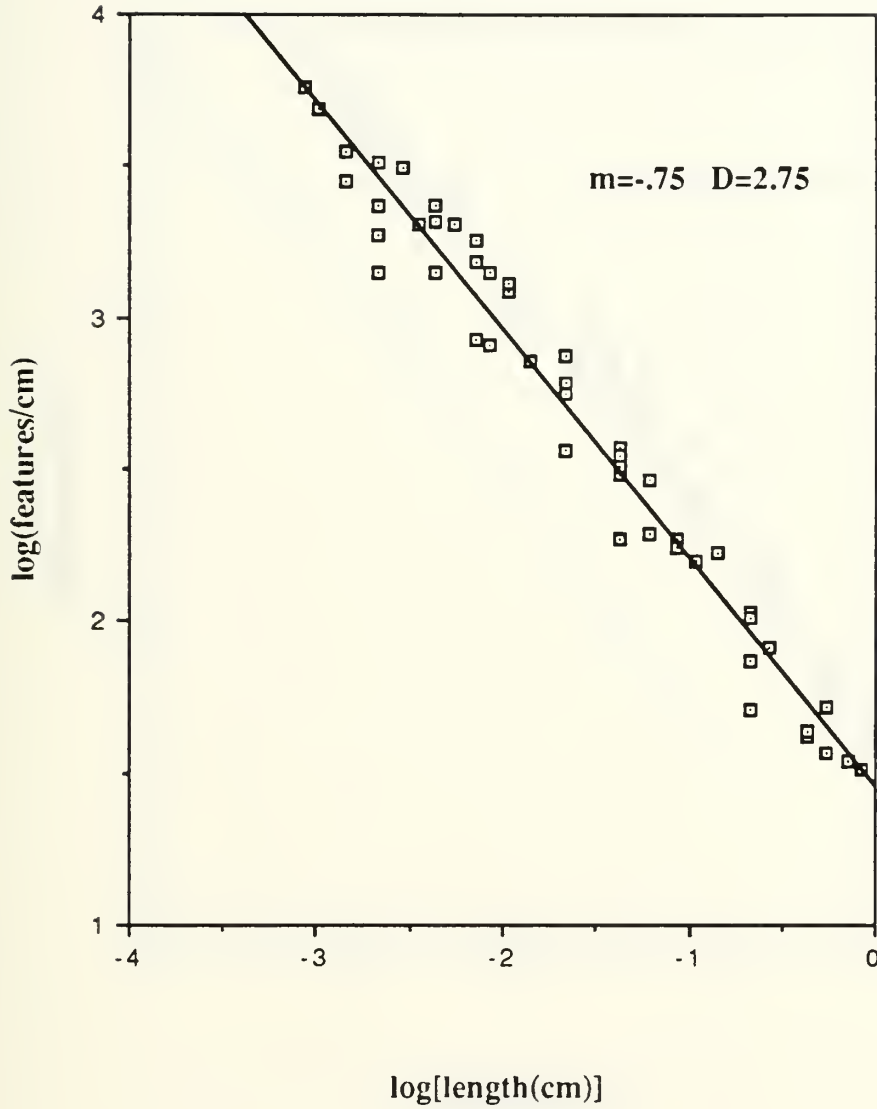


Figure 4-2: Log-log plot for Berea sandstone.

Frio Sandstone 9178.3 ft uncompacted

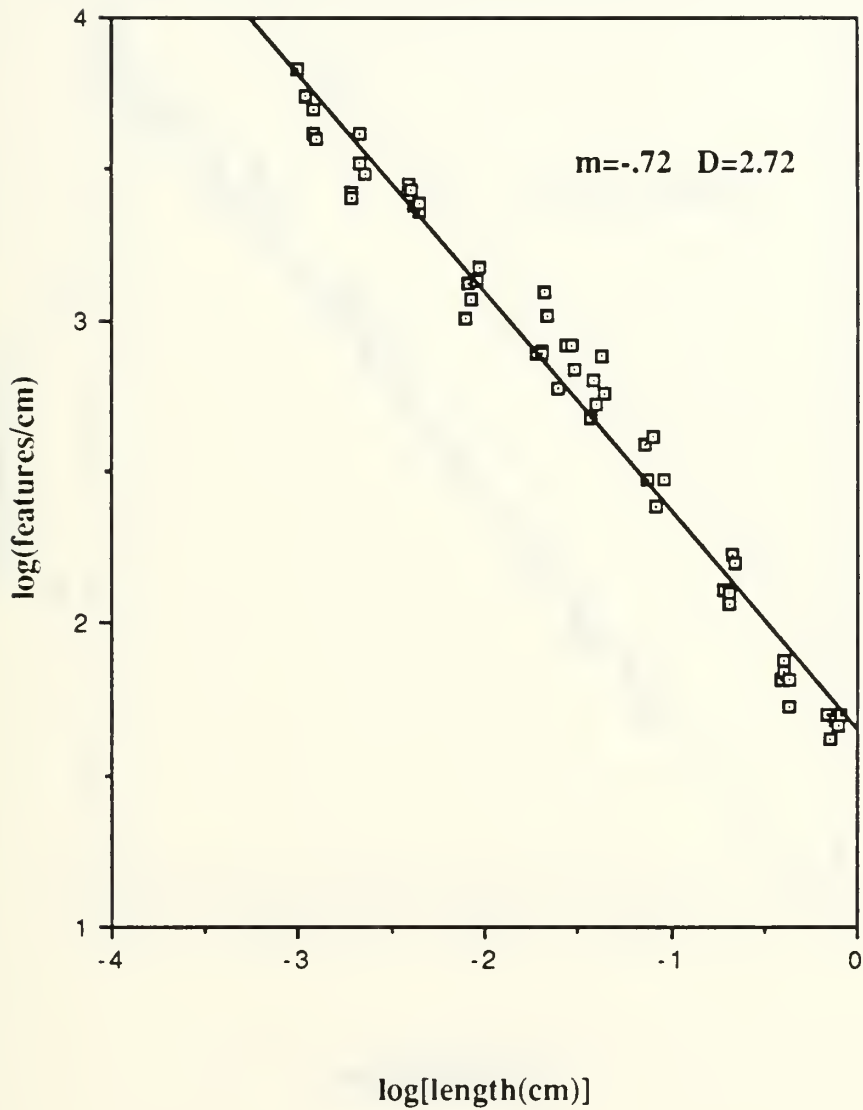


Figure 4-3: Log-log plot for uncompacted Frio sandstone, 9178.3 ft.

Frio Sandstone 9177.5 compacted

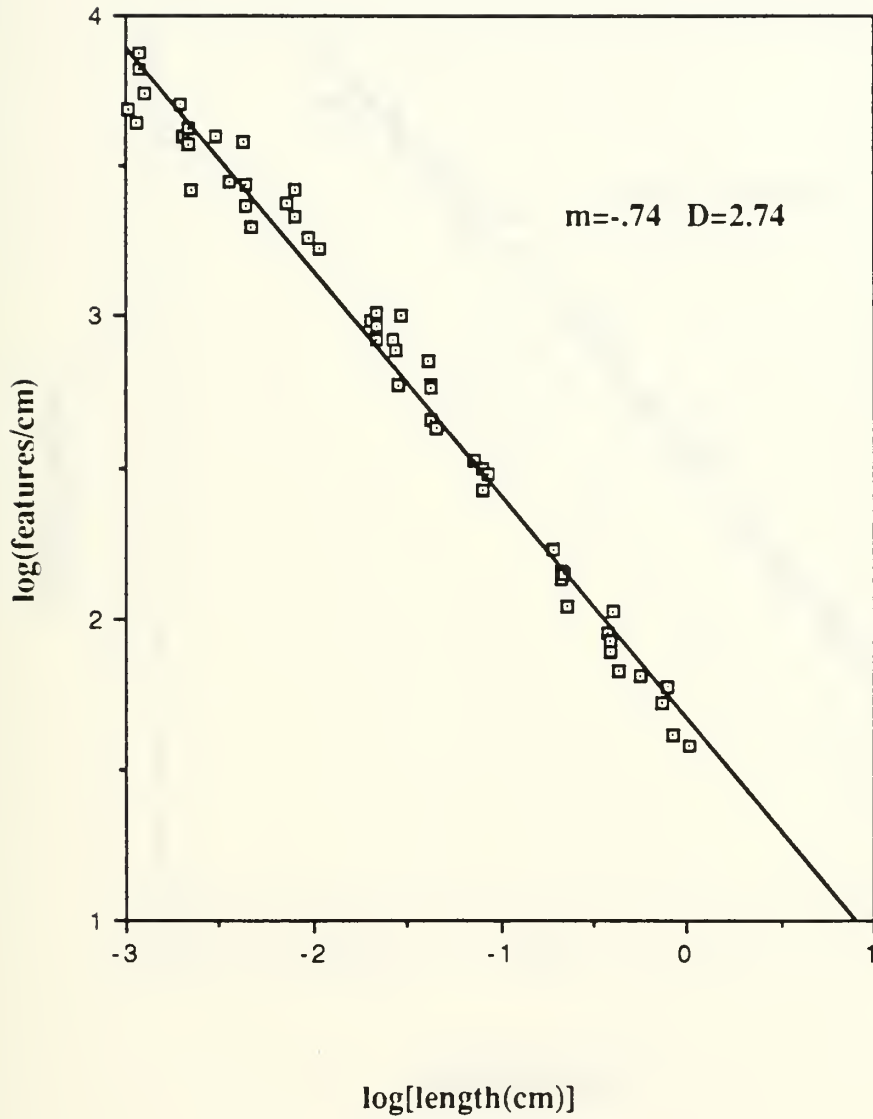


Figure 4-4: Log-log plot for compacted Frio sandstone, 9177.5 ft.

Frio Sandstone 9189.5 ft uncompacted

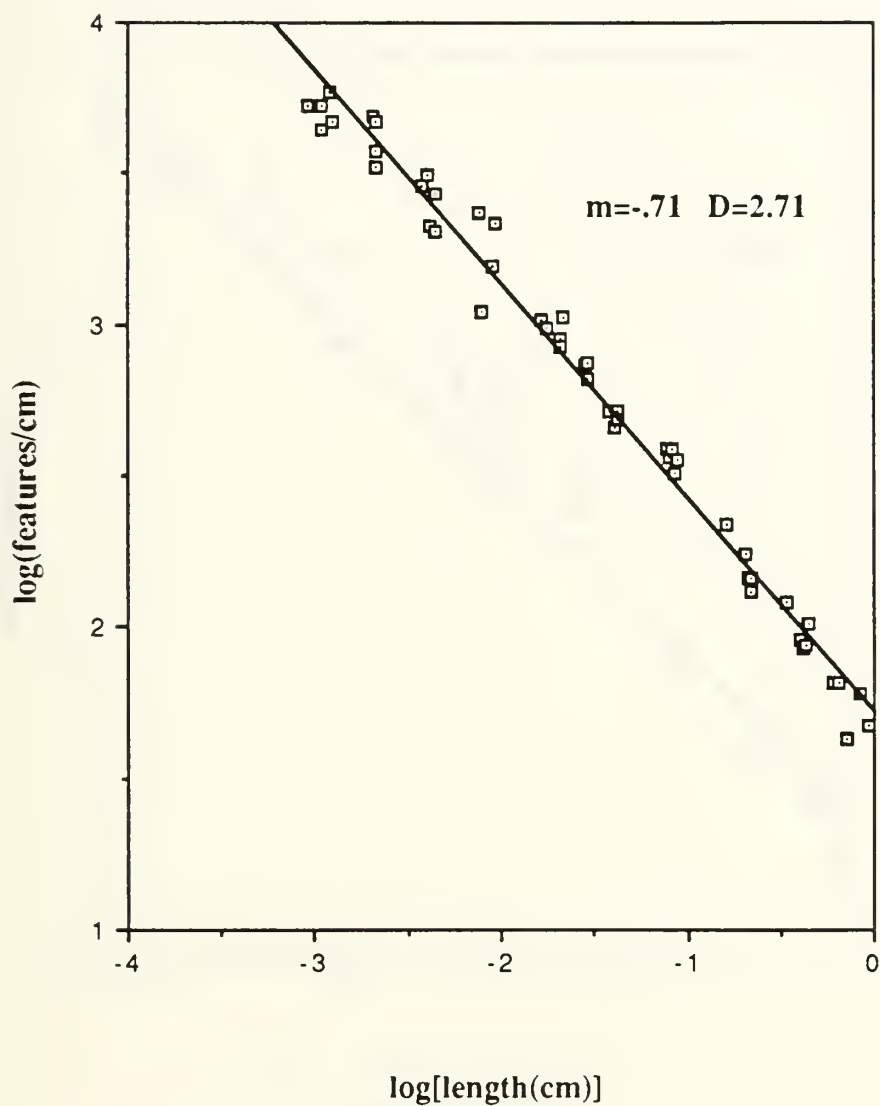


Figure 4-5: Log-log plot for uncompacted Frio sandstone, 9189.5 ft.

Frio Sandstone 9189.5 ft compacted

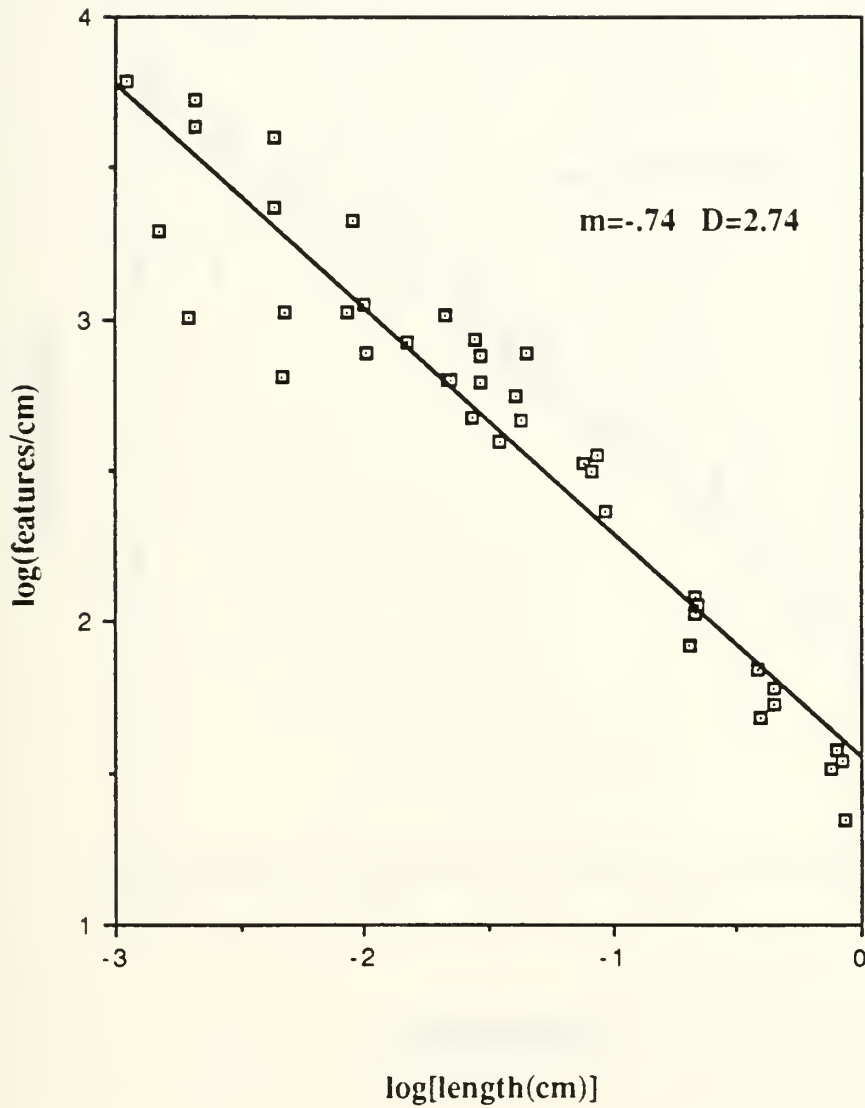


Figure 4-6: Log-log plot for compacted Frio sandstone, 9189.5 ft.

Travis Peak Sandstone 7449.4 ft

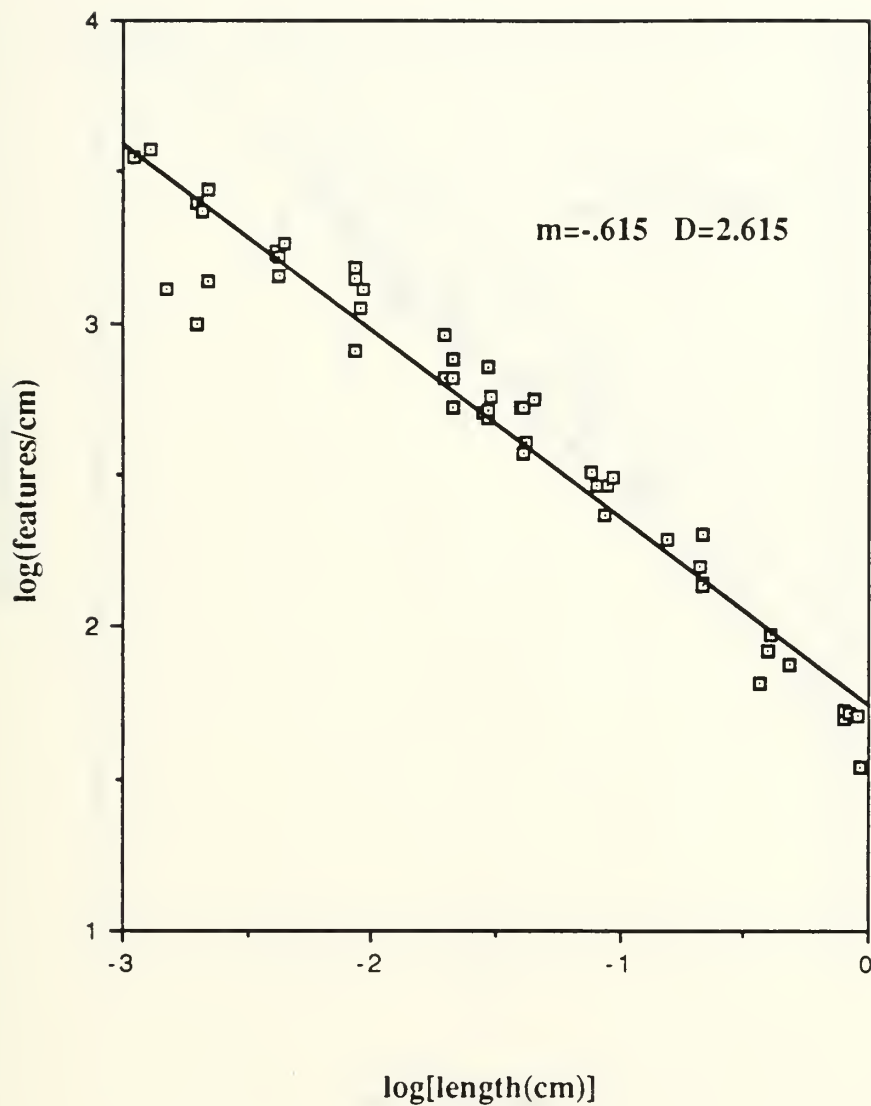


Figure 4-7: Log-log plot for Travis Peak sandstone, 7449.4 ft.

Travis Peak Sandstone 7456.3 ft

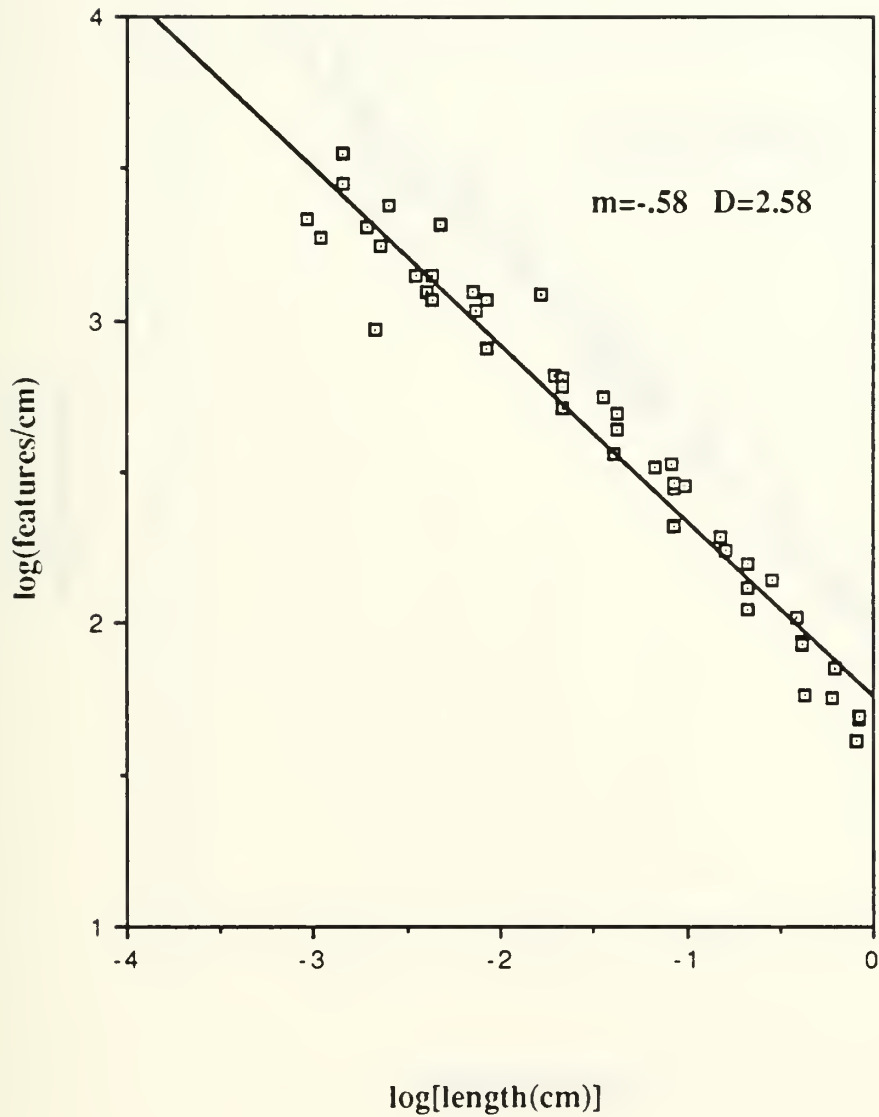


Figure 4-8: Log-log plot for Travis Peak sandstone, 7456.3 ft.

San Andres Dolomite 3350 ft

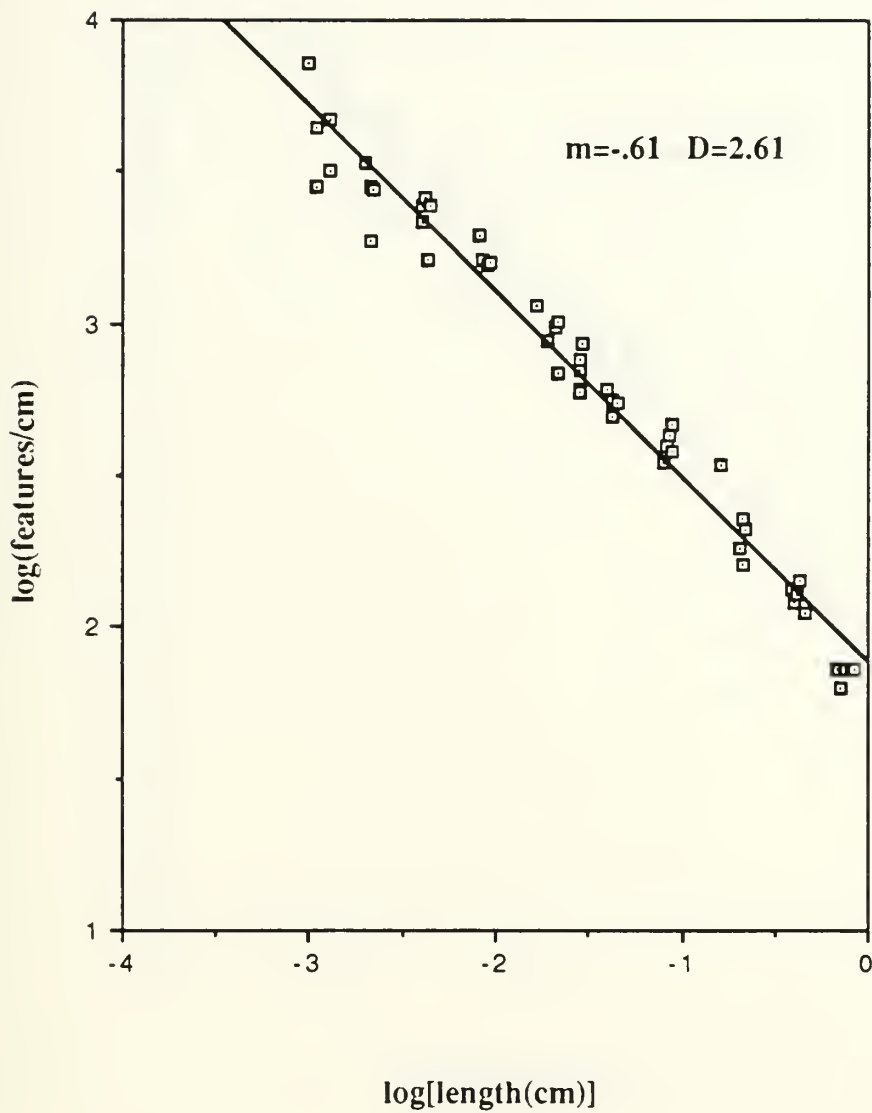


Figure 4-9: Log-log plot for San Andres dolomite, 3350 ft.

San Andres Dolomite 3414 ft

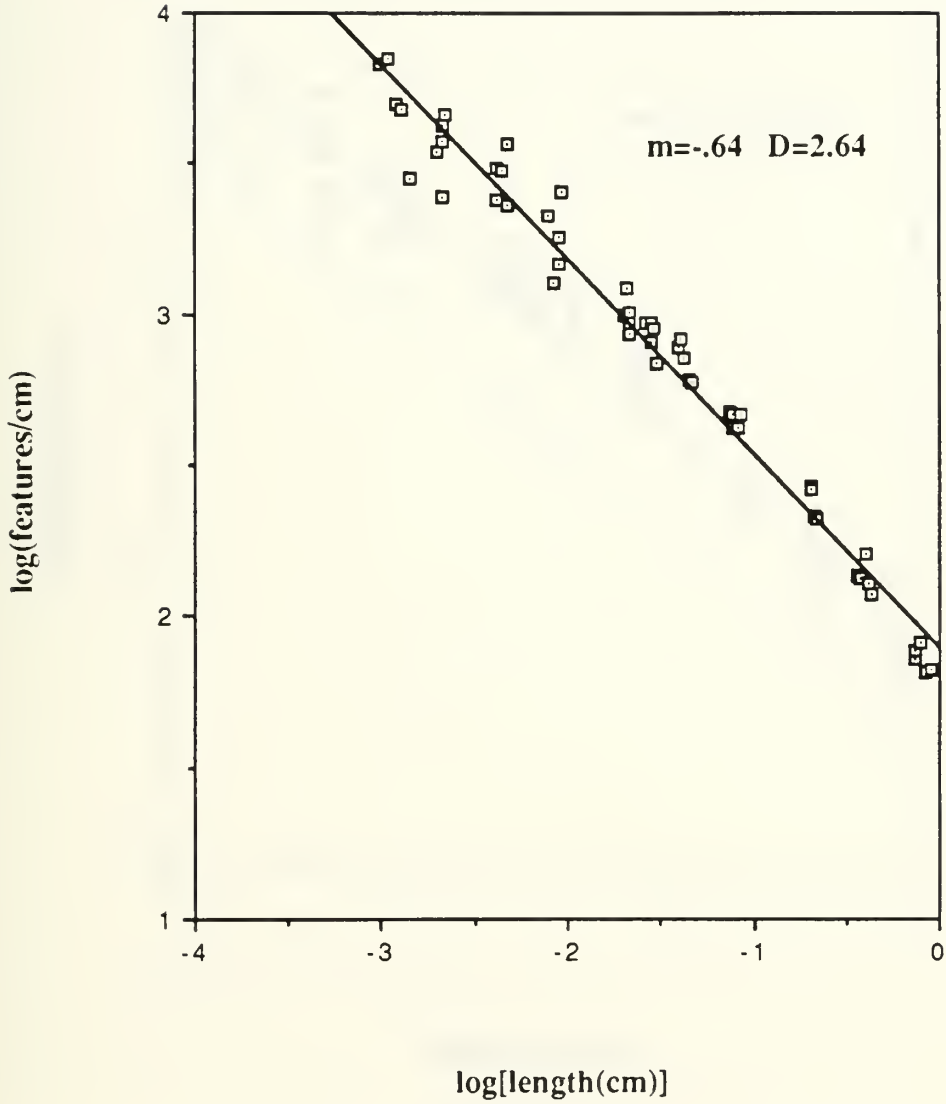


Figure 4-10: Log-log plot for San Andres dolomite, 3414 ft.

San Andres Dolomite 3464 ft

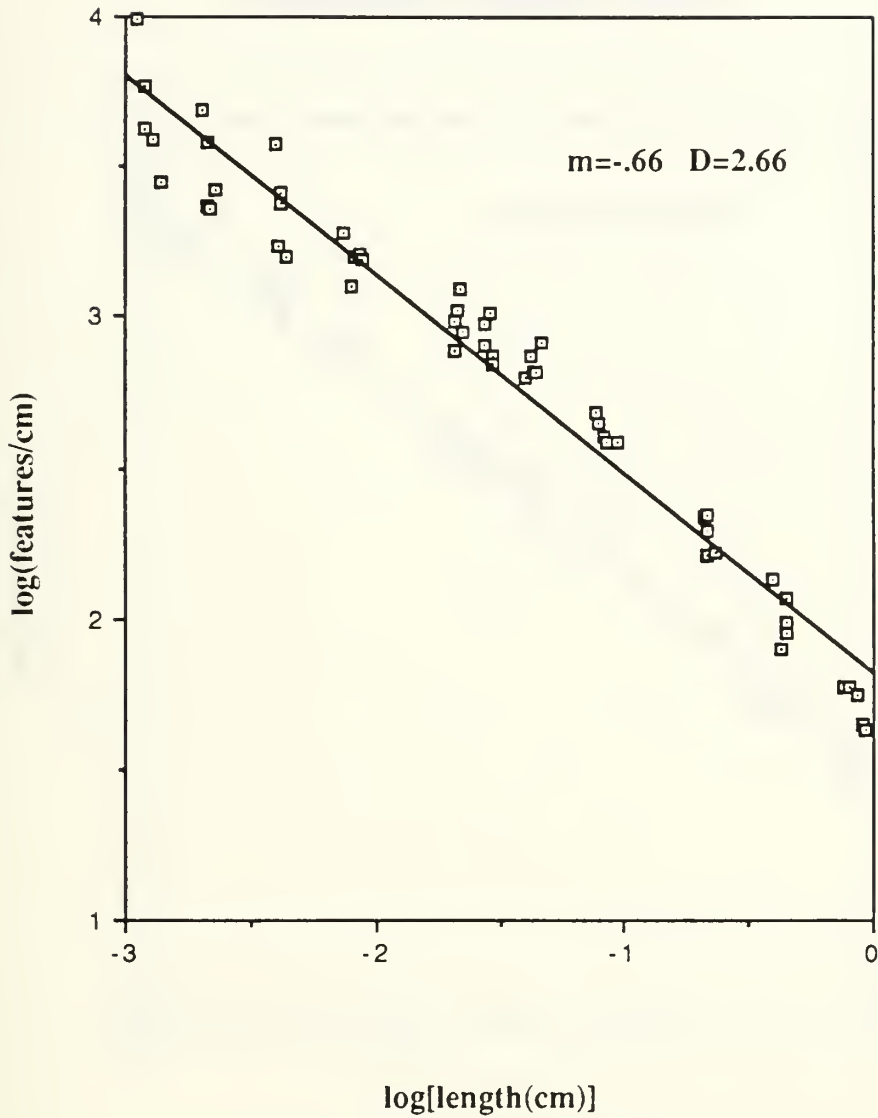


Figure 4-11: Log-log plot for San Andres dolomite, 3464 ft.

San Andres Dolomite 3492 ft

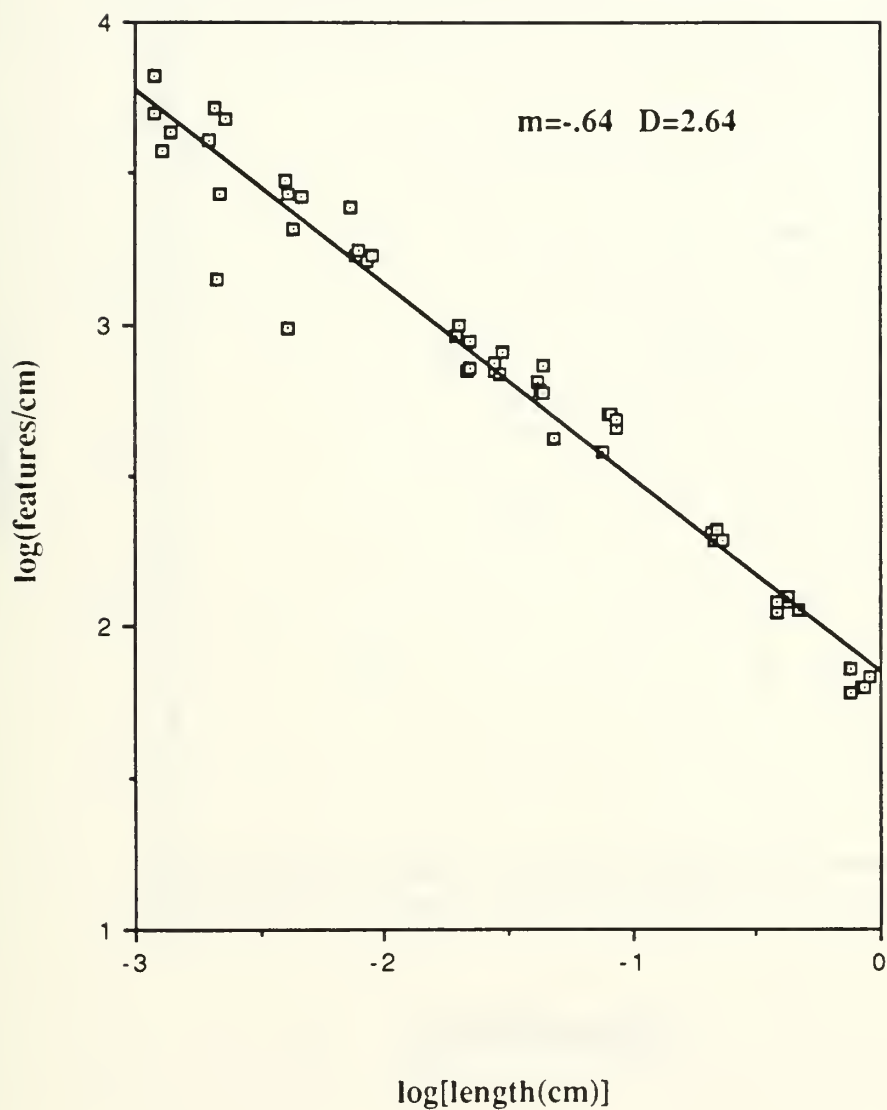


Figure 4-12: Log-log plot for San Andres dolomite, 3492 ft.

Porosity vs. Fractal Dimension

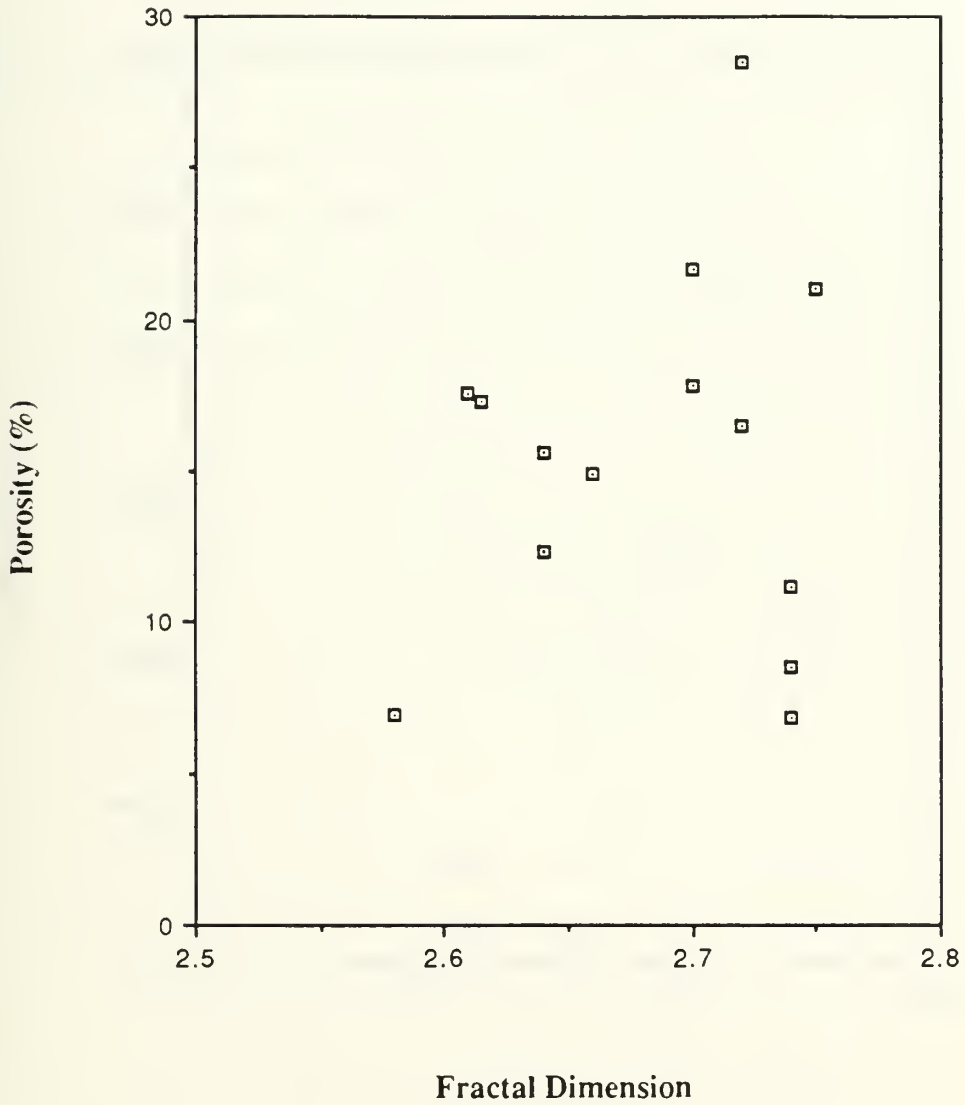


Figure 4-13: Porosity vs Fractal Dimension for all rock samples.

Permeability vs. Fractal Dimension

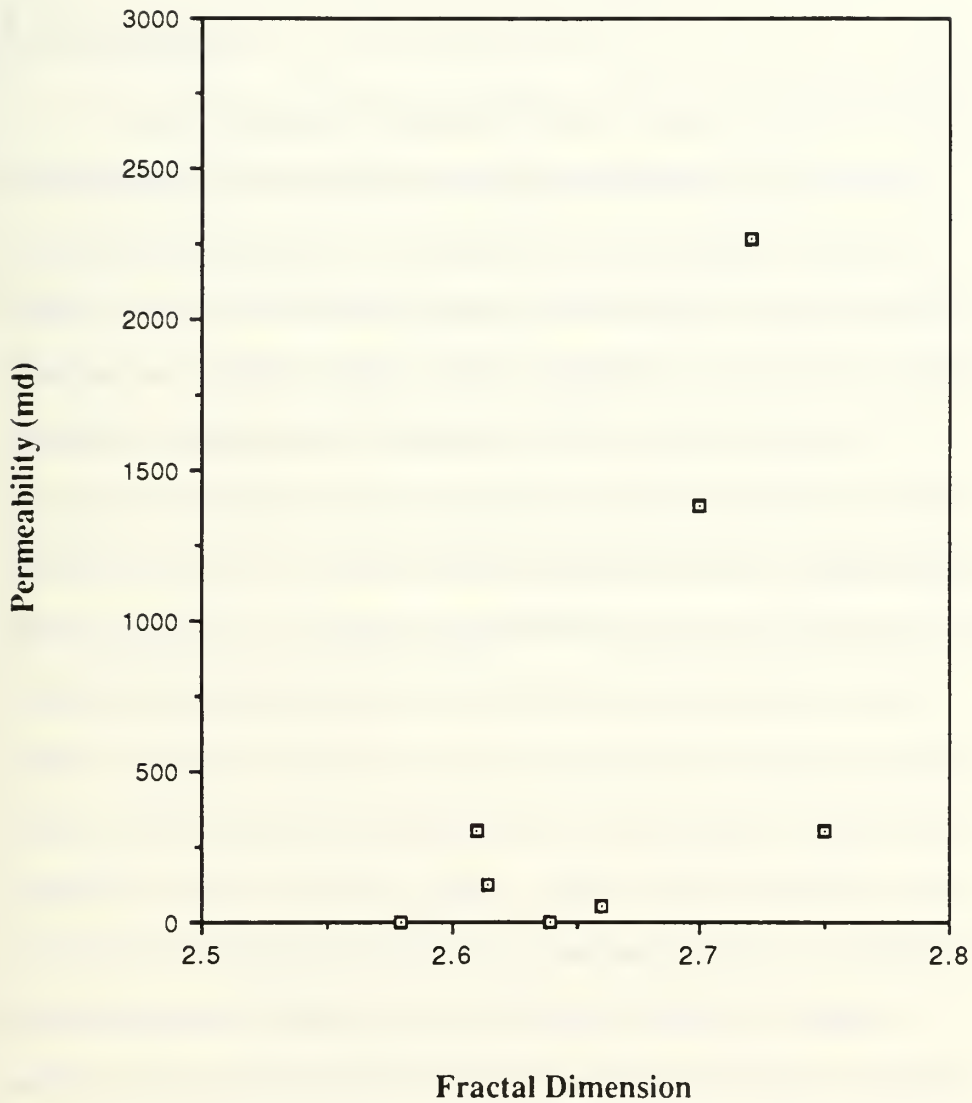


Figure 4-14: Permeability vs Fractal Dimension for all rock samples.

Chapter 5

Fractals and Transport Properties of Rocks

5.1 Summary

As the concepts of fractals become more common and easier to comprehend, more effort is being expended to find ways of utilizing this property. Attempts have been made to relate the fractal concept to phenomena such as two phase flow boundaries (Jacquin and Adler, 1985), energy transfer in porous Vycor glass (Schaefer, Bunker, and Wilcoxon, 1987), the formation of aggregates, dendrites and crystals from small colloidal particles (Skjeltorp, 1987) as well as other Diffusion Limited Aggregation (DLA) processes. It appears that fractals play an important role in many scientific phenomena that have been observed for many years. One area that has received a great deal of attention lately is that of fluid transport through rock and its relation to the fractal dimension of the rock pore space. Many of the references cited thus far in this paper provide very good support for the claim that the pore spaces of many porous rocks are fractal in nature; however, the relationship between the fractal pore space and the transport properties of the rock is still poorly understood.

Hewett (1986) attempted to relate the fractal properties of distributions of permeability and porosity on oil recovery

processes using simulation on a distributed field of properties with a correlation structure matching that in field measurements. In this paper, he discussed the geometric properties and spatial correlation structure of fractal distributions as well as methods for measuring the fractal character of log data. His approach holds much promise for the modeling of heterogeneous reservoirs.

The approach above considers petrophysical property distributions at large length scales (a few feet). The approach in this thesis is to consider a microscopic description of homogeneous rock. Rocks also exhibit fractal behavior at these length scales, not because of porosity or permeability heterogeneity, but because of pore surface features developed during diagenesis. It is at this length scale that we hope to adequately represent the pore structure by a fractal lattice.

5.2 Two Dimensional Model: The Sierpinski Carpet

As a starting point, Sharma and Gupta (1987) considered a two dimensional fractal lattice called the Sierpinski Carpet that is self-similar within the length scales L_1 and L_2 to model the pore space. As stated in Chapter 2, the Sierpinski Carpet is formed using a square initiator and a square generator in which the initial square is subdivided into b^2 subsquares and c^2 of these subsquares are

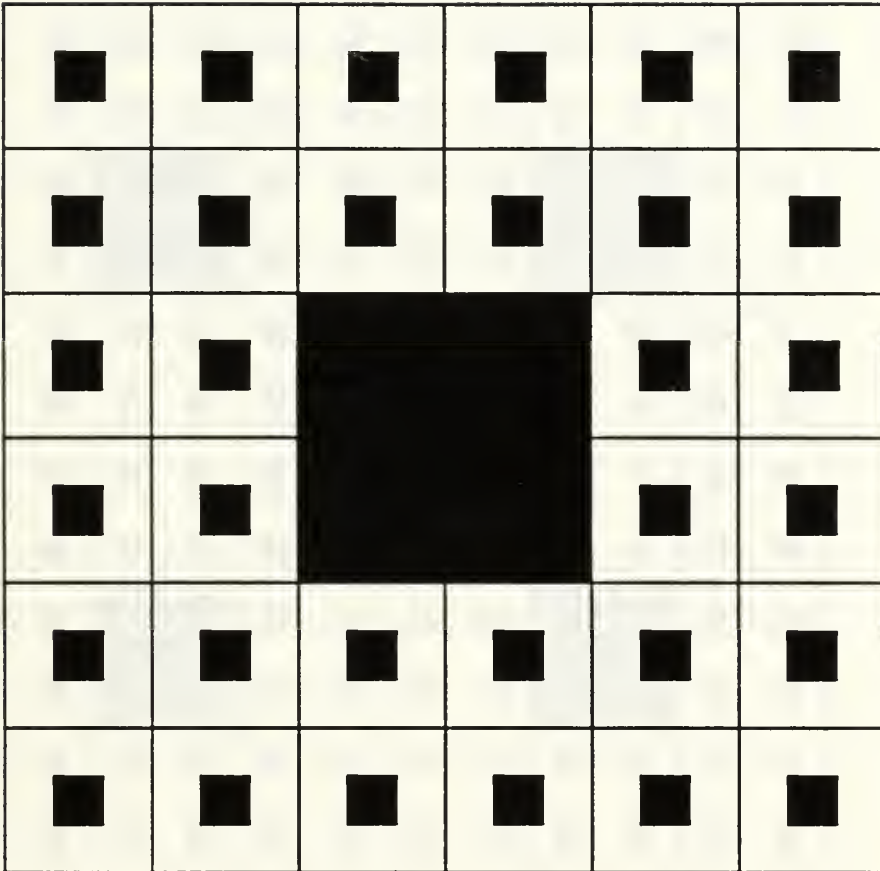
removed. When this procedure is repeated indefinitely on each daughter subsquare, the fractal dimension of the resulting lattice is

$$D = \frac{\log (b^2 - c^2)}{\log b} \quad (5.1)$$

where $1 \leq D \leq 2$.

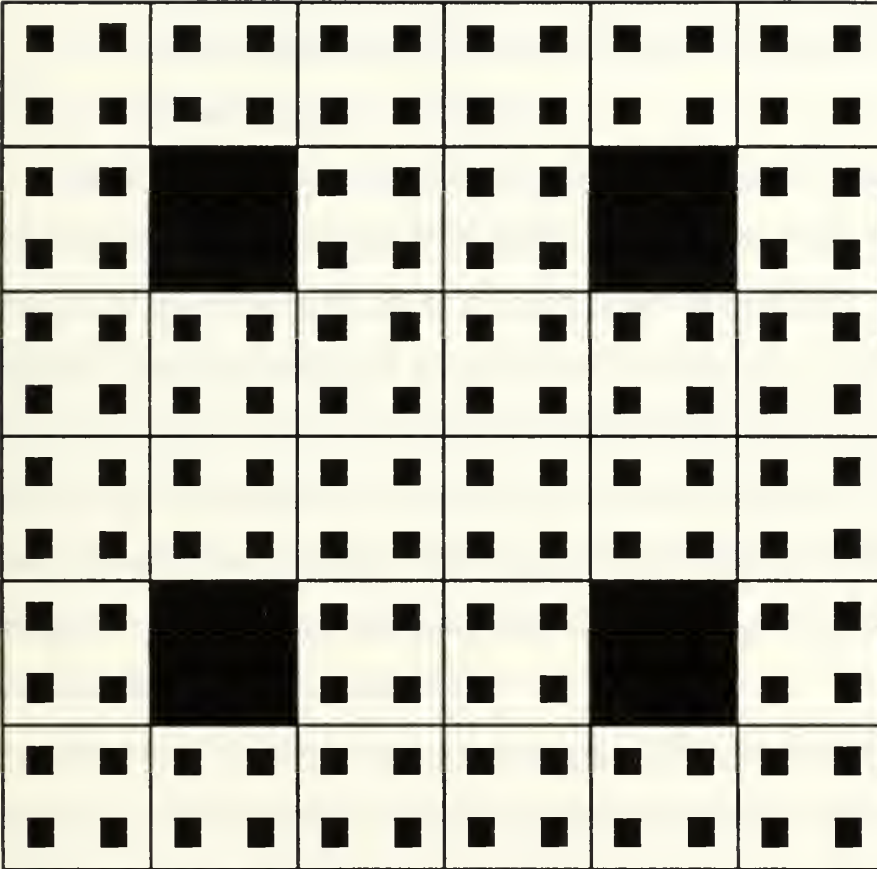
The classical Sierpinski Carpet has a value of $b^2 = 9$, $c^2 = 1$ and $D=1.8928$ (Mandelbrot 1983). Sharma and Gupta used a slight variation of the Sierpinski Carpet in which the values of b^2 and c^2 could be varied to form an infinite number of fractal configurations each with a unique fractal dimension. In addition, the locations of the c^2 removed subsquares could be varied. Figures 5-1 and 5-2 show two versions of the Sierpinski Carpet with identical fractal dimensions in which $b^2 = 36$ and $c^2 = 4$. Obviously, the two lattices are not identical, and hence, it is necessary to obtain more than just the topological and fractal dimensions to completely define a fractal. Other required properties to define a fractal are:

- (i) Order of ramification. This is a measure of the smallest number of significant interactions which one must cut in order to isolate an arbitrarily small bounded set of points. Intuitively this is related to the connectivity of the fractal network.



$b=6, c=2, d=4, D=1.9343$

Figure 5-1: Sierpinski Carpet with high lacunarity.



$$b=6, c=2, d=1, D=1.934.$$

Figure 5-2: Sierpinski Carpet with low lacunarity.

(ii) Lacunarity. A fractal is said to be lacunar if its gaps are large. Therefore, the fractal in Figure 5-1 is more lacunar than the one in Figure 5-2. Lacunarity is also a measure of the extent to which a fractal is translationally invariant.

Sharma and Gupta used the Sierpinski Carpet as a model for a two dimensional cross section of porous media. The holes created in the lattice from the removal of c^2 subsquares during each subdivision were regarded as pores through which flow occurred. This model was extended to represent a three dimensional porous structure by the extension of the holes to a series of parallel tubes through which flow occurred. Obviously, this extension to three dimensions was an oversimplification and has the same limitations as any parallel capillary tube model.

They used the following nomenclature throughout their experiment. The Sierpinski Carpet was considered to be self-similar between length scales L_1 and L_2 . Each side of the square initiator was divided into b segments to obtain b^2 subsquares. c^2 of these subsquares were removed in each generation. Of the squares removed, d squares were connected together. Thus, d was a measure of lacunarity. The higher the value of d , the more lacunar the fractal. Using this model, equations were developed for some of the petrophysical properties of the fractal lattice.

5.2.1 Porosity

Sharma and Gupta showed that the porosity of such a fractal lattice is equal to

$$\phi = k_1 \left[1 - \left(1 - \frac{c^2}{b^2} \right)^n \right] \quad (5.2)$$

where $n = \log(L_2/L_1) / \log b$

and $k_1 =$ a shape factor = (area of a pore equivalent size r) / r^2

$k_1 = 1$ for square pores.

This equation suggests that porosity is uniquely determined by the fractal dimension for a fixed value of L_2/L_1 , and that it is independent of lacunarity or the order of ramification. Figure 5-3 is an example of how porosity varies with fractal dimension for a fixed value of L_2/L_1 . Note that the porosity decreases from 1 to 0 as the fractal dimension varies from about 1.5 to 2.0.

Sierpinski Carpet

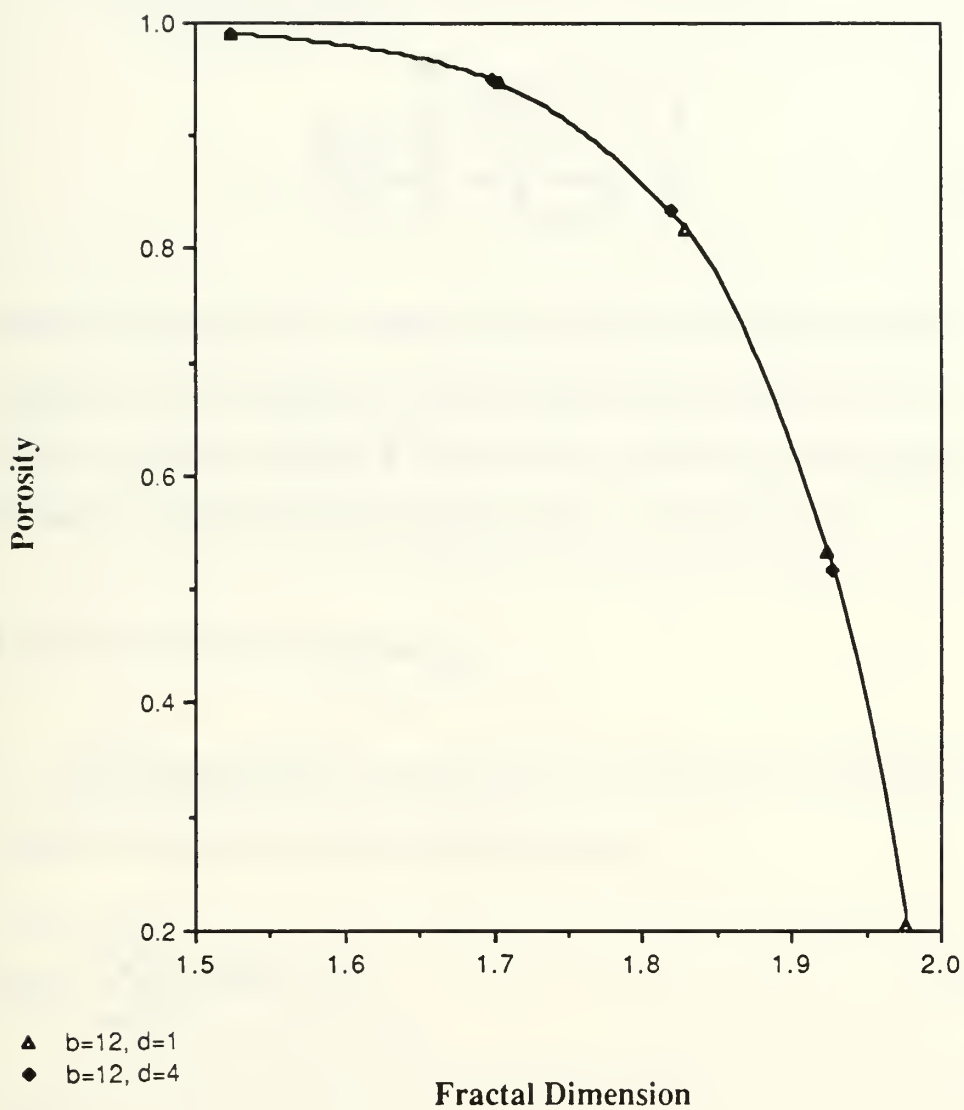


Figure 5-3: Porosity vs D for varying lacunarity.

5.2.2 Specific Surface Area

The specific surface area (S) can be written as

$$S = \frac{k_2 d^{1/2}}{L^2} \left[\frac{\left(\frac{b^2 - c^2}{b} \right)^n - 1}{b^2 - b - c^2} \right] \quad (5.3)$$

where k_2 is a geometric constant that relates the surface area of a single pore to the length of its side (Sharma and Gupta 1987). As shown from the equation, S is a function of the fractal dimension, lacunarity, and the limits of length scales of self similarity.

5.2.3 Pore Size Distribution

The number pore size distribution consisted of a series of delta functions that could be represented as

$$f_{pn} = \sum_{i=1}^n f_p(r_i) \delta(r - r_i) \quad (5.4)$$

where

$$r_i = \sqrt{d} (L^2/b^i) \quad (5.5)$$

and

$$f_p(r_i) = \frac{(b^2 - c^2)^{i-1}}{\left[\frac{(b^2 - c^2)^{n-1}}{b^2 - c^2 - 1} \right]} \quad (5.6)$$

$f_p(r_i)$ for each generation of pores depend on the fractal dimension but are independent of lacunarity; however, the radii of pores in each generation depend on lacunarity. Figure 5-4 shows pore size distribution for varying lacunarities. Note that the distributions are identical except for a scaling factor related to d (for the same fractal dimension).

It was also determined that the volume pore size distribution could be written as

$$f_{pv} = \sum_{i=1}^n f_{pv}(r_i) \delta(r - r_i) \quad (5.7)$$

where

$$f_{pv}(r_i) = \frac{\frac{c^2}{b^2} (1 - c^2/b^2)^{i-1}}{[1 - (1 - c^2/b^2)^n]} \quad (5.8)$$

and r_i are given as before. The conclusions made about the number size distribution are valid here as well.

5.2.4 Permeability

The flow rate in a single conduit of side r is given by

$$q = \frac{r^4 \Delta P}{k_3 \mu L} \quad (5.9)$$

where $k_3=28.8$ for a square conduit. Using this fact and a method analagous to the capillary tube model, it was determined that the permeability of the fractal lattice could be written as

$$k = \frac{c^2 d}{k_3} (L_2/b)^2 \left[\frac{1 - \left[\frac{b^2 - c^2}{b^4} \right]^n}{(b^2 - 1 - c^2/b^2)} \right] \quad (5.10)$$

(Sharma and Gupta 1987). As seen from the equation, the permeability shows a strong dependence on lacunarity, which seems reasonable because lacunarity is a measure of the size of the gaps. Figure 5-5 shows permeability as a function of both fractal dimension and lacunarity.

and r_i are given as before. The conclusions made about the number size distribution are valid here as well.

5.2.4 Permeability

The flow rate in a single conduit of side r is given by

$$q = \frac{r^4 \Delta P}{k_3 \mu L} \quad (5.9)$$

where $k_3=28.8$ for a square conduit. Using this fact and a method analagous to the capillary tube model, it was determined that the permeability of the fractal lattice could be written as

$$k = \frac{c^2 d}{k_3} (L_2/b)^2 \left[\frac{1 - \left[\frac{b^2 - c^2}{b^4} \right]^n}{(b^2 - 1 - c^2/b^2)} \right] \quad (5.10)$$

(Sharma and Gupta 1987). As seen from the equation, the permeability shows a strong dependence on lacunarity, which seems reasonable because lacunarity is a measure of the size of the gaps. Figure 5-5 shows permeability as a function of both fractal dimension and lacunarity.

Pore Size Distribution

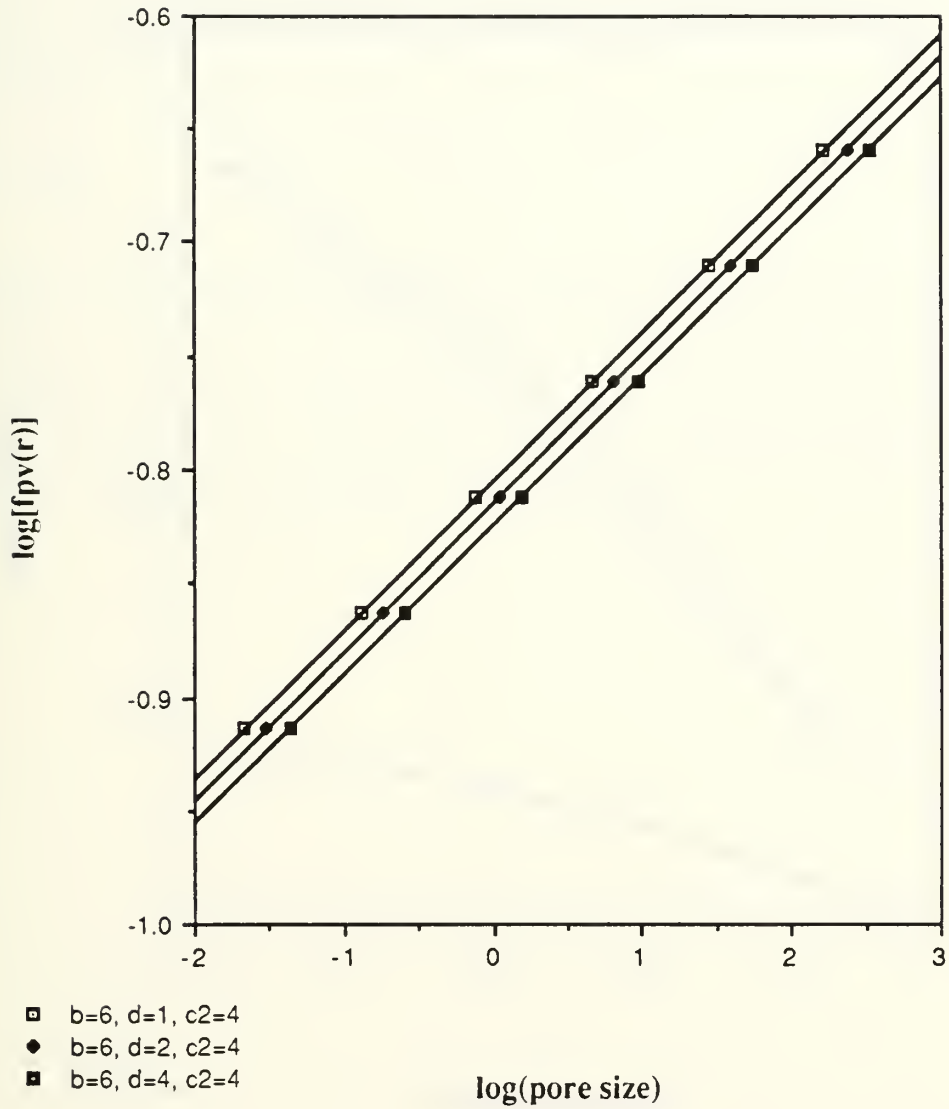


Figure 5-4: Pore size distribution for varying lacunarity.

Sierpinski Carpet

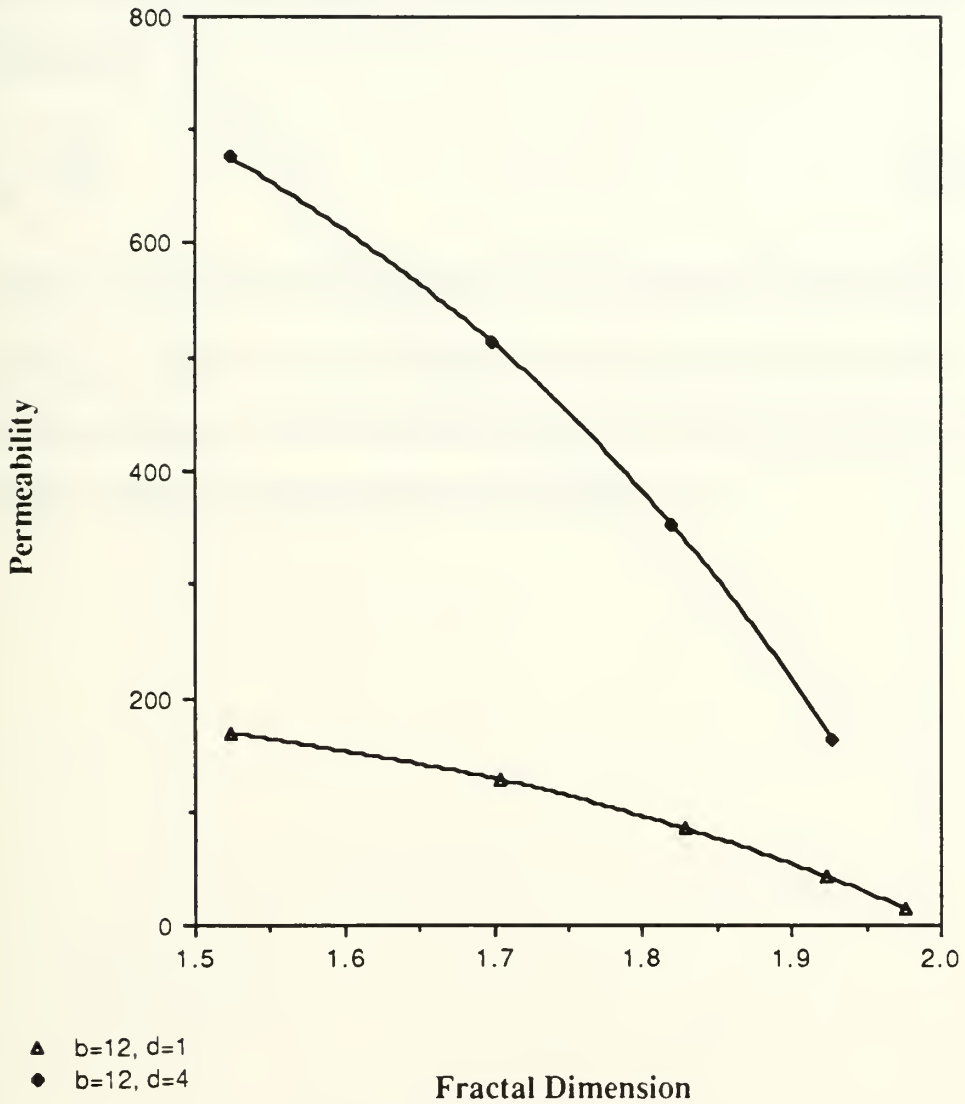


Figure 5-5: Permeability vs D for varying lacunarity.

5.2.5 Capillary Pressure Curves

If the non-wetting phase is allowed to enter the largest pores in accordance with capillarity, the capillary pressure curves can be constructed

$$P_c = \frac{k_4}{r} \quad (5.11)$$

where k_4 is a constant that depends on the interfacial tensions and geometry. Figure 5-6 shows some capillary pressure curves for varying lacunarity. Note that these curves are identical except for a scaling constant proportional to the lacunarity, d .

Capillary Pressure Curves

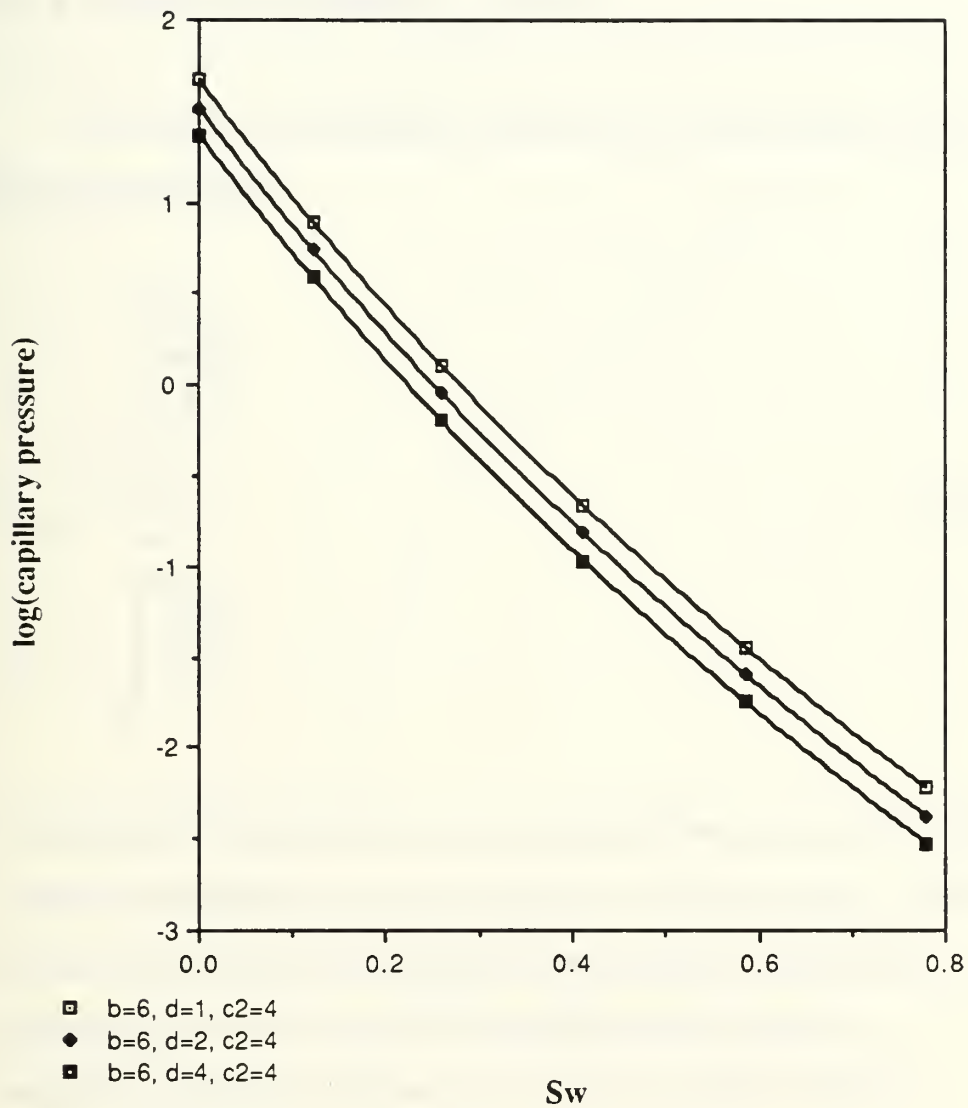


Figure 5-6: Capillary pressure curves for varying lacunarity.

5.2.6 Relative Permeability Curves

The relative permeability curves can be determined from the following equation

$$k_{rw} = \frac{\int_{S_w}^{\infty} \frac{dS_w}{P_c^2}}{\int_0^{\infty} \frac{dS_w}{P_c^2}} \quad (5.12)$$

All Sierpinski Carpets with the same fractal dimension had the same relative permeability curves irrespective of the lacunarity. This is an interesting result considering the fact that the single phase permeability and the pore size distribution both depend on lacunarity. Figure 5-7 shows how the wetting phase relative permeability curves vary with fractal dimension.

Relative Permeability Curves

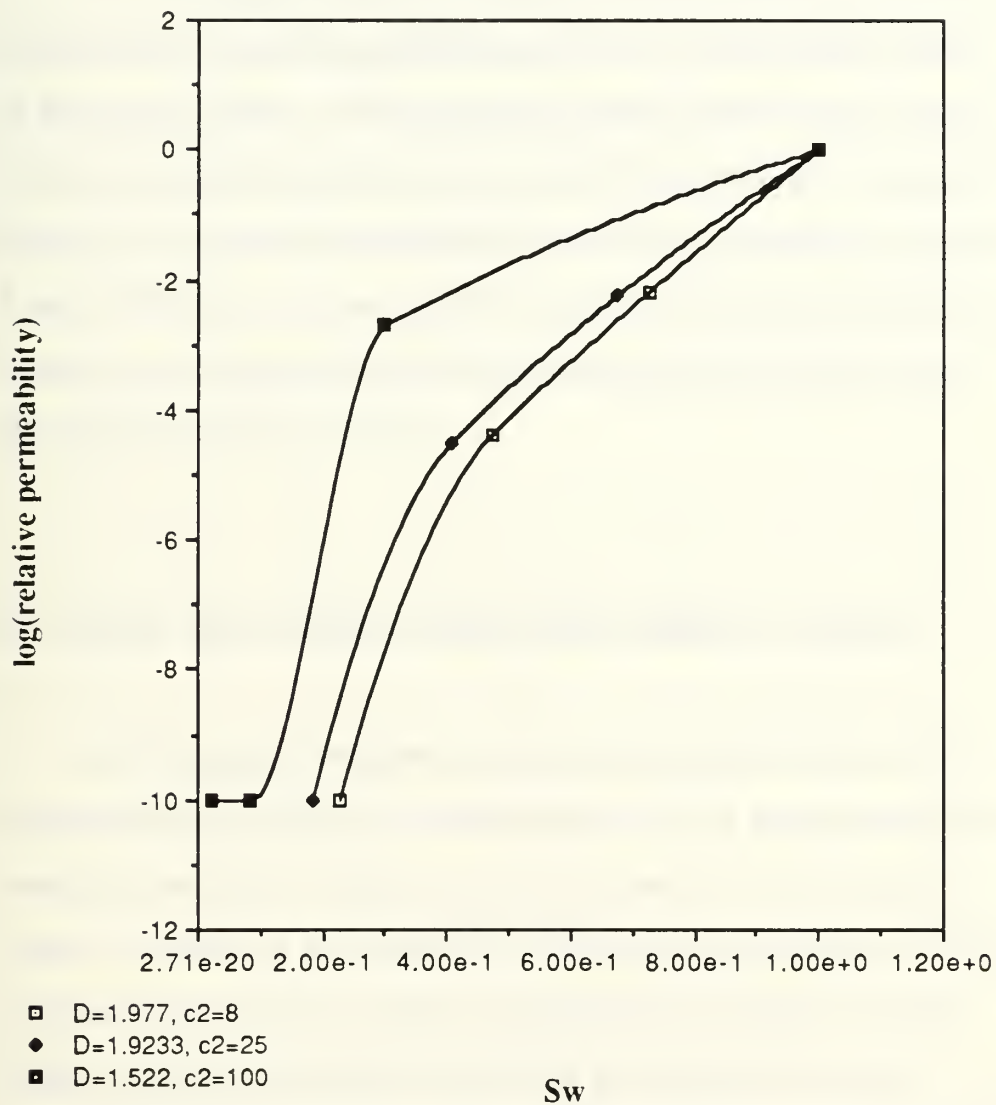


Figure 5-7: Relative permeability curves for varying fractal dimension.

5.2.7 Discussion

The theoretical results of this model could not be compared directly with experimental data due to the two dimensional nature of the fractal lattice. All Sierpinski Carpets created in this manner had fractal dimensions between 1 and 2; however, the rock samples that were measured on the SEM all had fractal dimensions between 2 and 3. Thus, it was not feasible to compare the core analysis data from the rock samples with the theoretical results obtained from the Sierpinski Carpet model.

5.3 Three Dimensional Model: The Menger Sponge

In this project an attempt was made to find a relationship between the measured fractal dimensions of rock samples and their transport properties using a model very similar to the Sierpinski Carpet . Instead of a converted two dimensional Sierpinski Carpet, the three dimensional version of the Sierpinski Carpet called the Menger Sponge was used to model the pore space of the rock samples. The goal of this project was to determine whether or not it could be accurately used to predict the physical properties of the rock samples.

The Menger Sponge is a generated fractal volume which was briefly described in Chapter two. The classic Menger Sponge is formed by dividing a cube of unit volume (sides equal to one) into a set of 27 smaller cubes as shown in Figure 2-7. The center cubes from each face, and the cube in the center of the entire figure, are removed to form some void space within the matrix of cubes. Each remaining cube is then divided into 27 smaller cubes, and the same cubes are removed from these smaller set of cubes. This process is repeated indefinitely to form the fractal volume known as the Menger Sponge.

In this project a slight variation of the Menger Sponge was used to model the rock samples. In the Menger Sponge described above, the original cube was initially divided into 27 (or 3^3) small cubes of side length equal to $1/3$. Note that there is a direct relationship between the inverse of the side length and the total number of small cubes. The relationship is

$$N = b^3 \quad (5.13)$$

where N is equal to the number of cubes resulting from the first division and b is the inverse of the length of the side of the cube (see Figure 5-8). In the example, b was equal to 3; however, in the model, other values of b were also used in order to determine if there were any values that gave reasonable results. The value of b

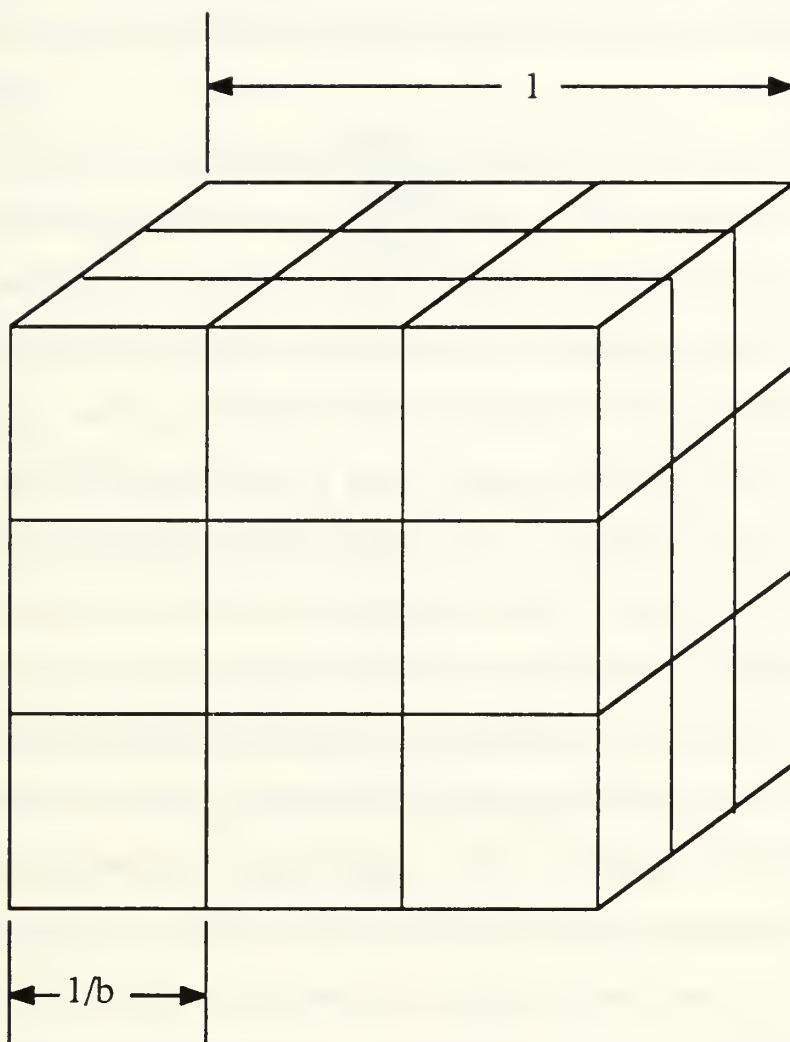
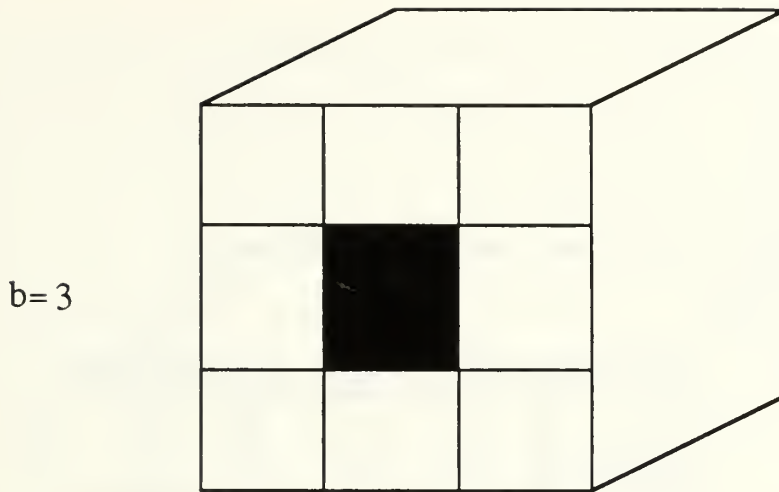


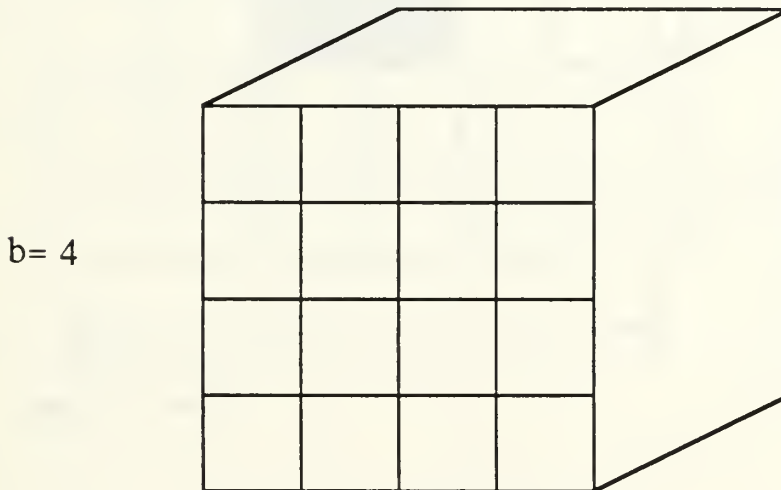
Figure 5-8: Original cube of side length 1 is divided into b^3 subcubes of side length $1/b$. In this example, $b=3$ and $N = 27 =$ number of subcubes.

was varied between 3 and 200 and the corresponding fractal dimensions and porosities were calculated through established formulas.

Before these values could be determined, there were several other parameters that required definition. In the example of the Menger Sponge, the center square of each cube face was removed (along with the center cube) during each division in order to create the fractal volume. However, as the value of b was increased from 3, the size of the subdivided cubes became relatively smaller, since the sides of the cubes were equal to $1/b$. Also, there was only a "center" cube on each face when the value of b was odd. Otherwise, there was no center cube to remove (see Figure 5-9). Obviously, the same procedure could not be repeated for all values of b . Thus, the number of cubes removed from the center of each side of the initial cube was varied depending on the value of b . Instead of removing just one cube from each face to create the fractal volume, the number of cubes removed was varied for each value of b . c^2 was defined as the number of cubes removed from each face so that c was equal to the number of consecutive cubes removed from any one row (see figure 5-10). This process was very similar to that used by Sharma and Gupta (1987) in their Sierpinski Carpet model, only they did not require that all squares be removed from the center only.



When b is odd, there will always be an odd number of rows and columns and a middle cube.



When b is even, there will be an even number of rows and columns and no middle cube.

Figure 5-9: Effects of changing the value of b .

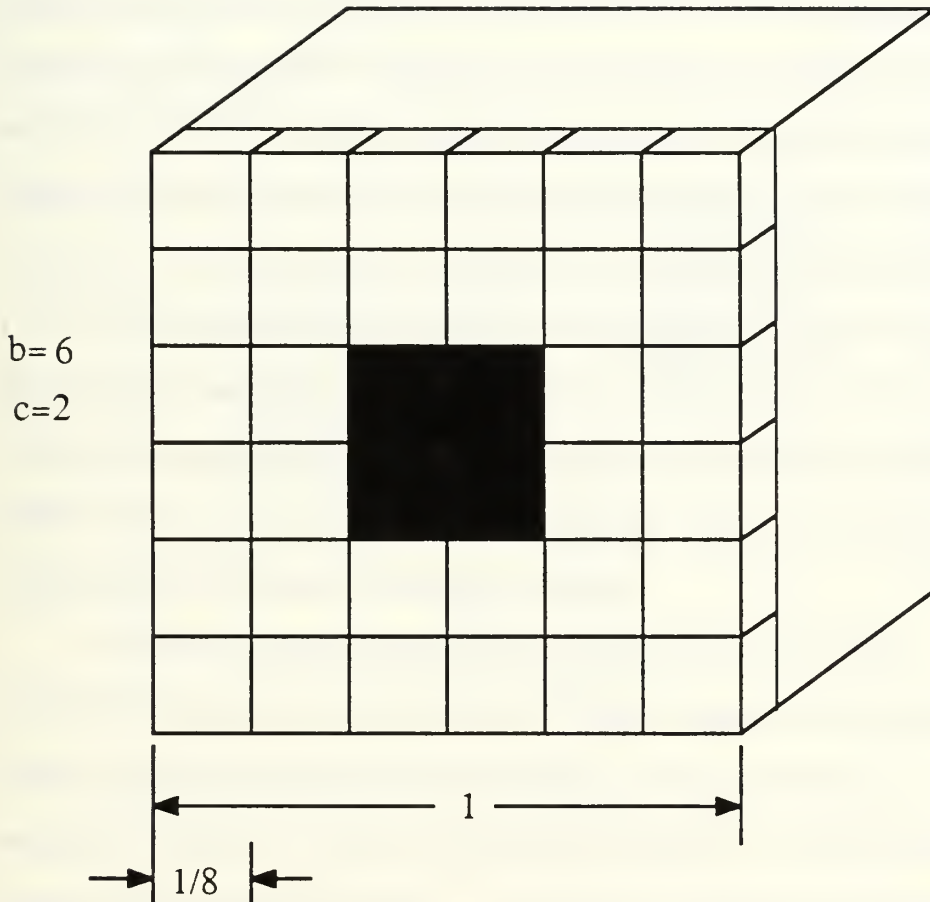


Figure 5-10: When $b=6$ and $c=2$, then the total number of cubes removed from the center of each face is c^2 or 4.

In order to keep the cube symmetrical, the value of c was always odd for odd values of b and even for even values of b . As long as this rule was followed, the volume of space removed was always located in the center of each cube face. For the purposes of this model, only center volumes were removed. It is important to note that not only were the small cubes on each large cube face removed, but so were all of the cubes between each face, thereby creating an empty pathway through the entire cube (see Figure 5-11). This removal of cubes within the original cube lattice creates the small pathways in which flow occurs. The pathways in the Menger Sponge are no longer unidirectional, parallel tubes, but rather form an intricate, intricate connected network of pores which yields a perfectly isotropic medium.

As b was varied between 3 and 200, the value of c was allowed to vary for each value of b . When b was an odd number, then c was allowed to take upon the value of all odd numbers between 1 and $b-2$. When b was an even number, c took upon all even values between 2 and $b-2$. Note that c was never allowed to be odd when the value of b was even, and vice-versa. The value of c could never be larger than $b-2$, otherwise the volume removed would either not be in the center of the original cube, or it would be the entire cube! Either condition would be unsatisfactory.

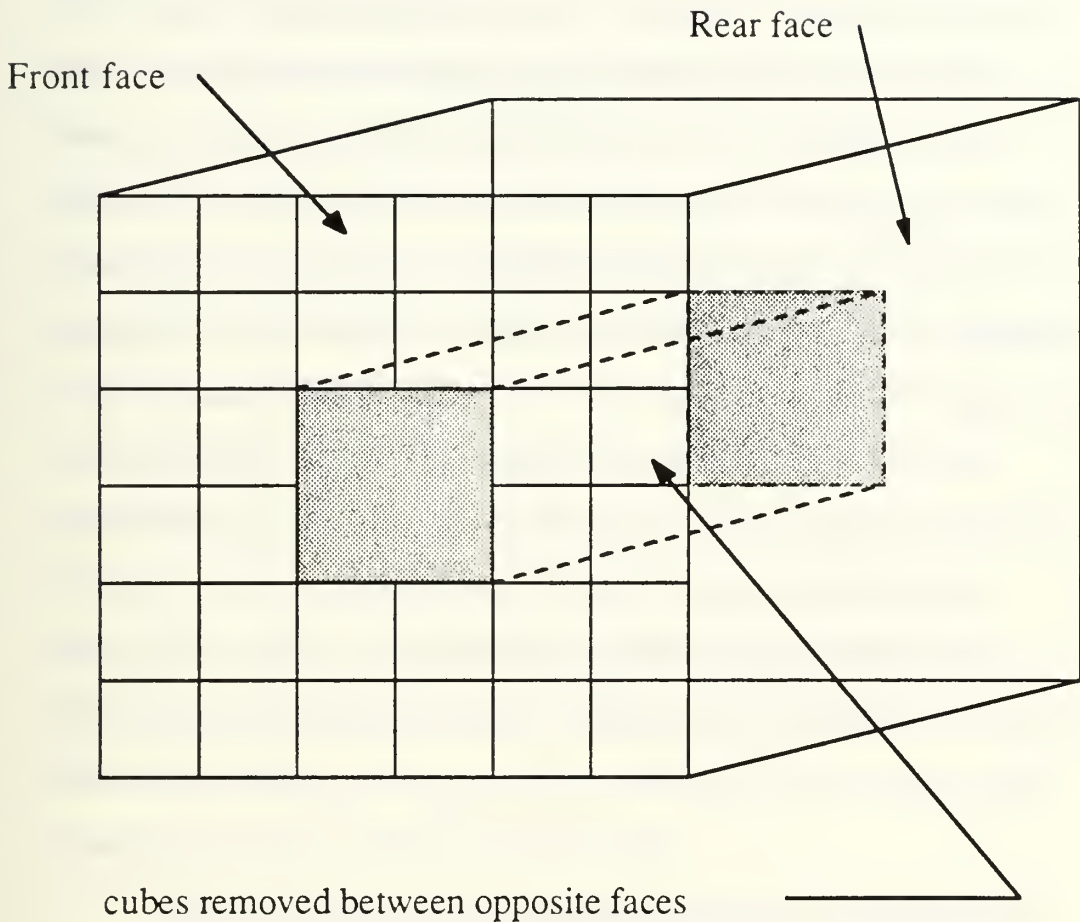


Figure 5-11: The cubes in between the faces are removed as well as the cubes on the faces, thereby creating an empty passageway between opposite faces. This example only shows two of the faces, but the same holds true for the other four faces as well.

Aside from b and c , the final parameter required before the porosity of the final volume could be determined was the ratio of the limits of fractal geometry, $L2/L1$, where $L2$ was the upper limit and $L1$ was the lower limit. As previously stated, most fractal structures do not exhibit fractal behavior over all length scales; rather, they usually exhibit fractal behavior over some upper and lower limits, $L2$ and $L1$. The data obtained from the SEM was not adequate to determine the values of $L2$ and $L1$. Katz and Thompson (1985) estimated the value of $L1$ to be approximately 20 Angstroms for sandstones, and she used autocorrelation data from optical measurements to determine $L2$ for both sandstones and carbonates. For this model, various values of $L2/L1$ were applied over the range $100 < L2/L1 < 35000$ which was the range determined by Krohn for most reservoir rocks. Applicable formulas were used to determine whether or not any of the values of $L2/L1$ in this range resulted in accurate estimates of porosity.

With all of the various parameters defined, the formulas for the fractal dimension and porosity could be determined. First, the fractal dimension for a Menger Sponge for any value of b and c defined above is

$$D = \frac{\log[b^3 - (3c^2b - 2c^3)]}{\log b} \quad (5.14)$$

where D is the fractal dimension. The numerator represents the log of the number of smaller cubes remaining after one generation, and the denominator represents the log of the length scale. When the generation process is repeated, the number of cubes remaining from any particular cube is the same as above. The only difference is in the fact that the cubes are smaller in each successive generation. Thus, only the number of cubes remaining after one generation is sufficient to determine the fractal dimension. When $b=3$ and $c=1$, the resulting figure is the classical Menger Sponge with $D=2.7269$. As the values of b and c are varied within the limitations already described, the value of D will always vary between 2 and 3. This fact should allow for a much better comparison of field data and theoretical data, since we already know that the fractal dimension of rock samples also lies within this range.

5.3.1 Porosity

Determination of porosity is a little more involved. First, the number of generations must be determined before the porosity can be calculated. Obviously, the more times the cubes are subdivided, the more the volume removed from the original cube, and the higher the porosity. Gupta (1987) determined that the

number of generations required for a sample is a function of $L2/L1$, and is defined as

$$n = \frac{\log(L2/L1)}{\log b} \quad (5.15)$$

where n is the number of generations. Hence, the larger the range of fractal behavior, the larger $L2/L1$, and the larger the value of n . Another parameter defined as the ratio of volume remaining after one generation to the original volume is defined as

$$r = \frac{b^3 - (3c^2b - 2c^3)}{b^3} \quad (5.16)$$

where r is the ratio. Gupta (1987) also determined that the porosity of a Menger Sponge for any value of b and c is

$$\phi = 1 - r^n \quad (5.17)$$

where ϕ is the porosity and r and n are defined above.

These formulas were used in a Fortran program in which the fractal dimension and the porosity were calculated for various values of b , c and $L2/L1$. Since the fractal dimension of all samples varied between 2.58 and 2.75, only the combinations of b , c and $L2/L1$ that resulted in values of D between 2.5 and 2.9 were selected. The corresponding value of porosity was also recorded in

order to determine if the Menger Sponge model accurately estimated the porosities of the rock samples. Note that porosity was the only petrophysical property of the rock that was investigated using this model. The complex nature of this model compared to that of the Sierpinski Carpet severely limited the number of properties that could be investigated. Obtaining similar formulas for permeability, specific surface area, etc. was much more complicated than in the case of the Sierpinski Carpet and was attempted.

5.3.2 Results

Figures B-1 through B-9 in Appendix B show the plots of porosity vs fractal dimension for various combinations of b , c and $L2/L1$. The program was run for values of $L2/L1$ equal to 1000, 5000, 10000, 20000, 30000, and 35000 in order to provide representative plots of the entire range of $L2/L1$ determined by Krohn (1987). For the three cases in which the values of $L2/L1$ were equal to 1000, 10000, and 35000, plots of porosity vs D were constructed for values of b equal to 10, 100, and 200. These graphs covered the entire spectrum of b values used in this project.

As previously stated, only the data points with $2.5 < D < 2.9$ were included in the Figures, because this was the range of D values

measured in the rock samples. The Figures all show the corresponding porosity values for this range of fractal dimensions. The range of c values was also shown on each graph in order to show which values provided the proper fractal dimensions. Note that in all cases, the porosity values were all greater than 50%! Table 4-1 shows that the highest porosity in any of the rock samples was around 28%. Obviously this model does not give adequate estimates of porosity. Thus, it was concluded that this version of the Menger Sponge cannot be used to predict the transport properties of rocks from fractal data.

5.4 Modified Menger Sponge

A slightly different version of the Menger Sponge showed some potential as it provided results more consistent with experimental data. After seeing that the porosity values were not feasible, it was determined that a slight modification of the model may provide more reasonable results. Instead of starting with a solid cube and removing subsquares, it was decided to start with an empty cube and add subsquares during each division. This process should result in a fractal volume with the same fractal dimension as the first model; however, the porosity would be equal to one minus the porosity of the first model, since the positions of pore space and

solid space were interchanged. Figures 5-12 and 5-13 show plots of porosity vs fractal dimension from the modified model for the cases of $L2/L1=1000$, $b=100$ and $L2/L1=35000$, $b=100$. These graphs show porosity values between 5% and 25% for the range of fractal dimensions measured in the rock samples. This range of porosity values is much more realistic than that determined for the first model, and it appears that this modified version of the Menger Sponge is a more appropriate model than the initial version.

5.5 Future Work

In this project, porosity was the only petrophysical property of the Menger Sponge that was calculated, because it was relatively easy to determine. Obviously, the first first version of the Menger Sponge does not seem to be an adequate model for the pore space of rocks, but the modified version shows potential. More work is required with this modified version to see if it accurately predicts some of the other petrophysical properties of rock samples. The other properties such as permeability, specific surface area, etc. would be much more difficult to calculate for the Menger Sponge model. Once these properties are determined, the results can be compared with actual core analysis data to check the feasibility of

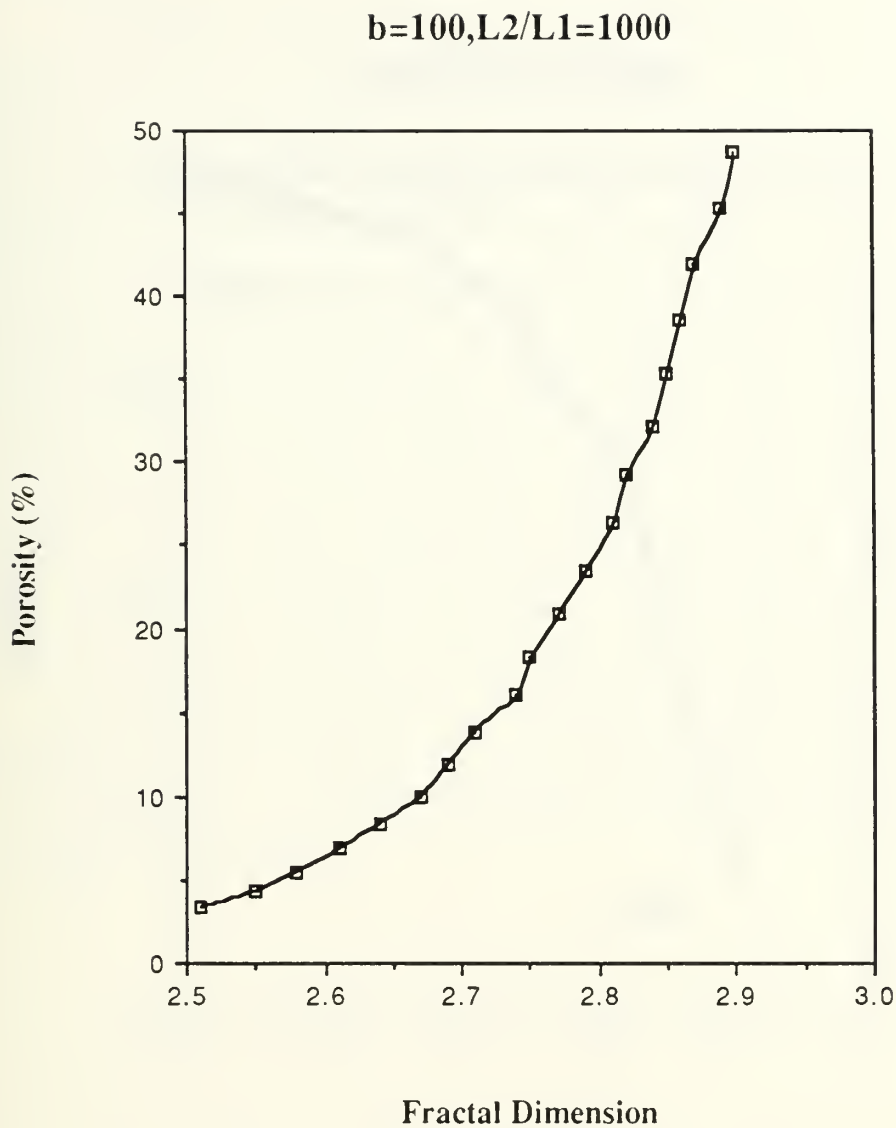


Figure 5-12: Porosity vs D for $b=100$ and $L2/L1=1000$ for the modified model.

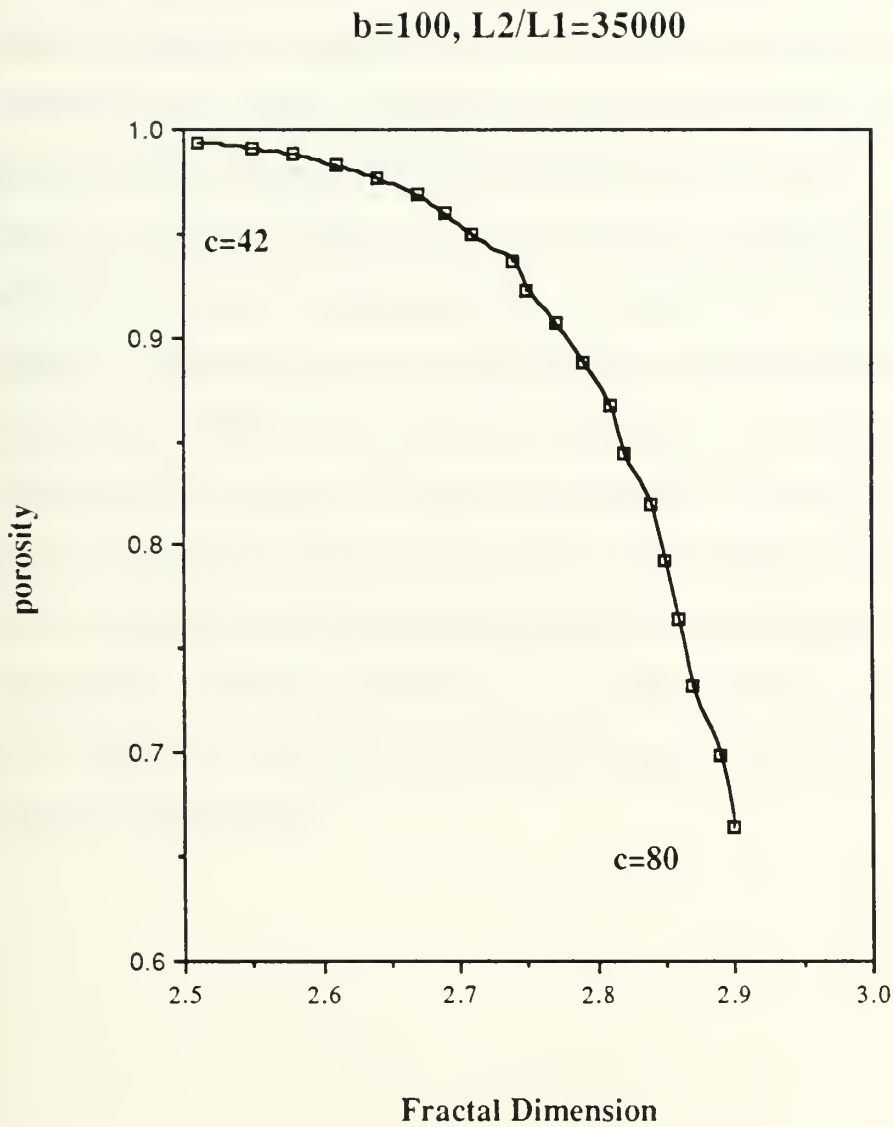


Figure 5-13: Porosity vs D for $b=100$ and $L2/L1=35000$ for the modified model.

this model.

In addition, nobody has yet determined whether or not the various methods of measuring fractal dimensions actually produce the same results. Katz, Thompson and Krohn (1987) produced identical results using both SEM data and thin section data; however, these two techniques rely on the same theoretical analysis and should produce consistent results. It would be interesting to determine whether or not two independent methods such as X-ray scattering and SEM data, or molecule adsorption and SEM data produce the same value of fractal dimension in rock pore spaces. If they do not, then the problem of finding a relationship between D and the properties of rocks becomes even more complicated. If they produce identical results, then we could confidently say that our D values are correct and that the pore space is indeed a fractal over some length scale.

Chapter 6

Conclusion

The results of the SEM measurements showed that the pore spaces of these particular rock samples were indeed fractals . The straight line relationship on log-log plots provided a method for the determination of the fractal dimension, since D is related to the slope of the line. Results showed that the fractal dimension of these rocks varied between 2.58 and 2.75. In general, the dolomites appeared to have values of D near the lower end of this range, while the sandstones appeared generally at the higher end.

Sample calculations on a Sierpinski Carpet showed that in principle the fractal property of lattices can be effectively utilized to obtain useful petrophysical properties. It was shown that the Menger Sponge was not an adequate model for the pore space of rocks. The values of porosity determined by the Menger Sponge model were much higher than those actually observed . A modified version, however, produced much better results and showed promise for accurately modeling the pore space of rocks. Much more work is required with this modified version before any definite conclusions can be made.

Appendices

Appendix A

Photographs



Figure A-1: Frio Sandstone, 9178.3 ft, x31, x53

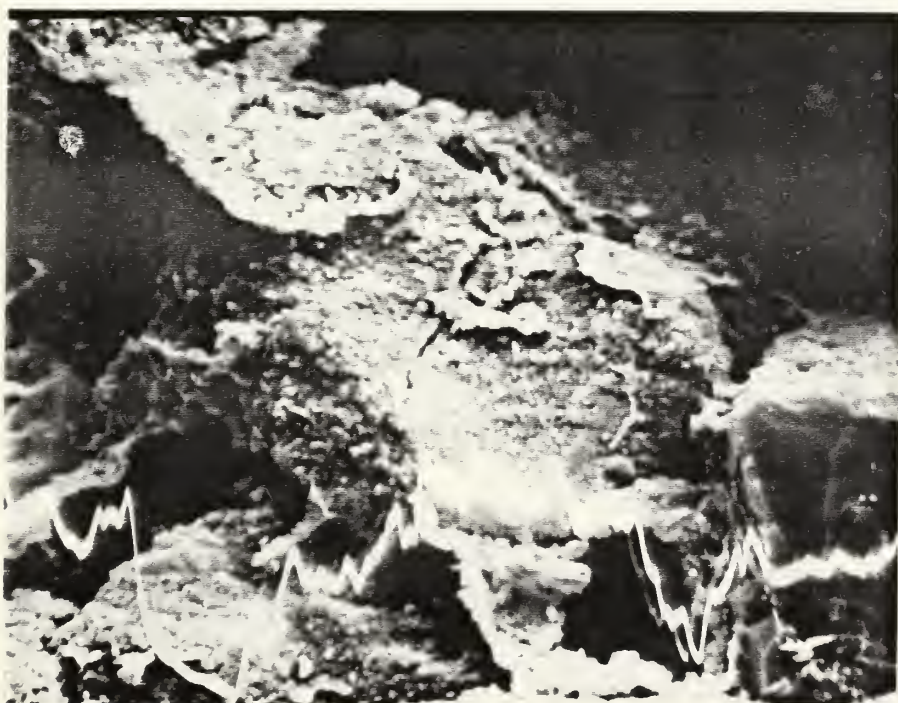


Figure A-2: Frio Sandstone, 9178.3 ft, x103, x260

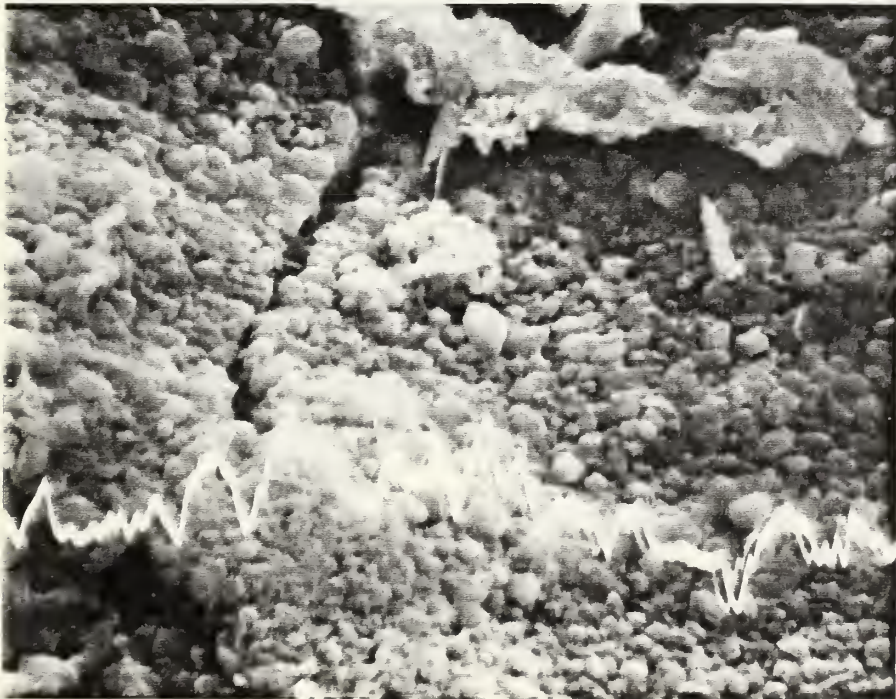


Figure A-3: Frio Sandstone, 9178.3 ft, x550, x1030

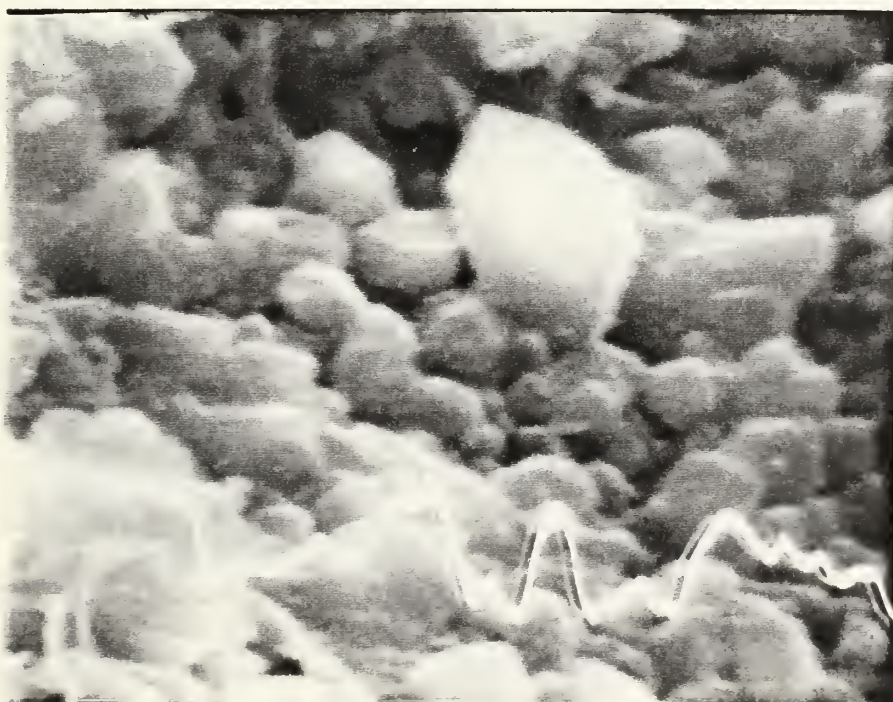


Figure A-4: Frio Sandstone, 9178.3 ft, x2600, x4800

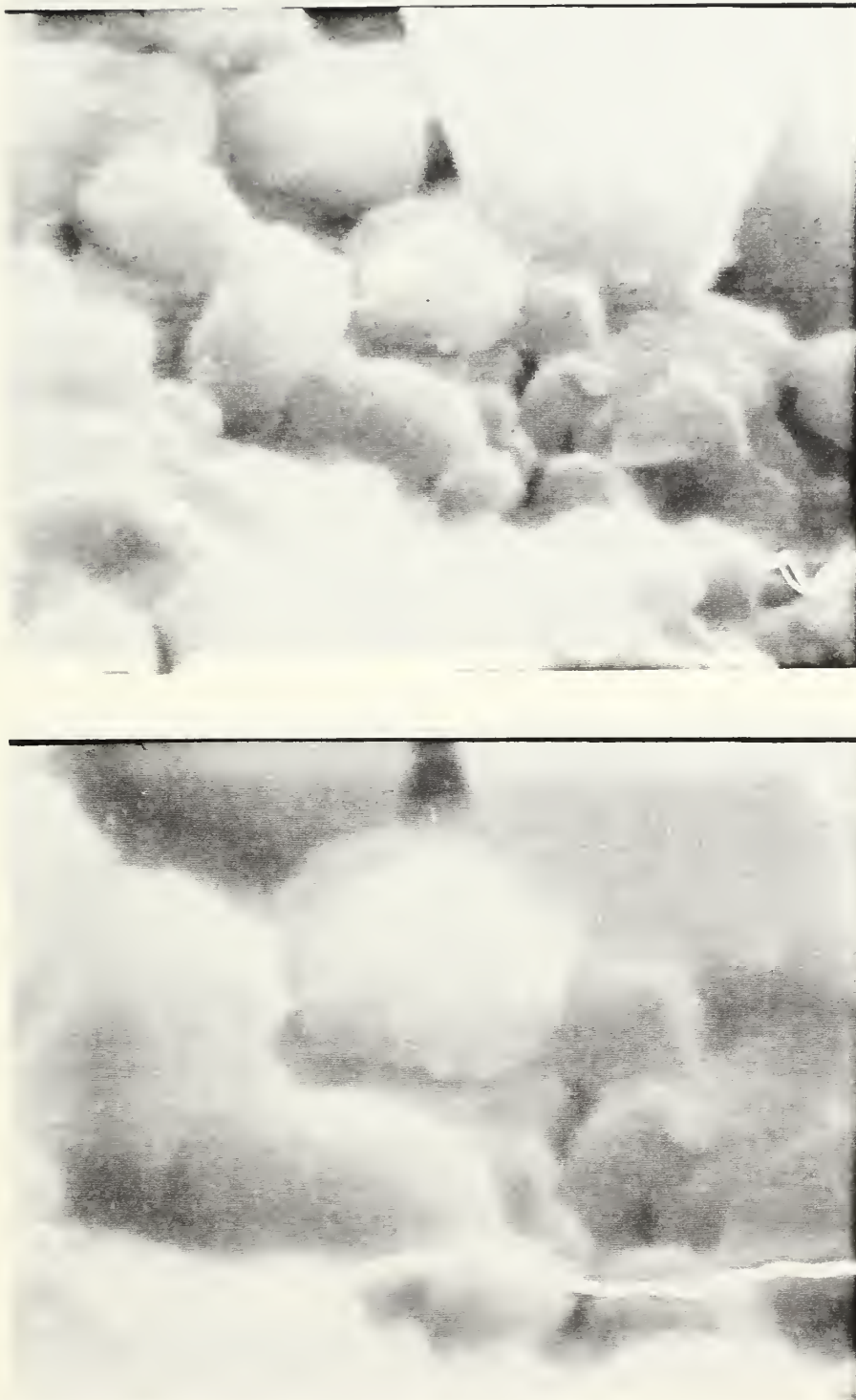


Figure A-5: Frio Sandstone, 9178.3 ft, x9300, x18500

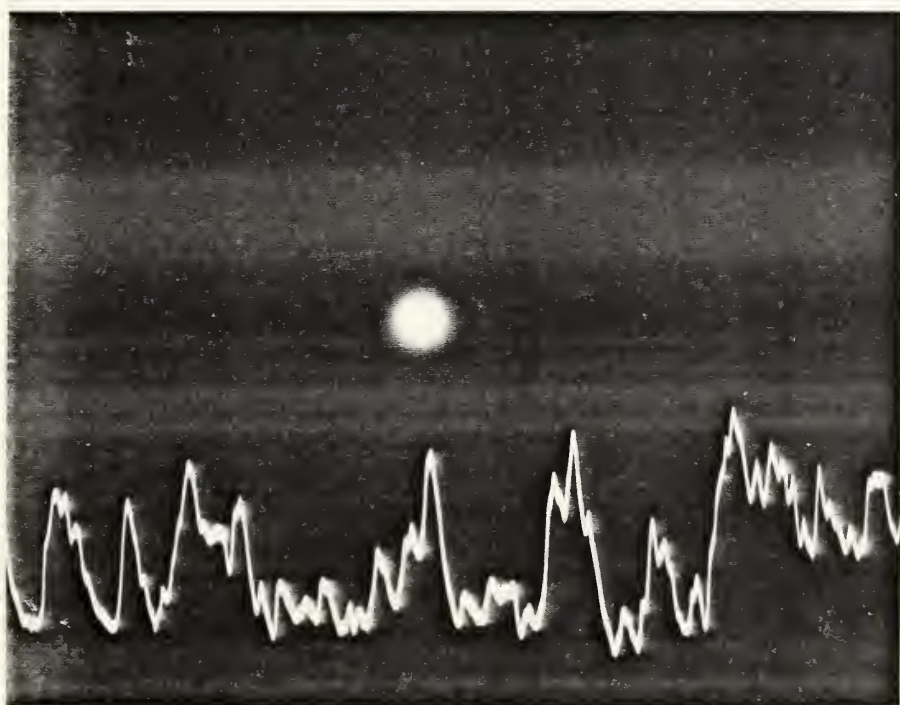
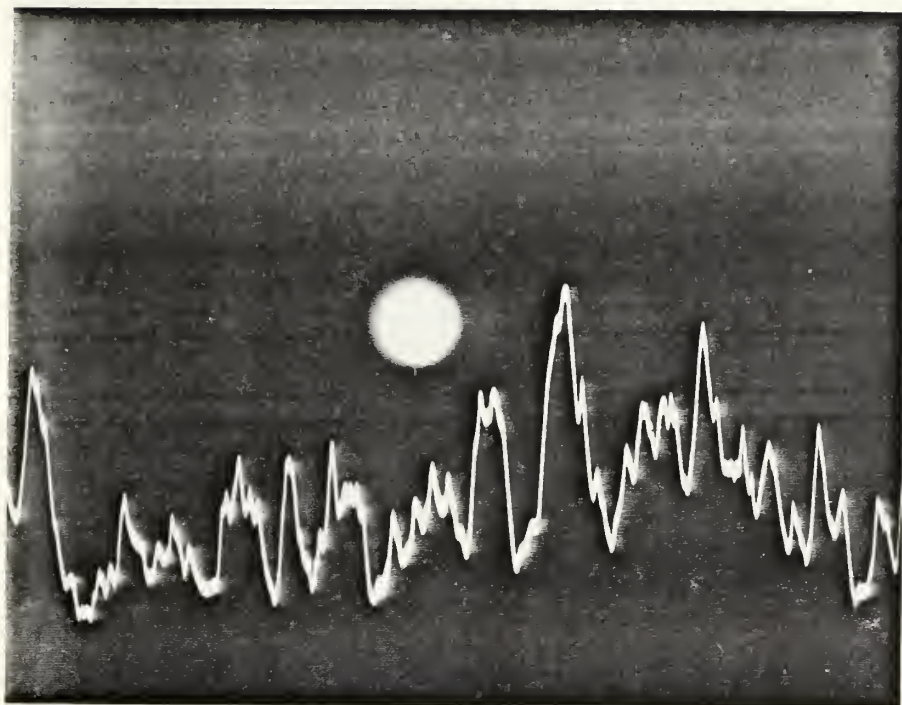


Figure A-6: Travis Peak Sandstone, 7456.3 ft, x34, x55

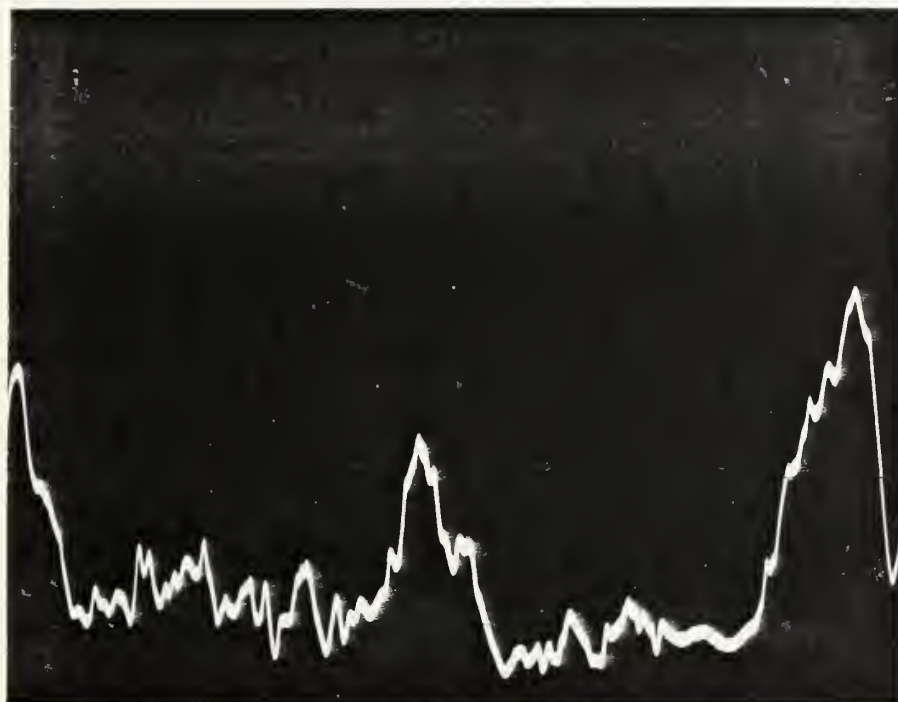


Figure A-7: Travis Peak Sandstone, 7456.3 ft, x130,
x220

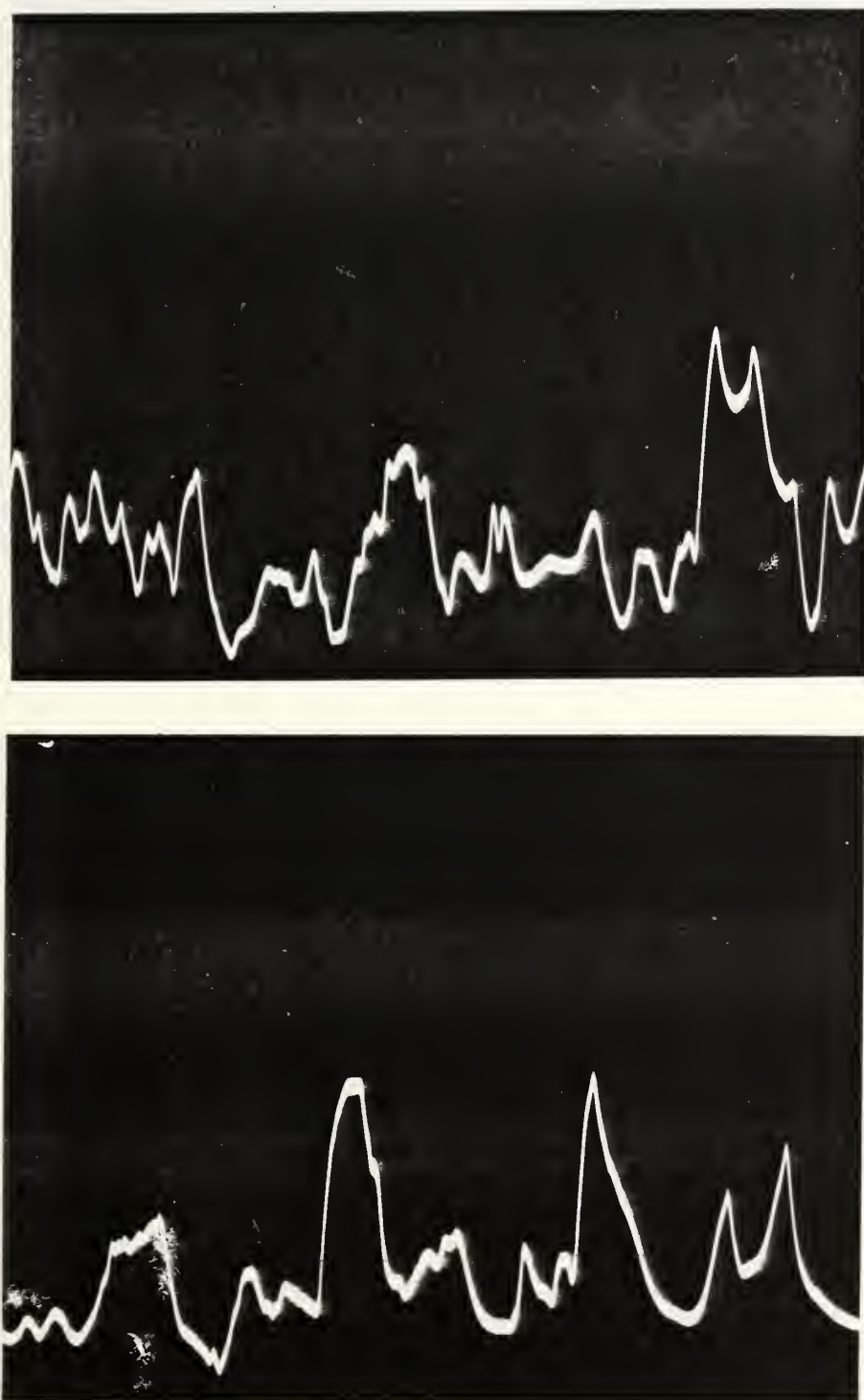


Figure A-8: Travis Peak Sandstone, 7456.3 ft, x260,
x520

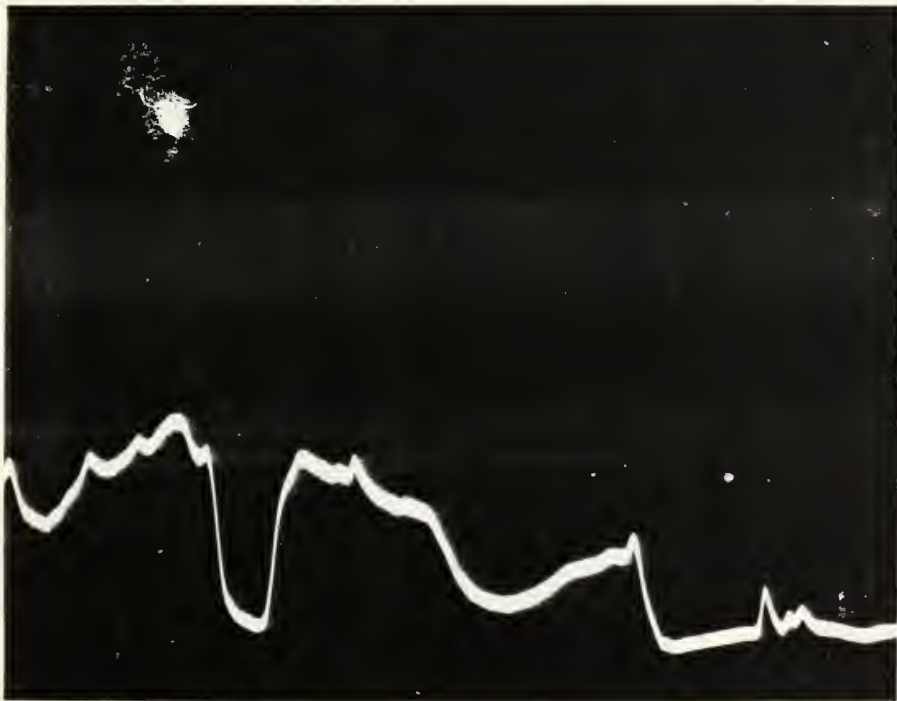
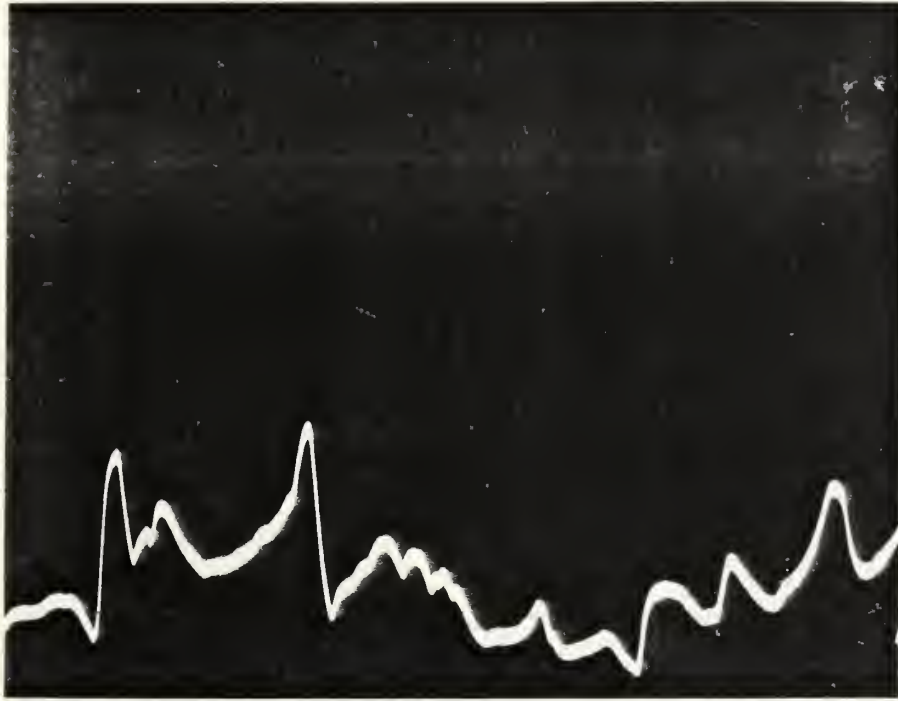


Figure A-9: Travis Peak Sandstone, 7456.3 ft, x1100,
x2900

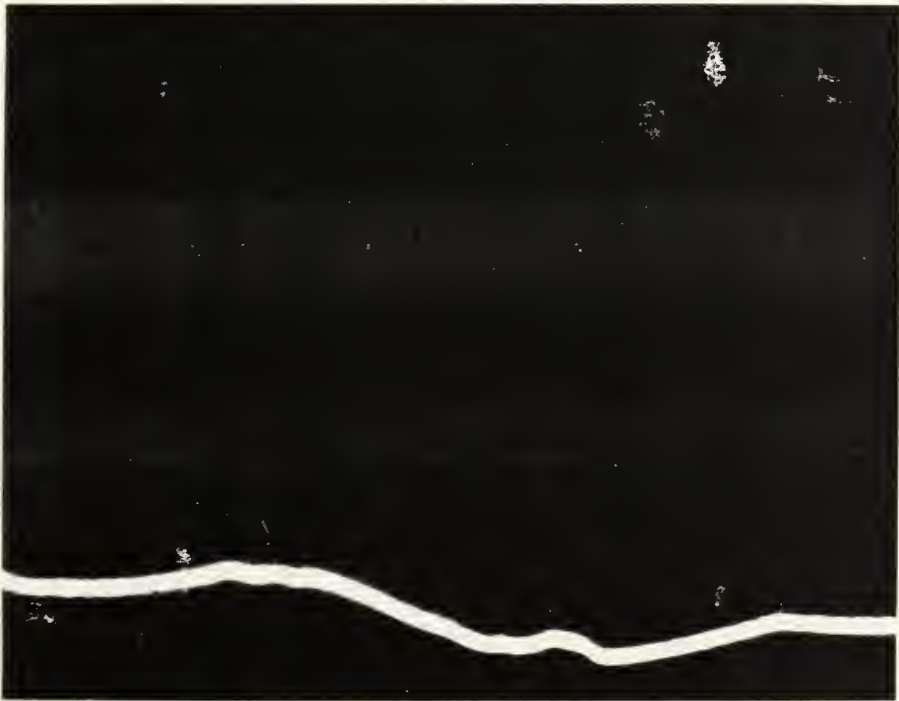
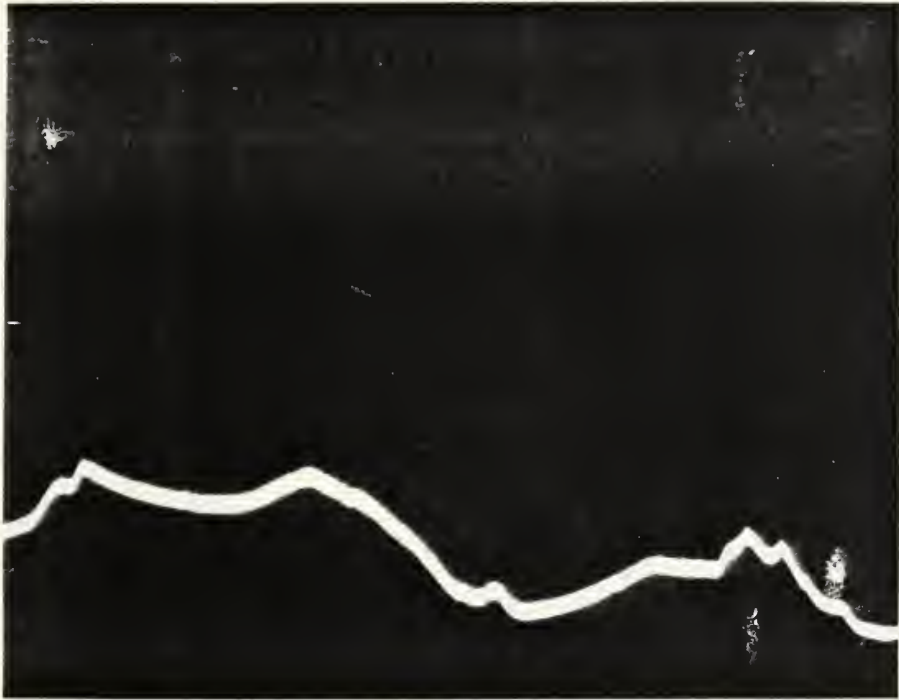


Figure A-10: Travis Peak Sandstone, 7456.3 ft, x5400,
x9500



Figure A-11: Frio Sandstone, 9189.5 ft, x29, x58

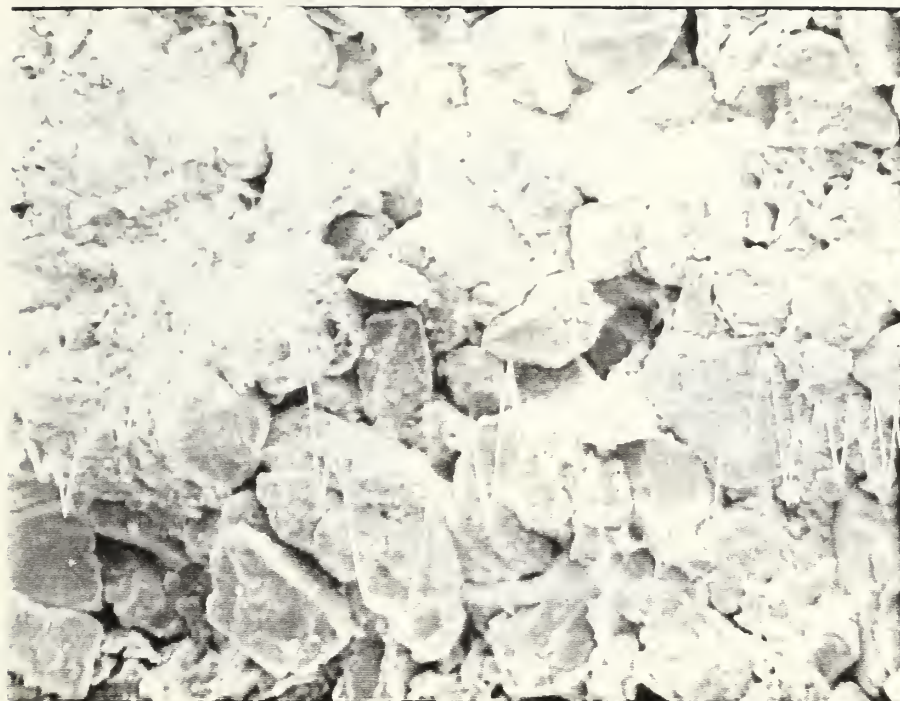


Figure A-12: Frio Sandstone, 9189.5 ft, x100, x250

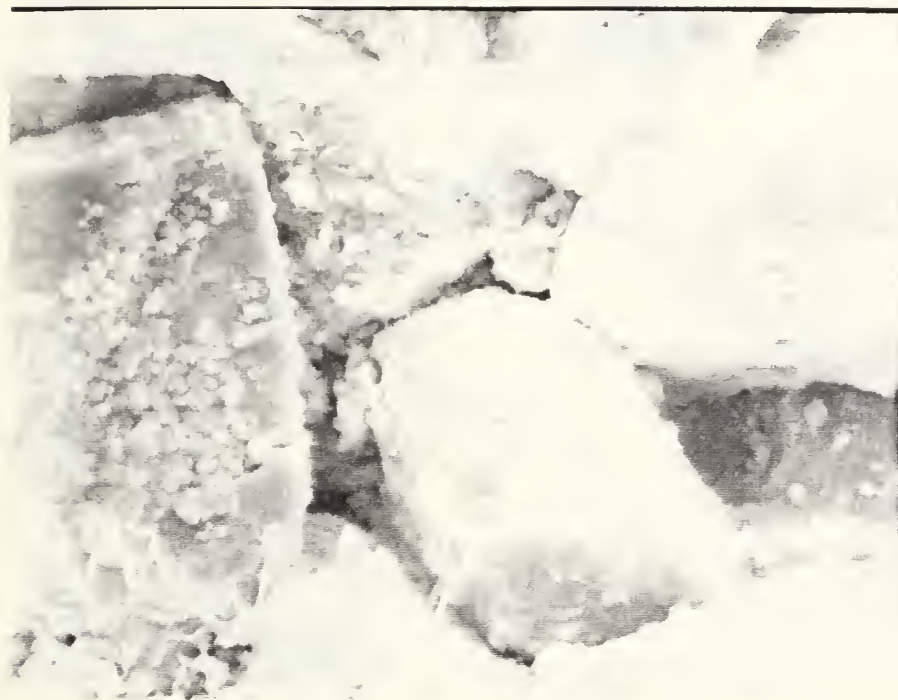


Figure A-13: Frio Sandstone, 9189.5 ft, x510, x750



Figure A-14: Frio Sandstone, 9189.5 ft, x1000, x2700

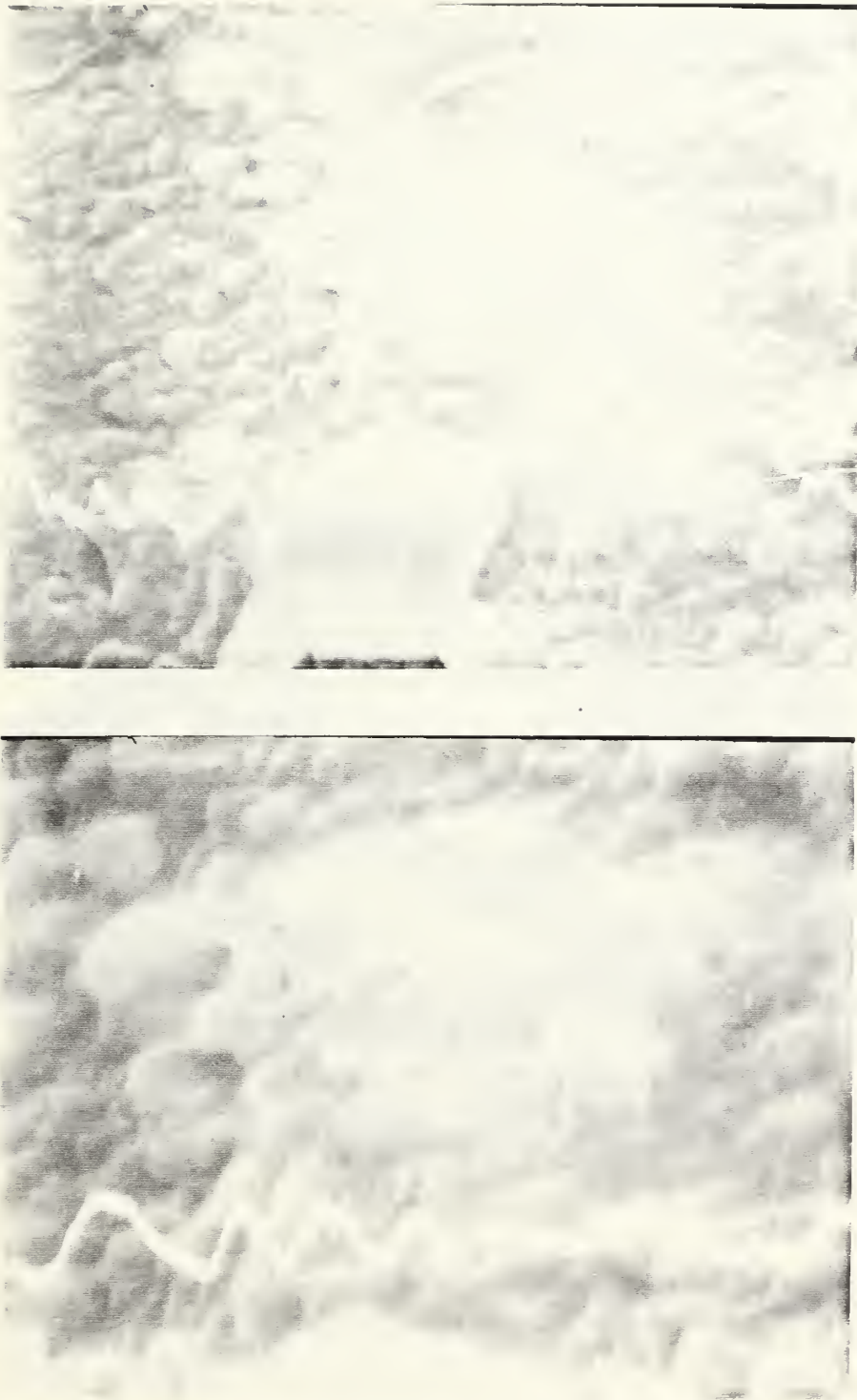


Figure A-15: Frio Sandstone, 9189.5 ft, x5100, x10000

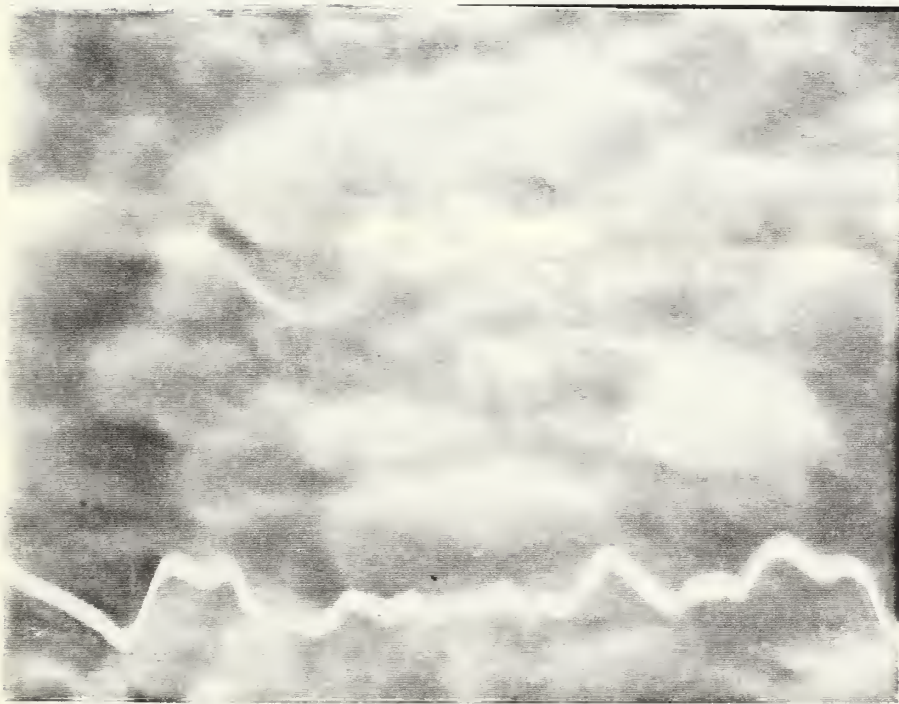


Figure A-16: Frio Sandstone, 9189.5 ft, x18000



Figure A-17: San Andres Dolomite, 3350ft, x31, x54



Figure A-18: San Andres Dolomite, 3350ft, x102, x240

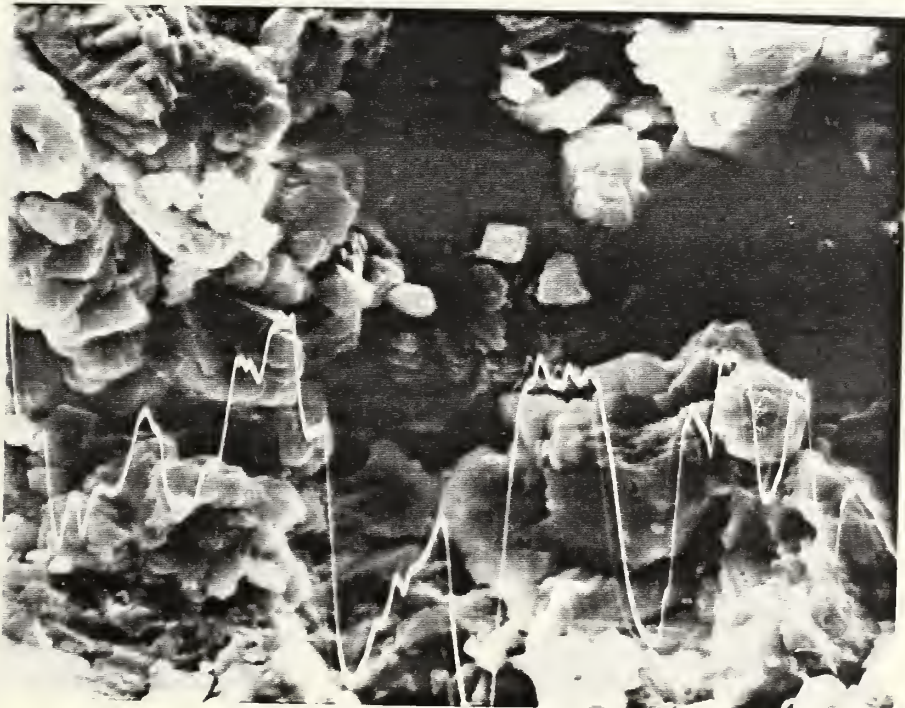
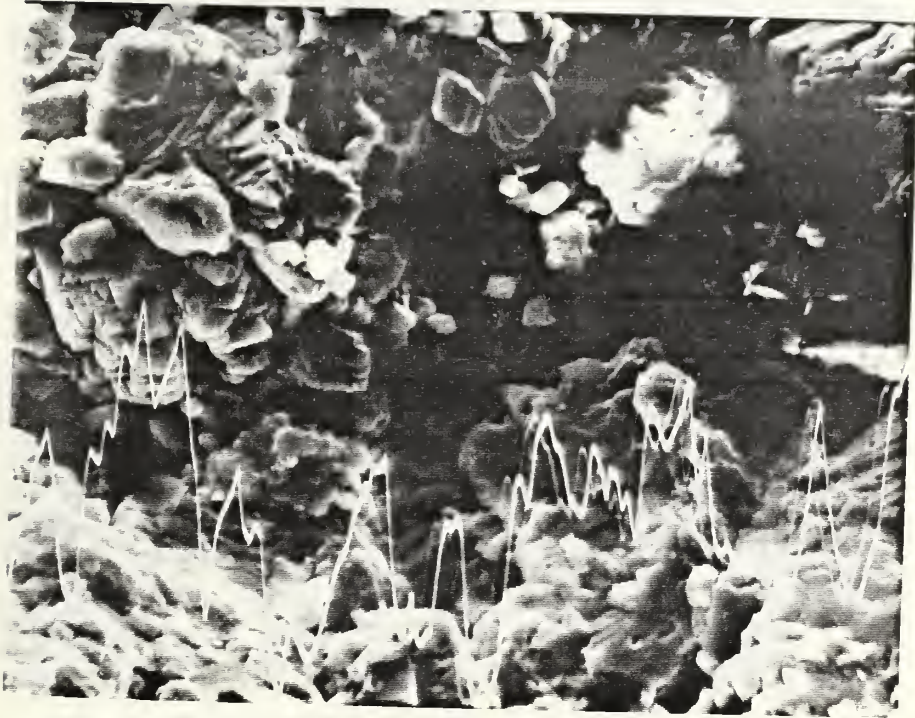


Figure A-19: San Andres Dolomite, 3350ft, x510, x760



Figure A-20: San Andres Dolomite, 3350ft, x990, x2500

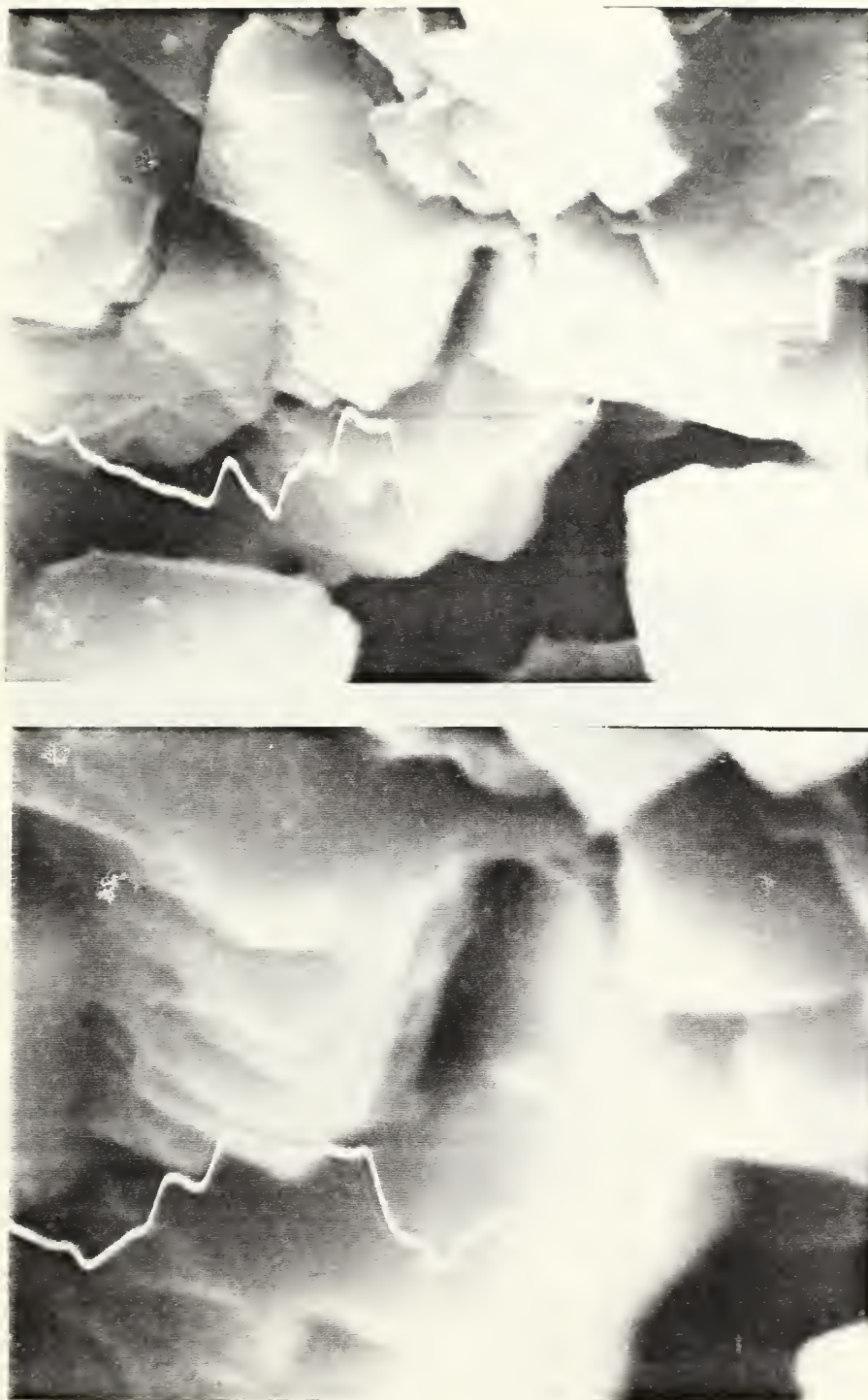


Figure A-21: San Andres Dolomite, 3350ft, x5200,
x10000

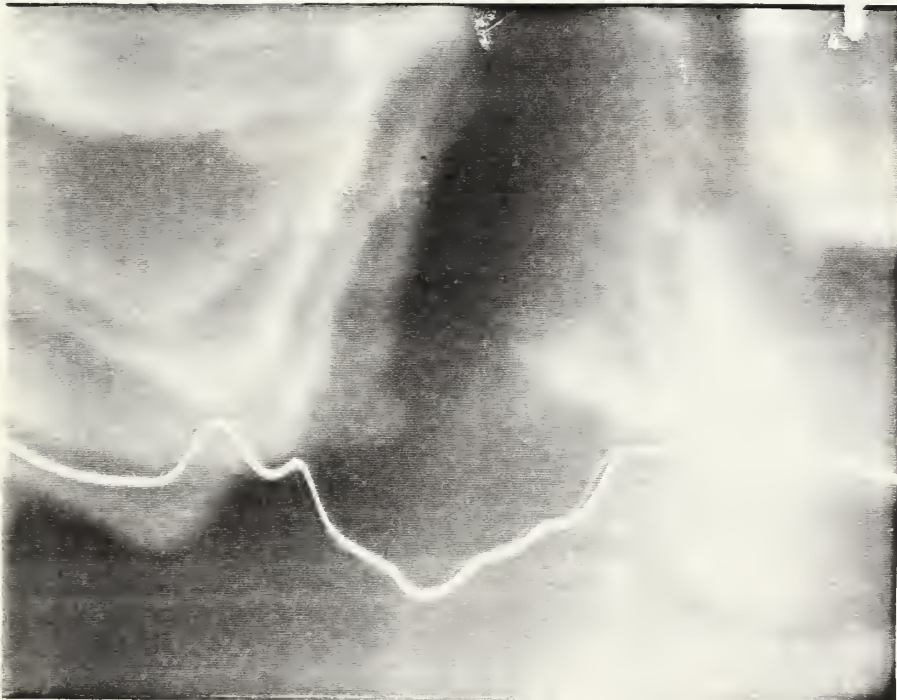


Figure A-22: San Andres Dolomite, 3350ft, x17000

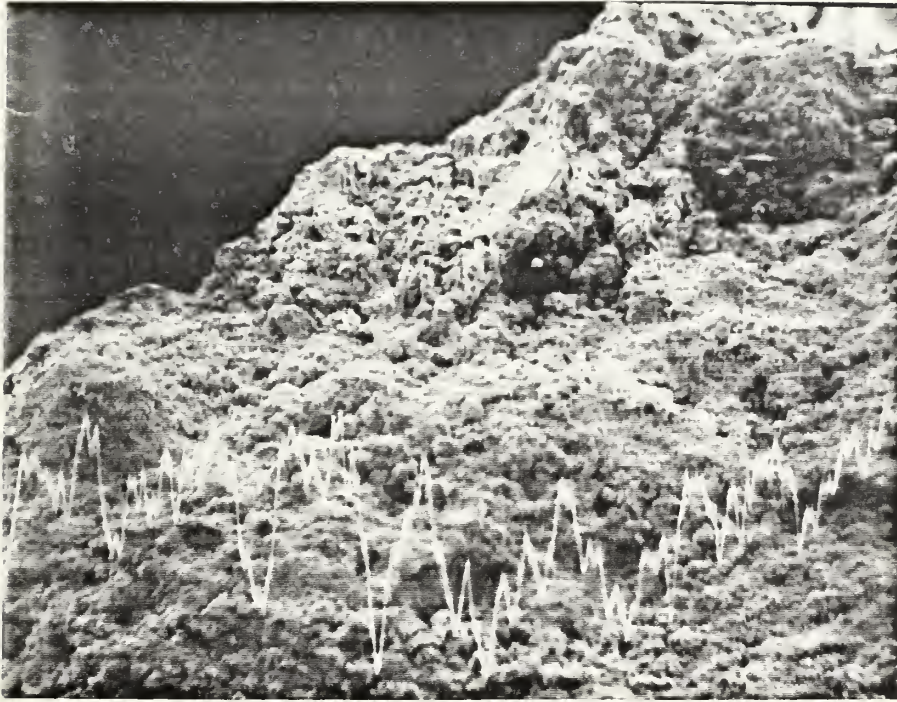


Figure A-23: San Andres Dolomite, 3464ft, x27, x54

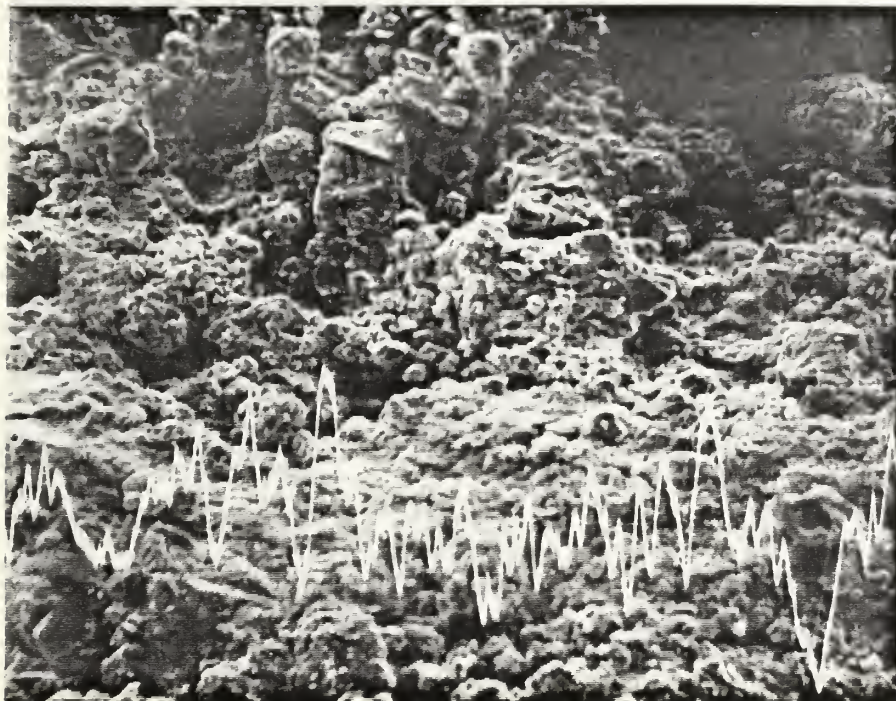


Figure A-24: San Andres Dolomite, 3464ft, x102, x230

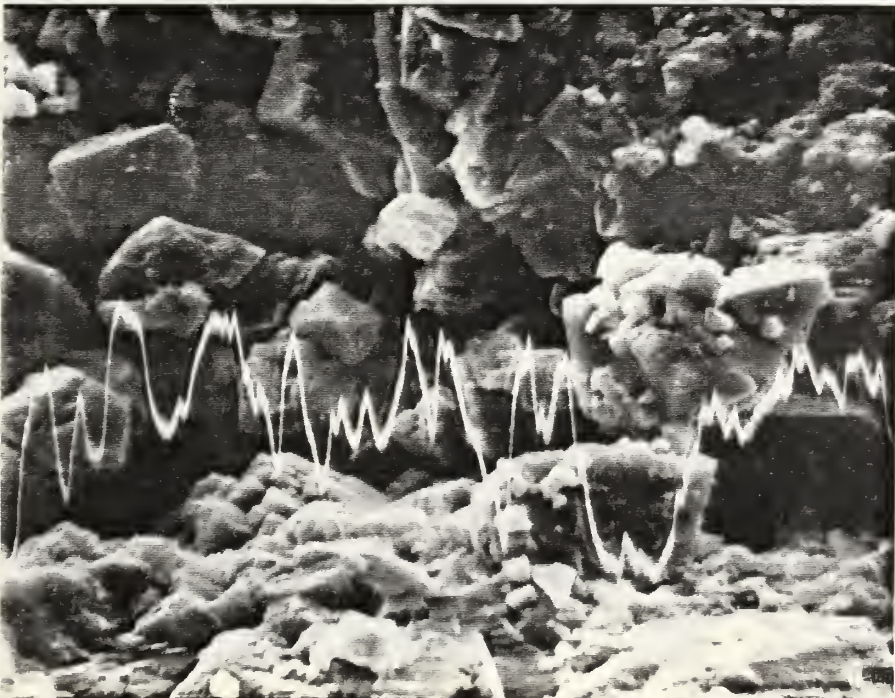


Figure A-25: San Andres Dolomite, 3464ft, x510, x730



Figure A-26: San Andres Dolomite, 3464ft, x1030,
x2400

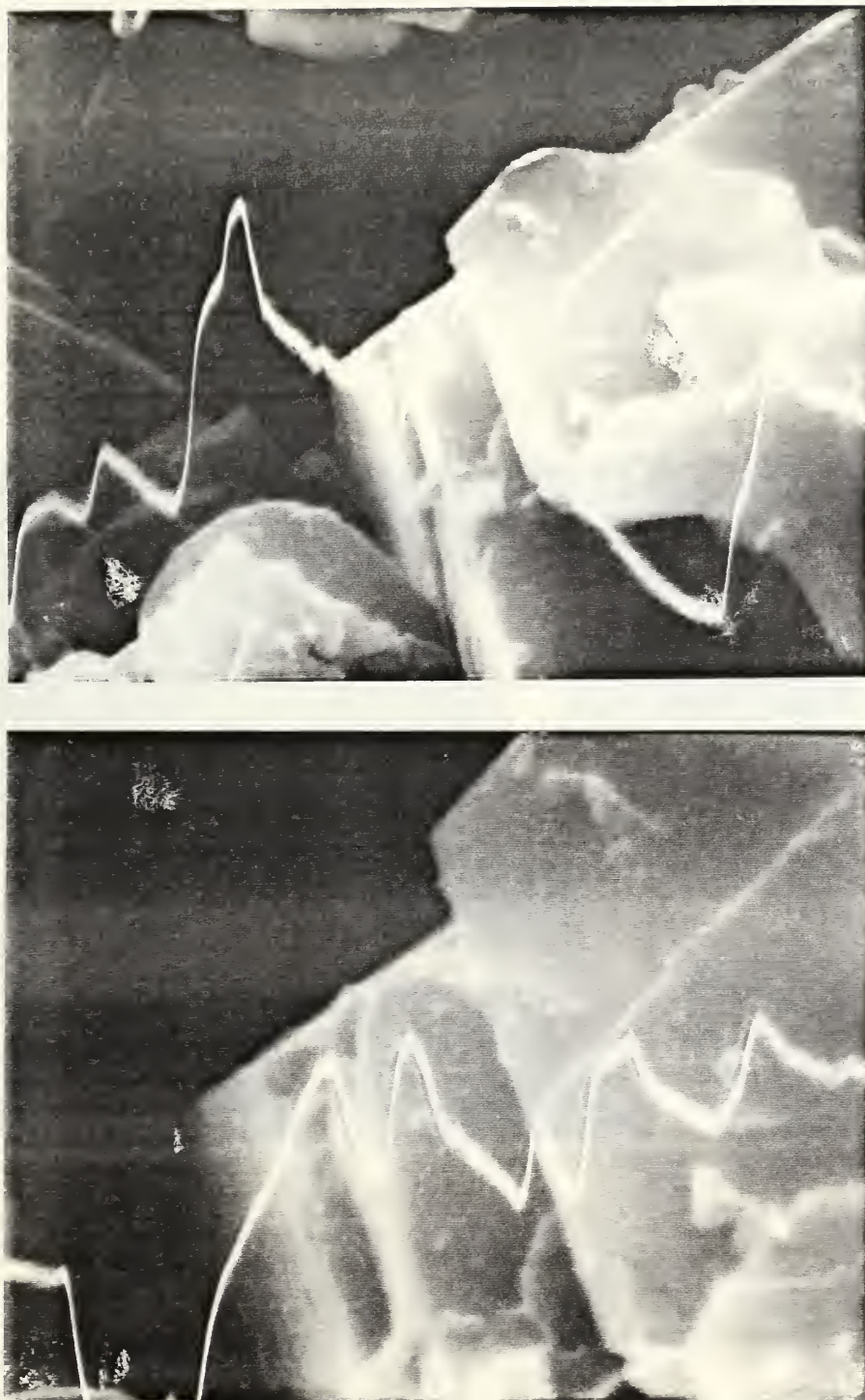


Figure A-27: San Andres Dolomite, 3464ft, x5100,
x10300



Figure A-28: San Andres Dolomite, 3464ft, x18300

APPENDIX B
MENGER SPONGE GRAPHS

$b=10, L2/L1=1000$

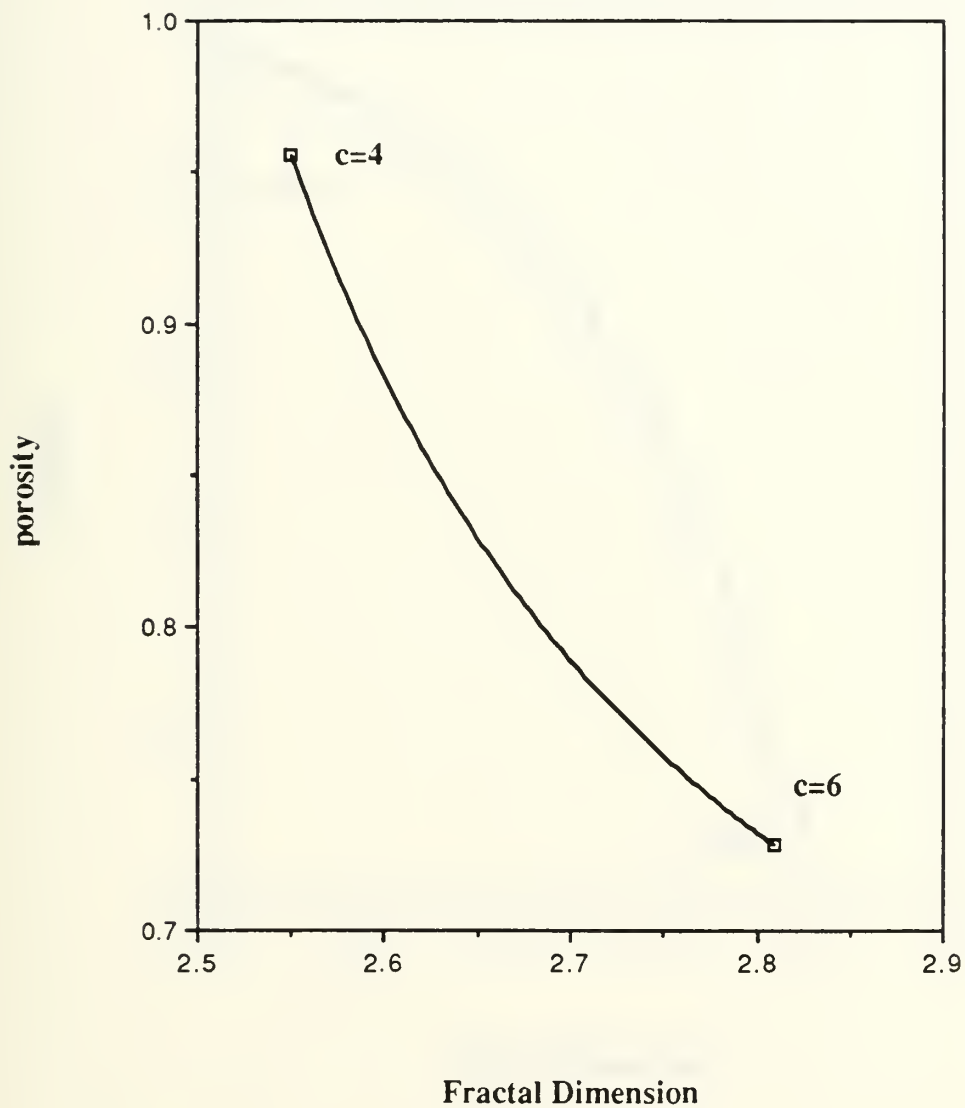


Figure B-1: Porosity vs D for $b=10$ and $L2/L1=1000$.

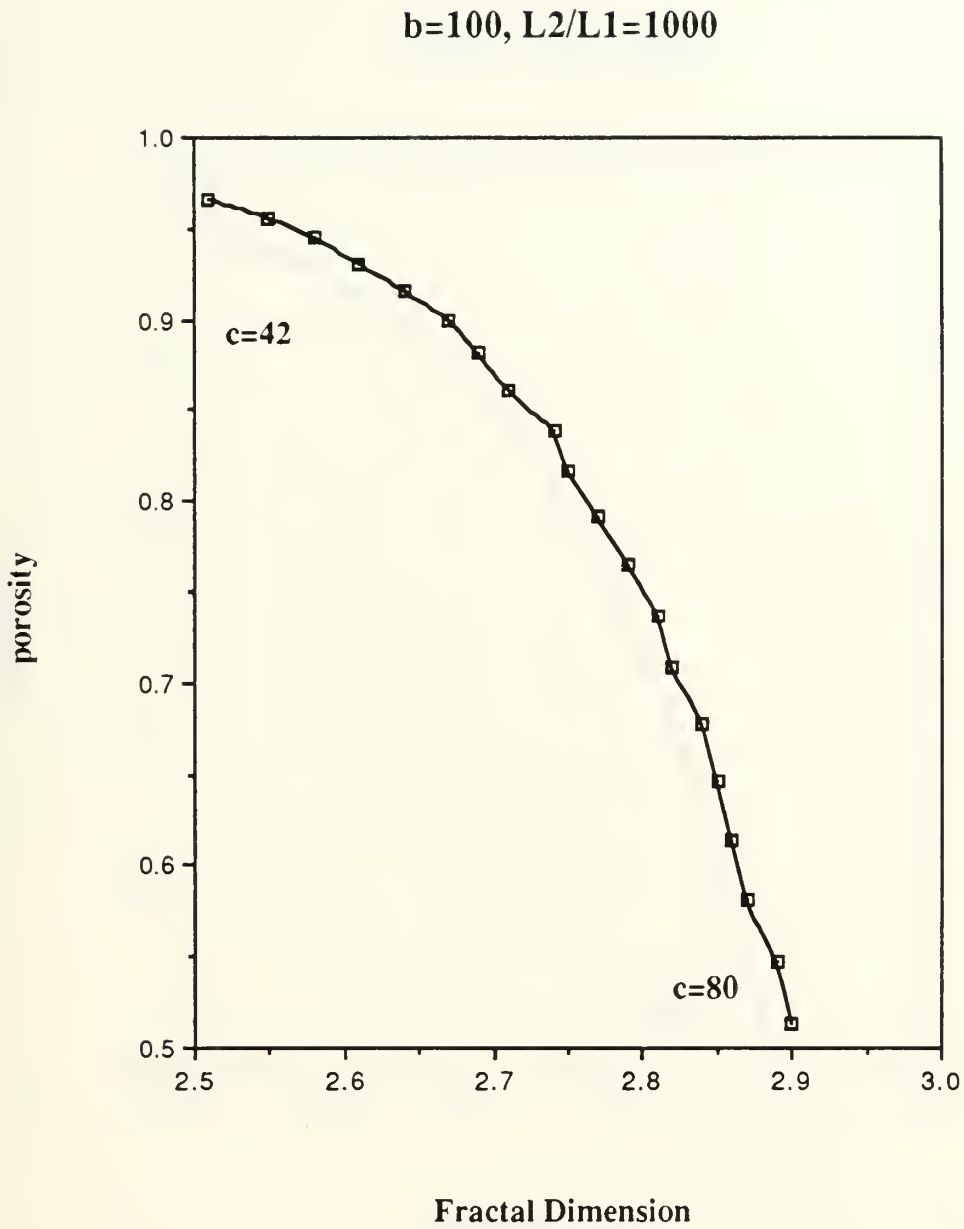


Figure B-2: Porosity vs D for $b=100$ and $L2/L1=1000$.

$b=200, L2/L1=1000$

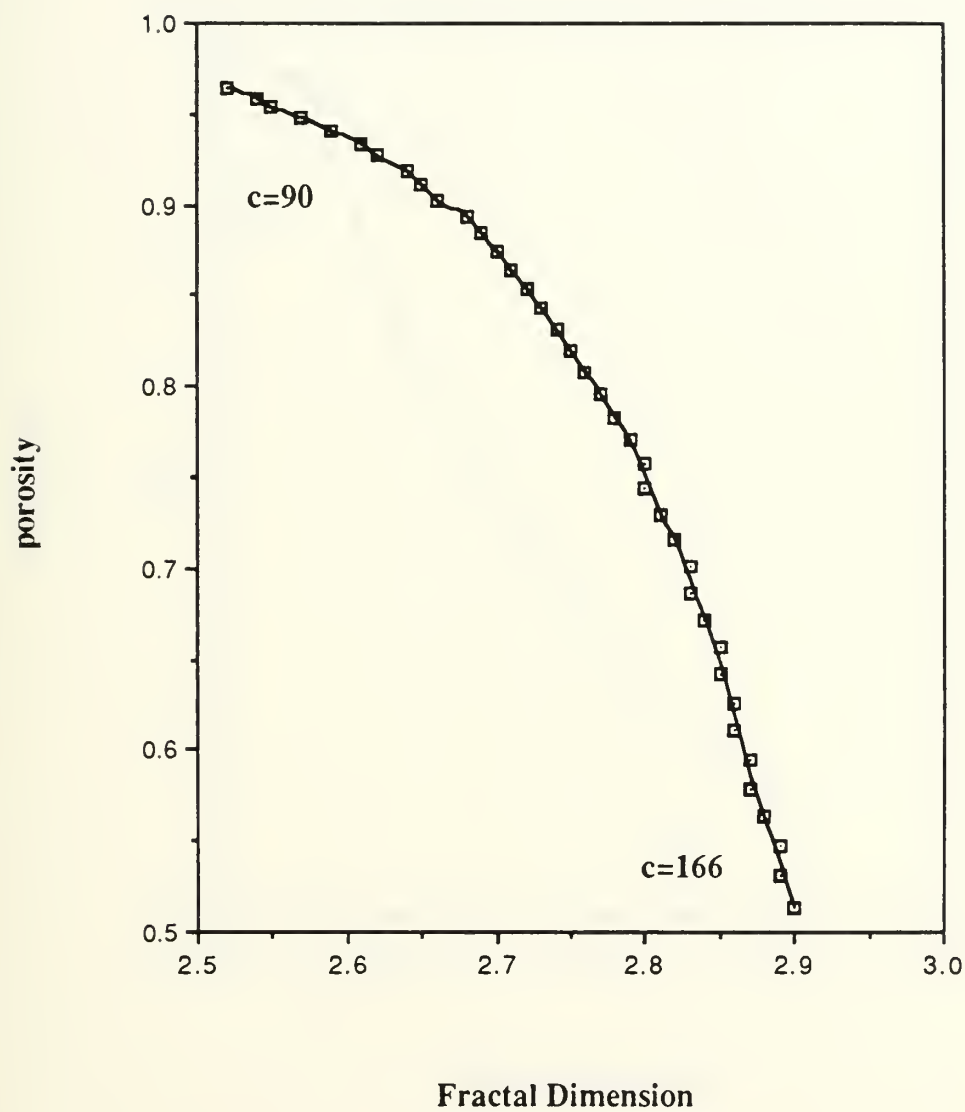


Figure B-3: Porosity vs D for $b=200$ and $L2/L1=1000$.

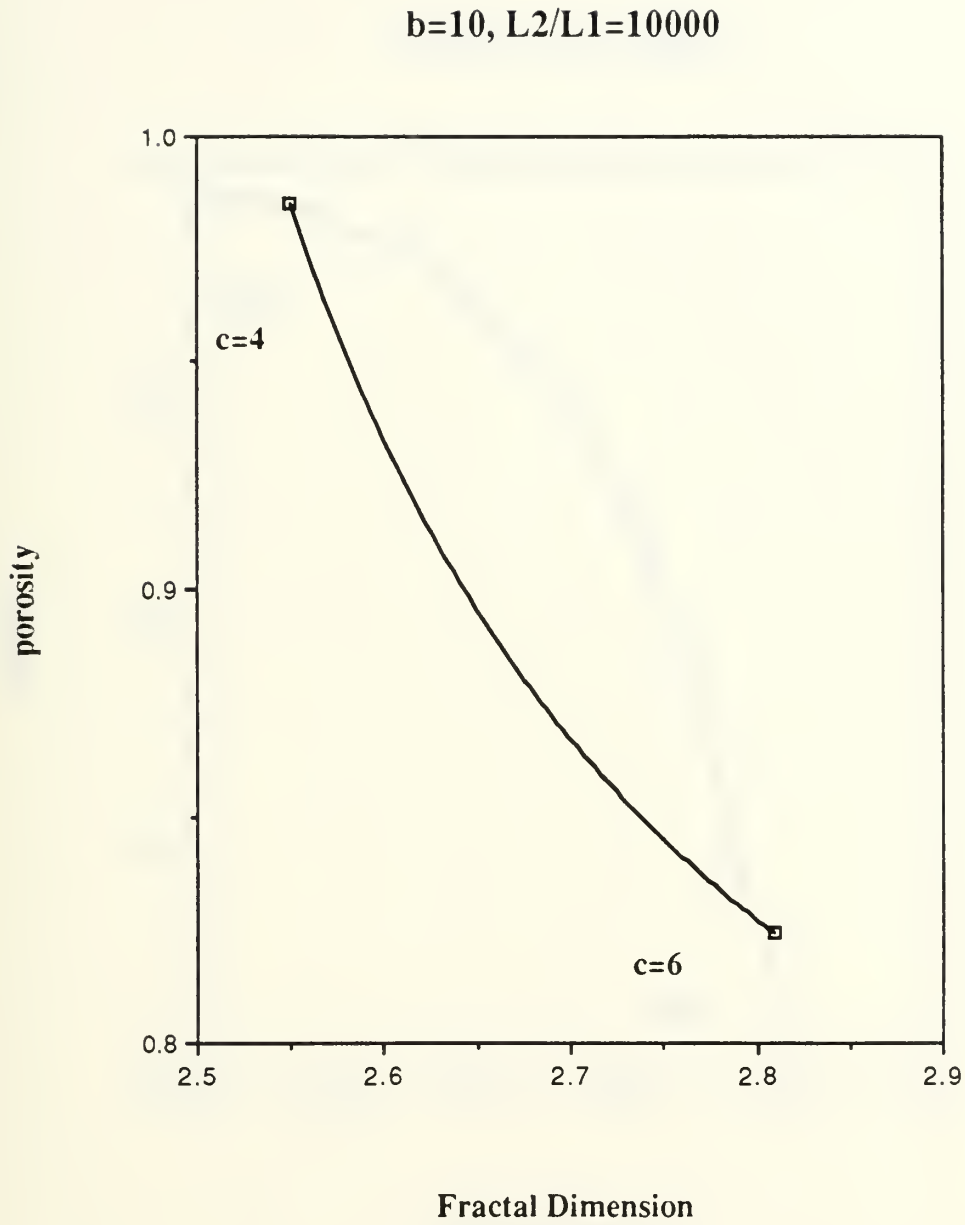


Figure B-4: Porosity vs D for $b=10$ and $L2/L1=10000$.

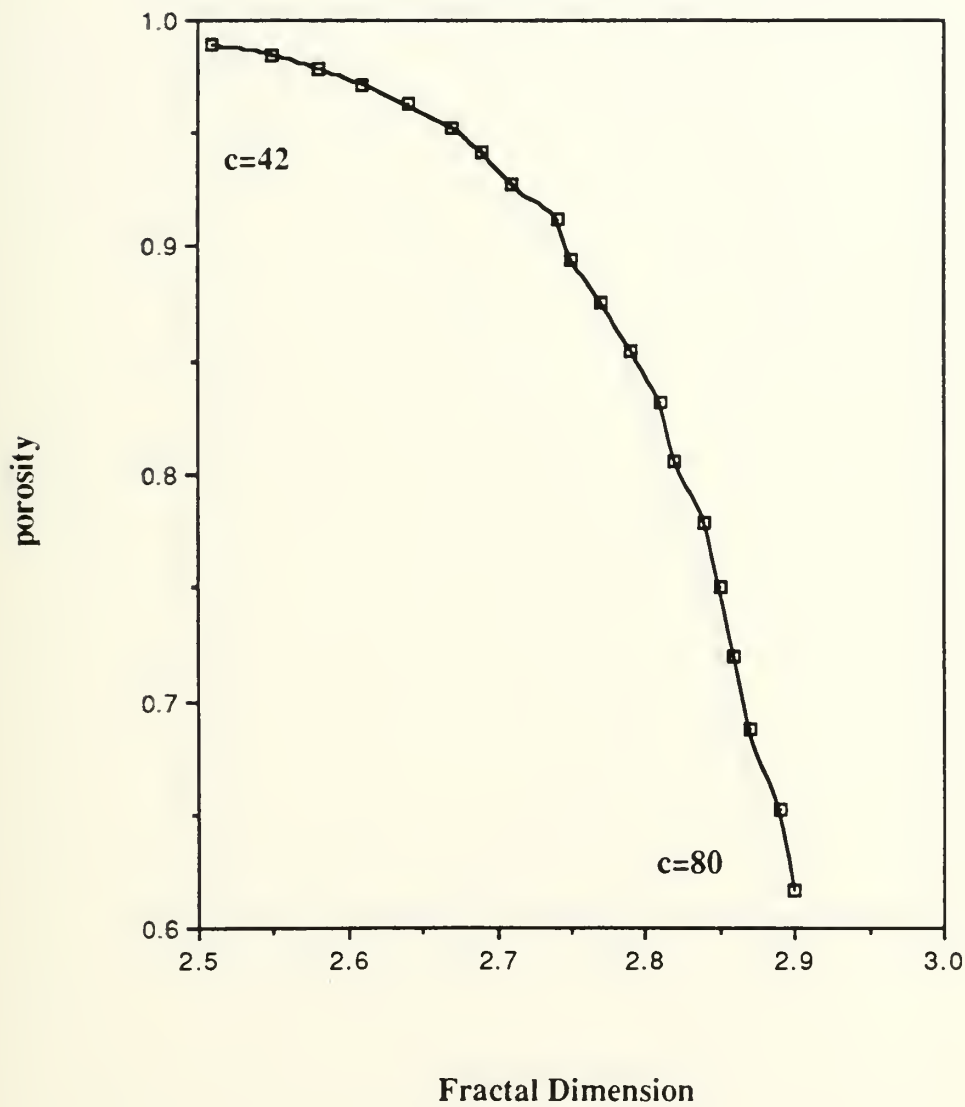
$b=100, L2/L1=10000$ 

Figure B-5: Porosity vs D for $b=100$ and $L2/L1=10000$.

$b=200, L2/L1=10000$

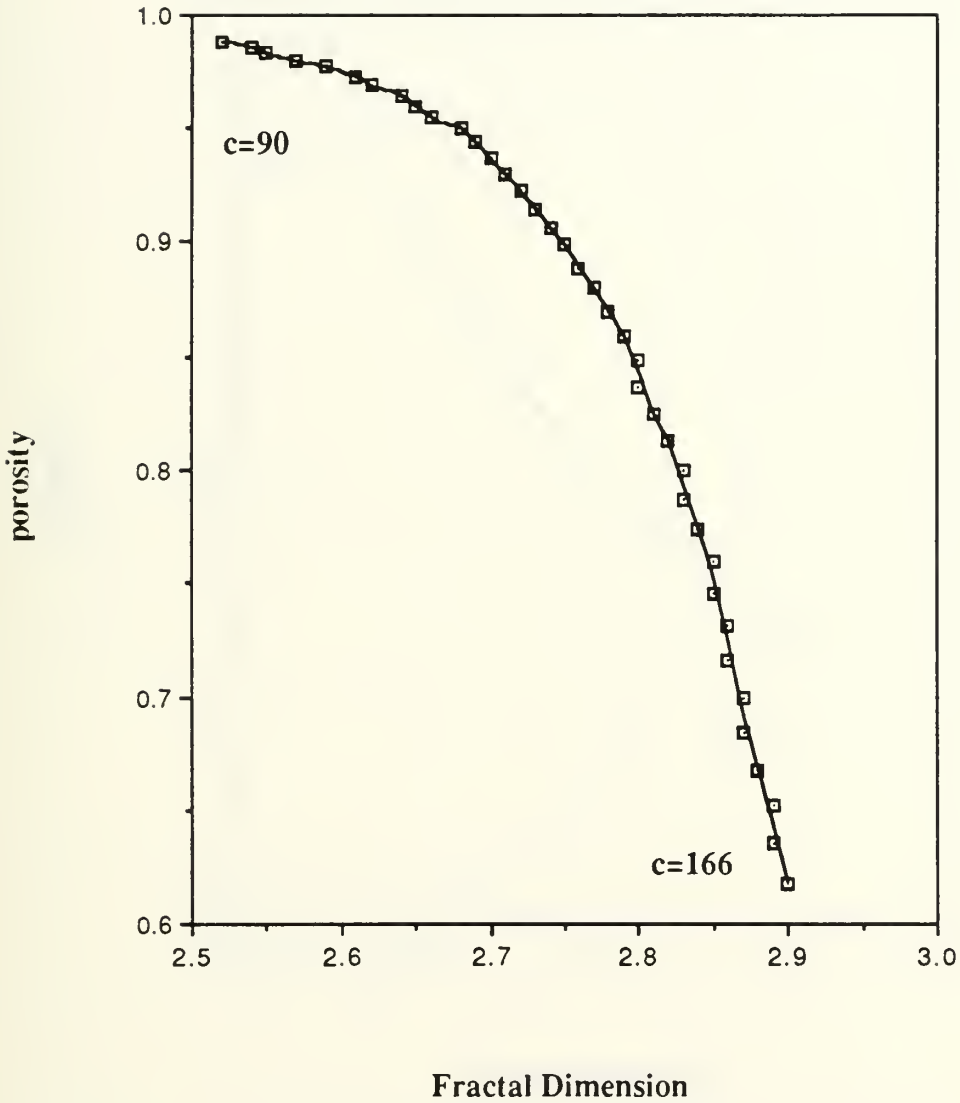


Figure B-6: Porosity vs D for $b=200$ and $L2/L1=10000$.

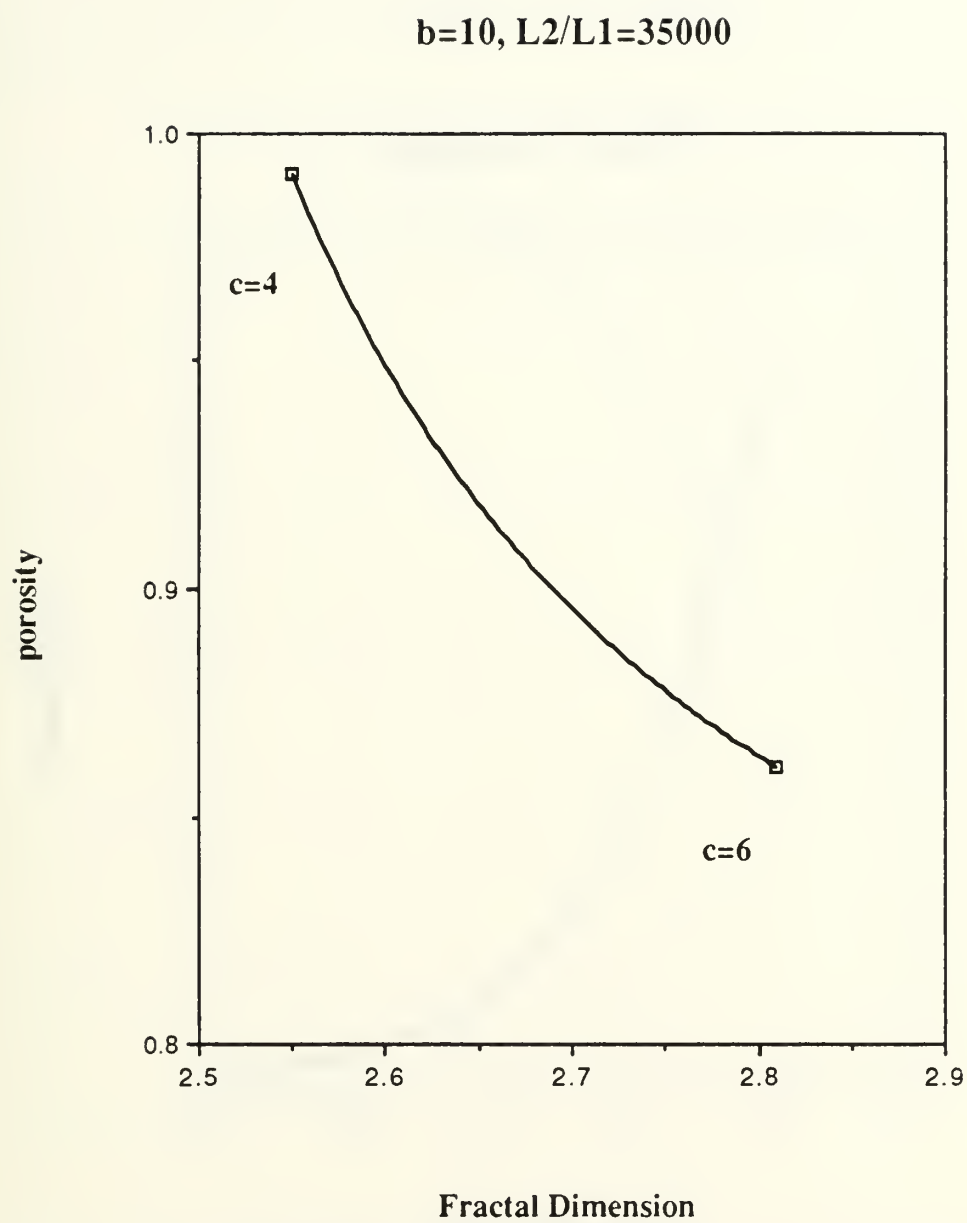


Figure B-7: Porosity vs D for $b=10$ and $L2/L1=35000$.

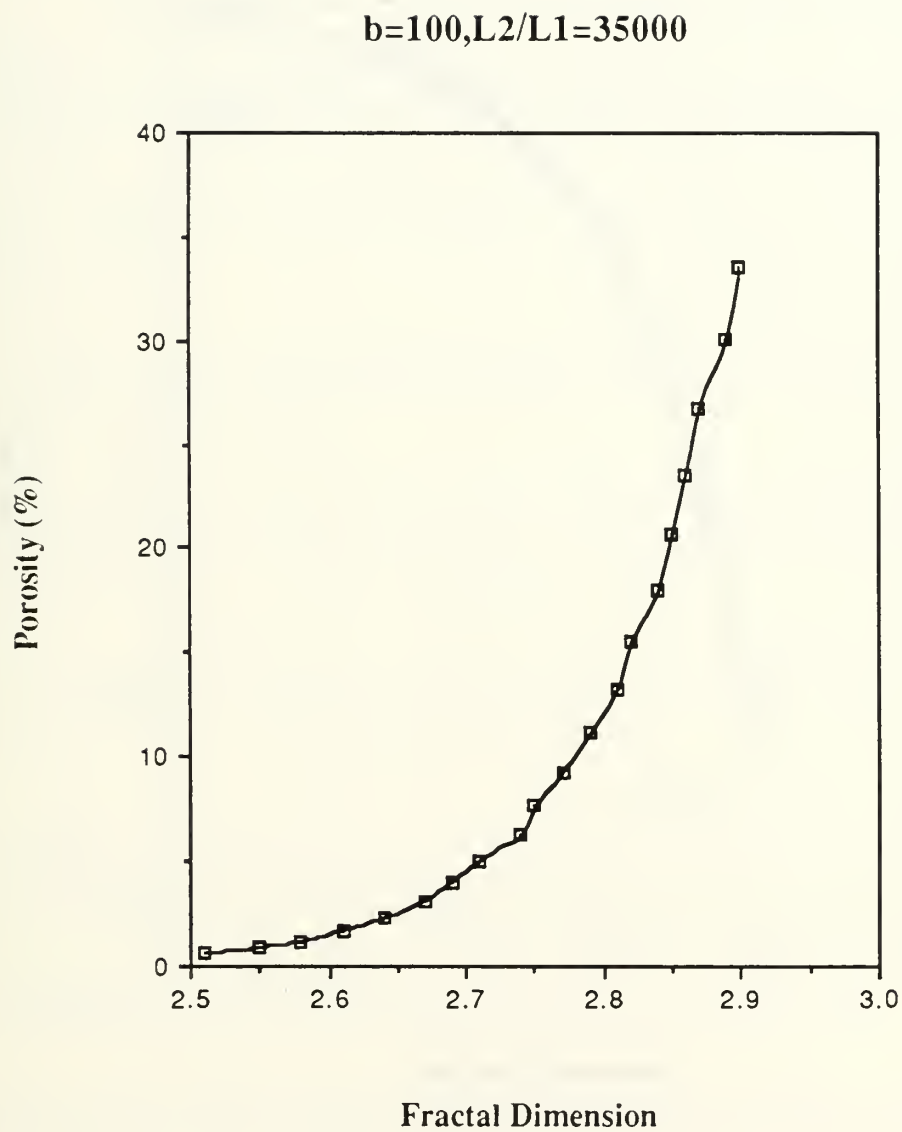


Figure B-8: Porosity vs D for b=100 and L2/L1=35000.

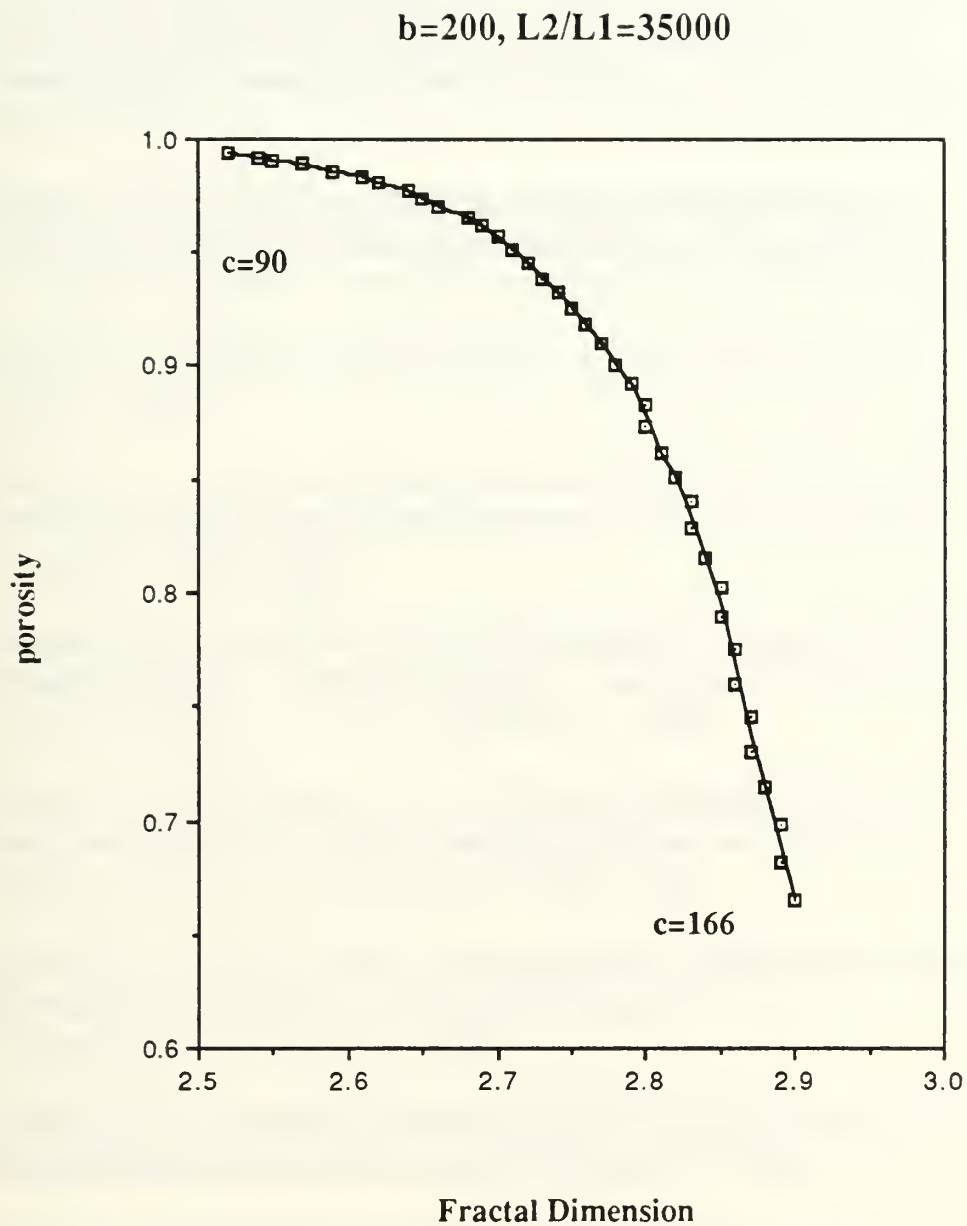


Figure B-9: Porosity vs D for $b=200$ and $L2/L1=35000$.

REFERENCES

- Avnir, D., Farin, D. and Pfeifer, P., "Chemistry in Noninteger Dimensions Between Two and Three II. Fractal Surfaces of Adsorbents", *Journal of Chemical Physics*, v 79, 7, pp. 3566-3571, 1983.
- Flook, A. G., "The Use of Dilation Logic on the Quantimet to Achieve Fractal Dimension Characterisation of Textured and Structured Profiles", *Powder Technology*, 21, pp. 295-298, 1978.
- Gupta, A., private communication at The University of Texas, 1987.
- Hewett, T. A., "Fractal Distributions of Reservoir Heterogeneity and Their Influence on Fluid Transport", *Society of Petroleum Engineers* 15386, 1986.
- Jacquin, C. G. and Adler, P. M., "The Fractal Dimension of a Gas-Liquid Interface in a Porous Medium", *Journal of Colloid and Interface Science*, v 107, 2, pp.405-417, 1985.
- Katz, A. J. and Thompson, A. H., "Fractal Sandstone Pores: Implications for Conductivity and Pore Formation", *Physical Review Letters*, v 54, 12, pp. 1325-1328, 1985.
- Kaye, B.H., "Specification of the Ruggedness and/or Texture of a Fine Particle Profile by its Fractal Dimension", *Powder Technology*, 21, pp. 1-16, 1978.
- Krohn, C. E., "Sandstone Fractal and Euclidean Pore Volumes", to be published, *Journal of Geophysical Research*, 1987a.
- Krohn, C. E., "Fractal Measurements of Sandstones, Shales and Carbonates", to be published, *Journal of Geophysical Research*, 1987b.

Krohn, C. E. and Thompson, A. H., "Fractal Sandstone Pores: Automated Measurements Using Scanning-Electron-Microscope Images", *Physical Review B*, v 33, 9, pp.6366-6374, 1986.

Mandelbrot, B. B., *The Fractal Geometry of Nature*, Freeman, New York, 1983.

Pentland, A. P., "Fractal-Based Description", *SRI Artificial Intelligence Center Technical Memo*, pp.973-981, 1983.

Pfeifer, P. and Avnir, D., "Chemistry in Noninteger Dimensions Between Two and Three. Fractal Theory of Heterogeneous Surfaces", *Journal of Chemical Physics*, v 79, 7, pp. 3558-3565, 1983.

Porod, G., *Kolloid Z.*, 124, p 83, 1951.

Schaefer, B. C., Bunker, B. C. and Wilcoxon, J. P., "Are Leached Porous Glasses Fractal?", *Physical Review Letters*, v 58, 3, pp. 284-285, 1987.

Schwarz, H. and Exner, H. E., "The Implementation of the Concept of Fractal Dimension on a Semi-Automatic Image Analyser", *Powder Technology*, 27, pp.207-213, 1980.

Sharma, M. M. and Gupta, A., "Transport in Fractal Lattices", *Center for Enhanced Oil Recovery Annual Report*, The University of Texas, pp. 215-245, 1987.

Skjeltorp, A. T., "Visualization and Characterization of Colloidal Growth from Ramified to Faceted Structures", *Physical Review Letters*, v 58, 14, pp.1444-1447, 1987.

Thompson, A. H., Katz, A. J. and Krohn, C. E., "The Microgeometry and Transport Properties of Sedimentary Rock", to be published, *Journal of Geophysical Research*, 1987.

Van Damme, H., Obrecht, F., Levitz P., Gatineau L. and Laroche C., "Fractal Viscous Fingering in Clay Slurries", *Letters to Nature* , v 320, pp. 731-733, 1986.

Winslow, D. N., "The Fractal Nature of the Surface of Cement Paste", *Cement and Concrete Research* , v 15, pp. 817-824, 1985.

Other related references:

Adler, P. M., "Transport Processes in Fractals II. Stokes Flow in Fractal Capillary Networks", *International Journal of Multiphase Flow*, v 11, 2, pp. 213-239, 1985.

Adler, P. M., "Transport Processes in Fractals VI. Stokes Flow Through Sierpinski Carpets", *Physics Fluids*, v 29,1, pp.15-22.

Normand, M. D. and Peleg, M., "Determination of the Fractal Dimension of a Particle Silhouette using Image-Processing Techniques", *Powder Technology*, 45, pp. 271-275.

Peleg, M. and Normand, M. D., "Mechanical Stability as the Limit to the Fractal Dimension of Solid Particle Silhouettes", *Powder Technology*, 43, pp. 187-188, 1985.

Van Damme, H. and Fripiat, J. J., "A Fractal Analysis of Adsorption Processes by Pillared Swelling Clays", *Journal Chemical Physics*, v 82, 6, 1985.

VITA

Kenneth Lee Cowan was born in Reno, Nevada, August 11, 1958, the son of Barbara Lee Cowan and Frank Alexander Cowan. The family then moved to San Jose, California where Kenneth grew up and attended public schools. He graduated from Oak Grove High School in San Jose in 1976 and attended The University of California at Berkeley in the Fall. After two years, he transferred to San Jose State University where he received his Bachelor of Science degree in Electrical Engineering in 1981. In 1981, he joined the Civil Engineer Corps of the United States Navy and has been employed by the Navy since that date. In 1986, he entered The University of Texas at Austin to pursue a Masters of Science degree in Petroleum Engineering.

Permanent Address: 8406 Cockney Drive
Austin, Texas

This thesis was typed by the author.

DOUBLE COPY LIBRARY
WELLS STATION, DUBLIN 2, IRELAND
MONYEAHILL, CO. DUBLIN 15, IRELAND

Thesis
C756924 Cowan
c.1 The fractal dimension
as a petrophysical
parameter.

Thesis
C756924 Cowan
c.1 The fractal dimension
as a petrophysical
parameter.

thesC756924

The fractal dimension as a petrophysical



3 2768 000 72901 6
DUDLEY KNOX LIBRARY